THEORETICAL INVESTIGATIONS OF FACTORS WHICH AFFECT THE MODE-SPECIFIC BEHAVIOR OF UNIMOLECULAR REACTION DYNAMICS

By

KAREN WALKER BINTZ

Bachelor of Science
Northeastern Oklahoma State University
Tahlequah, Oklahoma
1984

Master of Science
Oklahoma State University
Stillwater, Oklahoma
1986

Submitted to the Faculty of the
Graduate College of the
Oklahoma State University
in partial fulfillment of
the requirements for
the Degree of
DOCTOR OF PHILOSOPHY
July, 1992

THEORETICAL INVESTIGATIONS OF FACTORS
WHICH AFFECT THE MODE-SPECIFIC
BEHAVIOR OF UNIMOLECULAR
REACTION DYNAMICS

Thesis Approved:

Donald L. Thompson
Thesis Adviser

Lionel M. Raff

Paul Westhaus

J Paul Devlin

Thomas C. Collins
Dean of the Graduate College

ACKNOWLEDGMENTS

Many individuals have made contributions to my education and have influenced the direction that the research reported here has taken. Although I could never express the complete extent of my graditude for what each person listed here has done, I at least wish to acknowledge their participation in the process which has led to this dissertation.

Foremost, I express my sincere appreciation to my research adviser, Professor Donald L. Thompson. All of the essential components for conducting research were placed at my disposal through his successful endeavors. However, he provided much more in terms of intellectual stimulation and guidance. I have obtained invaluable insight from his instruction.

Thanks is also due the members of my committee, Professors Lionel Raff, J. Paul Devlin, Paul Westhaus, and H. L. Scott, for their time and advisement. I would like to give special thanks to Professor Raff for instructive conversations regarding power spectra and potential-energy surface fitting. I am also indebted to Professor Devlin for explaining certain aspects of the absorption spectroscopy used in the CF_2Br_2 photodissociation experiments. I am appreciative for the interactions that I have had with the physicists on my committee, Professors Westhaus and Scott. I have learned much from both of them and am grateful that they both agreed to serve as "out-of-area" members of my committee again.

Professor Mark Gordon and Ms. Theresa Windus were very gracious hosts during my visit to North Dakota State University last year. I would also like to thank Theresa for her patience in sending me numerous sets of *ab initio* results.

Dr. Tim Gosnell suggested the dynamics study of the CF_2Br radical. He was an active participant in the research and I benefitted immensely from a number of very illuminating telephone conversations with him.

I am appreciative for having been a member of a research group from which I obtained scientific inspiration and comradeship. I owe Tommy Sewell a Coke for many valuable conversations regarding various aspects of my research and his. I learned immeasurably from our discussions. I would also like to thank Candee Chambers for many scientific discussions and for companionship. I am grateful to Yue Qin for insightful discussions. I would like to acknowledge beneficial interactions with the two postdocs, Alison Marks and Dave Sahm. I would also like to acknowledge Huadong Gai and Eric Wallis.

This research was supported in part by the Air Force Office of Scientific Research. I would also like to express sincere thanks to the Robert Glenn Rapp Foundation and Phillips Petroleum Company for support in the form of fellowships.

Special thanks are extended to Alliant Computers, IBM, and Pinnacle Office Systems for outstanding support service. Without their help, I could not have completed the calculations reported here in a timely fashion.

My most heartfelt thanks are due my husband, Dan Bintz, for his understanding and encouragement during the course of this work. Without his patience and love, this would not have been possible. I would also like to thank my parents, Jack and Thelma Walker, for their love, support, and encouragement during the past 32 years.

TABLE OF CONTENTS

LIST OF TABLES

LIST OF FIGURES

CHAPTER I

INTRODUCTION

Literature Review

Mode Specificity

As early as 1933, the importance of mode-specific behavior in polyatomic molecules was beginning to emerge. During that year, Hinshelwood and Fletcher[1] put forth the following proposition: "In a molecule of moderate, but not too great, complexity, it seems possible that there may be several different modes of activation, corresponding to particular divisions of part of the energy among a limited number of vibrational (or rotational) states. To a first approximation, each of these modes may be associated with a separate probability of transformation, because, in the absence of collisions, internal redistribution may be difficult." The extent and rate of intramolecular vibrational energy redistribution (IVR) at chemically significant energies are still of active interest. Specifically, as to whether the energy, following an excitation process, is randomly distributed throughout the molecule on a timescale less than that required for chemical reaction. It has generally been observed that the energy randomization occurs on the order of picoseconds.[2] However, although the nature of the intramolecular dynamics at energies near or above that required for chemical reaction has generally been considered to be chaotic (corresponding to complete energy randomization), there is substantive evidence for regular (quasiperiodic) motion embedded in "chaotic" regions of phase space.[3,4,5,6,7,8]

Regular behavior at chemically significant energies is of fundamental

importance to IVR, specifically as it relates to the possibility for mode-specific chemistry. That is, if regular states exist near or above the dissociation barrier, then there is the possibility of exploiting the situation such that products are formed selectively. Exploitation of regular states requires the highly selective preparation of a state from which the process of interest can occur during the lifetime of that state. Regular states have been discussed by Hose and Taylor.[4] They proposed that a state be classified as regular if any of the coefficients of expansion of that state in the zero-order states used to define the coupled Hamiltonian are greater than 50 percent. Correspondence has been found between classical regular dynamics and regular quantum states on the basis of that criterion.[3] However, there are also cases for which quantum regularity has been found at energies for which the classical dynamics are chaotic.[9,10] In addition, studies of a number of model systems demonstrate that classical quasiperiodic motion occurs in regions of phase space classified as chaotic on the basis of the long-time behavior.[3,4,5]

The existence of regular states at energies that are high, but less than that required for chemical reaction, has been discussed and analyzed by Hose and Taylor.[5] They divided the vibrational structure of polyatomic molecules into three subspaces. They define Region I as the low-energy structure corresponding to sparse level density and quasiperiodic motion. Region II is the quasicontinuum which is a few quanta above the vibrational ground state. The quasicontinuum corresponds to dense level spacing and extends to the first dissociation threshold. The continuum is Region III and is the region of unbounded states including resonance states. They note that the quasicontinuum has been generally thought to consist of mode-mixed delocalized states.

Hose and Taylor[5] use the phrases "mode-localized states" and "mode localization" to characterize decoupled states embedded in the quasicontinuum. Mode

localization is descriptive of a molecular mode which is decoupled from the other molecular modes. The ideal limiting case for mode-localized behavior is the zeroth order normal-mode description whereby the molecule is represented as an assembly of uncoupled harmonic oscillators. Although the normal-mode description is invalid at high energy because the anharmonic terms in the potential cannot be neglected, there is substantial evidence for mode localization at energies near or above that required for chemical reaction (see Ref. 5 and references therein). Hose and Taylor have attributed mode localization at high energy to extreme motion, that is, large amplitude motion of the localized mode. They found that extreme motion "generates adiabatic dynamic potentials that localize the motion and decouple the normal or local modes."

Hose and Taylor[5] reviewed experimental evidence for mode localization in the quasicontinuum. They cited two types of experiments: those which excite molecules from the ground state into the quasicontinuum and those which measure the spectrum of molecules which have been excited into the quasicontinuum. They argued that the main feature of the overtone excitation experiments is that overtone progressions as high as ten quanta are observed for both normal- and local-bond-type modes. If the quasicontinuum "consisted solely of evenly mode-mixed states, such non-uniform distributions (of electric transition moments between vibrational states) leading to overtone progressions in a particular active mode, could not have been seen."[5] They discussed experiments which prepare states in the quasicontinuum at energies where dissociation may occur *via* single-photon absorption. They pointed out that regular energy levels must be present in the quasicontinuum to account for the experimental observations.

Among the experimental evidence cited by Hose and Taylor[5] is that due to the work of Coggiola, Cosby, and Peterson,[11] who used electron-impact ionization to prepare highly excited CF_3I^+ and CF_3Br^+ which they subsequently dissociated with a

low-power cw CO_2 laser. The absorption profile of the CF_3^+ fragments is narrow and centered near a fundamental line of the ion. Hose and Taylor noted that those experiments demonstrate that photodissociation occurs due to a transition from a bound vibrational state slightly below the dissociation energy " to a specific point in the continuum that is one fundamental quantum higher in energy than the bound state."[5] Hose and Taylor observed that the absorption profile would not have been narrow had the transition occurred between two delocalized states.

Experimental evidence of mode-localization at high energy continues to be reported. Choi and Moore[12] used stimulated emission pumping spectroscopy to examine the highly vibrationally excited states of HFCO above its dissociation threshold. They found that states with the most quanta in the out-of-plane C-H bending mode (ν_6) are the most decoupled from other states. They attributed the unusually stable vibrational states in HFCO to extreme motion states. They compared their results to the theoretical predictions of Hose and Taylor[5] and concluded that "mode specificity in the state mixing of highly vibrationally excited HFCO comes from mode localization of states with ultra-high overtone excitation of ν_6."[12]

Studies of IVR in a series of substituted acetylene compounds have been carried out by Lehmann, Pate, and Scoles.[13,14] They used optothermal detection of the acetylenic C-H stretch or its first overtone absorption spectrum in a cold, collimated molecular beam. They found that, for this series of molecules, IVR is statistical (that is, the energy becomes randomly distributed throughout the molecular modes), but that the IVR lifetimes are 200 ps or greater. The relaxation rates were found to be very similar for the different molecules that were examined with no apparent dependence on the bath states. Those results are also discussed in terms of Hose and Taylor's[5] extreme-motion states. It is proposed that a model which could account for the observed consistency in the rates is that the $\equiv$C-H stretch is a

localized mode in this series of molecules. In order to relax, tunneling must occur through a dynamical barrier. If the barrier is the same for all of the molecules in the series, the relaxation rates will be of similar order.

Hose and Taylor[5] also discussed the theoretical basis for mode localization. As a foundation for their subsequent analysis, they reviewed studies of the classical dynamics of two coupled oscillator systems. It has been well established that classical trajectories of such systems are quasiperiodic at low energy and that irregular trajectories appear at higher energy, becoming increasingly more dominant as the energy is increased. However, quasiperiodic trajectories can still be found at very high energy. Hose and Taylor argue that if quasiperiodic trajectories exist at high energy then the "intuitively analogous" mode-localized states should also exist in the same energy range. They observed that studies of a two degrees-of-freedom system demonstrate the existence of mode-decoupled states embedded in a mode-coupled quasicontinuum. Furthermore, they proposed that if the mechanism underlying the mode-decoupled states in the two degrees-of-freedom system could be revealed, that extension could be made to systems of higher dimensionality. They concluded that the mechanism responsible for localization is extreme-motion. In addition, they calculated "adiabatic" potentials (functions of a fixed "slow" variable) that have adiabatic wells which are responsible for the observed localization. Hose and Taylor concluded that the mode-localized states in the quasicontinuum are responsible for structure at high energies and that these states carry the big oscillator strengths when the transition begins in a local state.

Quasiperiodic dynamics have also been observed *above* the dissociation threshold.[7,15,16] Hase and coworkers[3,6,7,8] extensively studied the dissociation of the alkyl radical. Hase and Wolf[8] investigated the dynamics of this unimolecular reaction to determine the effects of potential energy surface on the unimolecular lifetime

distribution, the product energy partitioning, and the presence of long-lived vibrational states. Hase and Wolf used eleven model potential-energy surfaces in their study of the alkyl radical reaction dynamics. Two properties were varied for those surfaces: the coupling between the HCC bend and the HC stretch and the coupling between the CH and CC bonds. Linear and non-linear HCC equilibrium geometries were also considered. They investigated the dynamics on each of these surfaces for evidence of intrinsic non-RRKM[17] behavior. (A system is called intrinsically non-RRKM if it has a nonrandom lifetime distribution even when the initial conditions are random.) They determined that the extent of HCC bend and HC stretch coupling do not affect the lifetime distributions. Earlier barriers for H-C-C → H + C=C dissociation and a linear HCC equilibrium geometry are the surface properties which are correlated with the observation of intrinsically non-RRKM behavior.

Hase and Wolf[8] also determined that a relationship exists between the number of nonreactive quasiperiodic trajectories and the nature of the unimolecular lifetime distribution. Specifically, they found that the potential-energy surface with the most intrinsically non-RRKM lifetime distribution had the largest fraction of quasiperiodic trajectories. In addition, there was only a small percentage of quasiperiodic trajectories for the potential-energy surfaces with intrinsically RRKM lifetime distributions. More importantly, however, is their finding of large fractions of quasiperiodic trajectories above the dissociation energy of their model for some of the anharmonic potential energy surfaces in their study.

Wolf and Hase[7] determined that intrinsic non-RRKM lifetime distributions were observed for potential-energy surfaces for which internal coordinate motions are only weakly coupled to the reaction coordinate. They also found a correspondence between intrinsically non-RRKM lifetime distributions and quasiperiodic dynamics.

Plots of the internal coordinate planes were presented which show that for the surface with a linear equilibrium geometry (surface VA in their study) that none of the nonreactive trajectories is chaotic. Analagous plots for the other surface considered (which has an equilibrium bending angle coordinate which varies between 109° and 90° as a function of the H-CC bond and which they labeled surface IA) are not as regular as for the linear equilibrium geometry surface. However, about 20 percent of the nonreactive trajectories for that surface could be classified as regular. In addition, there were regions of regular behavior embedded in the "stochastic" trajectories representing the remaining 80 percent of the nonreactive trajectories.

Wolf and Hase[7] approximated the internal coordinate vibrational kinetic energy using the G-matrix representation.[18] Analysis of the diagonal and off-diagonal terms revealed that the diagonal representation of the internal coordinate momenta for the bonds is similar in form to that obtained from a local-mode approximation to the momenta. They also found that for linear configurations, the off-diagonal terms representing bond-angle interactions are zero. Therefore, for linear configurations there is no vibrational kinetic coupling between the bonds and the angle. They also pointed out that the bond-bond coupling is small.

Noid and Koszykowski[16] found classically bound states above the dissociation threshold for a model Hamiltonian. The bound trajectories, attributed to compound-state resonances, exhibited quasiperiodic behavior. The path integral method was used to assign semiclassical quantum numbers. The results are in good agreement with those from an exact quantum mechanical scattering calculation.

Classical and quantal evidence of regular dynamics/states above the dissociation threshold was also found for a model of a linear triatomic molecule.[15] The classical results showed that with increasing energy the asymmetric motions are more stable than the symmetric motions. This behavior is in agreement with the

extreme-motion model proposed by Hose and Taylor[5] which predicts stable regions of phase space associated with large-amplitude motion in asymmetric modes. Similar behavior was observed in the quantum results.

Shirts and Reinhardt[19] reported classical trajectory studies of the Hénon-Heiles[20] model system and the Barbanis Hamiltonian.[21] They determined that, for these two model systems, there are approximate constants of the motion at energies for which the classical dynamics, based on long-time behavior, are chaotic. The approximate constants of the motion fluctuate with time. For the Hénon-Heiles system, an approximate constant of the motion was found which is relatively stable in value for about 75 vibrational periods. The motion during this interval was attributed to a circulating motion. A "transition period" of about 75 vibrational periods ensued during which the value of the "constant" shifted to a lower value. The lower value was then stable for about 75 vibrational periods. The motion during this interval was attributed to pendular type motion. They attributed the short-time regular behavior to vague *tori*. Vague *tori* are defined as remnants of *tori*. They proposed that the shift in the value of the approximate constant of the motion is due to transitions between two vague *tori*.

A number of methods are available for classification of dynamics as regular or chaotic. Semi-classical quantization has been used to classify the regular *vs.* chaotic nature of model systems over a wide range of energies.[4] Hose and Taylor[5] have defined the general behavior of molecular systems in terms of a critical energy below which the system is generally quasiperiodic and above which the system is generally chaotic (again with some regular energy levels present). The nature of the dynamics can be characterized for two degrees-of-freedom systems by examining the Poincare´ surfaces of section.[22] A two degrees-of-freedom system which has a constant of the motion in addition to the total system energy will have trajectories which form a

closed curve as they intersect the surface of section. At low energy, the surface of section plots are well-defined, indicating quasiperiodic dynamics. The lack of structure of surfaces of sections at higher energies is indicative of chaotic dynamics. Surfaces of section can be used to study systems of higher dimensionality. However, their interpretation is somewhat less well defined than for the two degrees-of-freedom case.[22] Instead of a smooth curve as is the case of regular trajectories, the intersection of the trajectories with the surface of section fill an annulus of finite area. The thickness of the annulus is related to the degree of separability in the surface of section coordinates. Surface of section plots have been calculated for three degrees-of-freedom systems.[23] Trajectories can also be classified as regular or chaotic on the basis of the Liapunov exponent, a measure of the exponential rate of divergence of nearby trajectories.[22]

Most of these techniques are not tractable for polyatomic molecules of even modest size. One must therefore rely on other methods of analysis. Noid, Koszykowski, and Marcus[24] calculated the power spectra of classical trajectories of anharmonic molecules and classified the trajectories as regular or chaotic on the basis of the calculated spectra. They illustrated that spectra consist of sharp lines when the dynamics are quasiperiodic and of broadened lines when the dynamics are ergodic. They noted that the broadened spectra corresponding to the ergodic regime are composed of intensity bands centered on certain frequencies.

Sewell, Thompson, and Levine[25] used power spectral analysis methods to investigate the dynamics of three molecular systems using realistic potential energy surfaces. They interpreted the spectra as evidence for non-chaotic dynamics at high energies.

Dumont and Brumer[26] performed a detailed study of the applicability of power spectra for classifying dynamics. They argued that power spectra of individual

trajectories could not in principle be used to differentiate between regular and chaotic dynamics, but that statistics of ensembles of power spectra do provide a measure of the nature of the dynamics. A more comprehensive review of power spectral methods and applications is given in Chapter II.

Although quasiperiodic dynamics set the stage for mode specificity with respect to the rate for unimolecular reaction, there are other factors which are operative that play a critical role in determining whether the unimolecular reaction rates will be mode specific. One such factor that can affect the mode-specific behavior of a molecule is the extent of projection of the excited mode onto the reaction coordinate. Waite and Miller[27] examined the reaction dynamics for one and three-dimensional Hénon-Heiles potentials. The 1-D potential exhibits classical regular dynamics at energies below the dissociation energy and gives mode-specific quantum mechanical unimolecular decay rates. However, although the dynamics of the 3-D potential are regular, the quantum mechanical decay rates are statistical. The results were attributed to projection of the excited mode onto the reaction coordinate. Motion in the *y* direction of the model avoids the saddle point for the 1-D potential, therefore excitation in the *y* direction is not conducive to promoting reaction. However, there is no mode for the 3-D potential which does not project onto one of the three reaction coordinates. Excitation in any direction is effective in causing reaction.

Projection of the excited mode onto the reaction coordinate has also been found to be a relevant factor in van der Waals molecules.[28,29] Ewing[29] developed a model for vibrational predissociation of van der Waals molecules which contain a vibrationally excited, chemically bonded molecule. The model ignores angular momentum changes during the reaction and thus only applies to vibrational to translational energy transfer. A steric factor is included in the model as a parameter

and describes the projection of the vibrationally excited chemical bond along the van der Waals bond. The model is successful in reproducing the observed mode specificity of $(HF)_2$. However, the projection effect was not sufficient to account for mode specificity in $(NO)_2$.[28]

Neither regular dynamics nor the degree of projection of an excited mode onto the reaction coordinate can, in solitary measure, provide a predictive indicator of mode-specificity of unimolecular rates of reaction. However, both factors have been found to play a role in systems for which the rates are mode specific. No one factor can be singled out as being the crucial determiner. It is important to realize that many factors are intertwined and must be considered simultaneously in studies of mode specificity. The role of regular dynamics and projection is examined in the studies described here.

Potential-Energy Surfaces from *Ab Initio* Results

An analytic expression for the potential-energy surface is a prerequisite to classical dynamics calculations. One approach to defining the potential-energy surface is to obtain the equilibrium structure, vibrational frequencies, and thermodynamic properties from the available experimental data. A reasonable functional form is then assumed for the potential. The form chosen can be based on a theoretical derivation on the basis of the atomic wavefunctions and/or chemical intuition. Parameters of the analytic expression for the potential-energy surface are then "fit" to reproduce the experimental data.

Often the experimental data are not sufficient to completely define the potential-energy surface.[30] It is therefore useful to augment the experimental data with *ab initio* results. The results from *ab initio* calculations have been used to obtain global potential-energy surfaces for a few tri- and tetra-atomic molecular systems.

However, *ab initio* methods are computationally expensive. Non-linear polyatomic molecules possess 3N-6 vibrational degrees of freedom. Therefore if *n* points per degree of freedom *d* are required to define a global surface, $n^d(n^3-1)$ additional points are required for each additional atom. Full scale *ab initio* methods are therefore prohibitive for anything larger than three or four atom systems.

An additional consideration is the analytic form used to represent the potential-energy surface. A number of forms have been used to develop surfaces for triatomics. Extension has been made of the triatomic potential functions to larger molecular systems. However, such usage requires simplifying approximations to reduce the dimensionality of the system. Dynamical effects which might be due to the neglected degrees of freedom are lost. It is therefore desirous to develop methods which make efficient use of *ab initio* results for polyatomic molecules at a limited number of surface points while maintaining the full dimensionality of the system.

Potential-energy surfaces for triatomic scattering systems, such as the LEPS (London-Eyring-Polanyi-Sato)[31] potential, are based on semiempirical valence bond theory. The LEPS potential has been used to treat the reaction dynamics of systems larger than three atoms by using a three-body model. For example, the methyl group in the reaction $Cl^- + CH_3Cl \rightarrow ClCH_3 + Cl^-$ has been treated as a single "atom" thereby reducing the six-body problem to a three-body problem.[32] The LEPS function has limitations which have been discussed elsewhere.[33] Some of the limitations have been dealt with by the inclusion of additional empirical parameters in the function.[34,35,36,37]

Another method which has been applied successfully to triatomics and tetra-atomics is the many-body expansion method. Murrell and coworkers[38] have used this method to define a number of potential-energy surfaces.

Cubic spline interpolation has been used to define global potential-energy

surfaces.[39,40,41,42,43,44,45,46,47,48,49,50,51] Wall and Porter[39] used the method in conjunction with a rotated Morse function to investigate the sensitivity to the potential-energy surface of the exchange-reaction probabilities for the reaction $H + H_2 \rightarrow H_2 + H$.

McLaughlin and Thompson[40] constructed a potential-energy surface for the reaction $HeH^+ + H_2 \rightarrow He + H_3^+ (C_{2v})$ using two-dimensional cubic splines to fit *ab initio* results. Comparisons of individual trajectories calculated using one-, two-, and three-dimensional cubic spline-based potentials and analytic (LEPS) potentials were made by Sathyamurthy and Raff.[41] They found that the 1-D splines were very accurate, 2-D splines were considerably less accurate than the 1-D, and that 3-D splines were less accurate than 2-D splines but with less relative decrease than between the 1-D and 2-D cases. They also noted that "point-by-point" matches were not achieved between the spline trajectories and the analytic-function trajectories but that ensemble properties were reasonably matched.

Molecular systems larger than three or four atoms generally require application of functions with less sound theoretical foundation. For example, an equilibrium potential function for a polyatomic molecule can be constructed by assuming that the bonds are Morse oscillators, the bond and wag angles are harmonic oscillators, and that the dihedral angle potentials can be represented by a truncated cosine series. Quadratic interaction terms can also be incorporated into the function. The parameters (force constants and interaction constants) from the assumed functional form are adjusted to fit experimental data. Trial and error or variational methods can be applied to improve the quality of the fit (insofar as reproducing the experimental vibrational frequencies). However, the experimental data do not usually provide enough parameters to completely define the potential-energy surface.[30,38] Furthermore, it is desirable to incorporate features into the potential that are not known from experiment. Specifically, the *ab initio* Hessian can be used to define the

normal mode vectors.[30]

Dasgupta and Goddard[30] have described a method for combining experimental data with *ab initio* results in a manner which provides for fitting the *ab initio* Hessian simultaneously with the experimental frequencies. The method consists of diagonalizing the Cartesian Hessian H obtained from theory:

$$HL = L\lambda \ , \tag{1}$$

where L is the matrix of eigenvectors, and λ is the diagonal eigenvalue matrix. Equation (1) can be solved for H

$$H = L\lambda L^{t} \ . \tag{2}$$

The experimental frequencies (λ_{exp}) are then substituted for the calculated frequencies (λ) to obtain an "experimentally biased Hessian"[30] (H_{exp}):

$$H_{exp} = L\lambda_{exp}L^{t} \ . \tag{3}$$

Prior to application of Eq. (3), Dasgupta and Goddard scaled the *ab initio* Hessian to fit the experimental frequencies. Furthermore, the experimental geometry was used in the *ab initio* calculations. After determination of H_{exp}, an analytic expression was assumed for the potential-energy function in an internal coordinate representation. Nonbonded terms and cross terms were included in the function. A set of initial potential parameters was chosen for the force and interaction constants. Variational methods were then employed to fit the internal coordinate Hessian H_{FF} to H_{exp}. (H_{FF} is the Hessian calculated from the analytic form of the potential.) Alternatively, H_{exp} may be transformed directly to an internal coordinate Hessian. (For a description of the method, see Chapter III).

The foregoing method is straightforward to apply at stationary points on the potential-energy surface where experimental data and *ab initio* results are generally

available. It therefore provides a very tractable method for defining an acceptable analytic description of the *equilibrium* potential for the reactant and product molecules. The method may similarly be applied at the transition state. However, a global analytic form for the potential-energy surface, designated by **f**, requires that the stationary points be connected. This can be accomplished by expressing **f** as a function of the reaction coordinate(s). Thus, all parameters associated with the potential (i.e., force constants, interaction constants, "equilibrium" values for the internal coordinates, bond dissociation energies, etc.) are written as explicit functions (commonly called switching functions) of the reaction coordinate. The switching functions must be continuous, single valued, and have continuous first derivatives. A number of functional forms are commonly used as switching functions.[52] The switching functions used in the present studies of the reaction dynamics of the CF_2Br radical and the N_2O_3 molecule are described in Chapter III.

Complex reactions may require switching functions to connect regions of the potential-energy surface corresponding to several reaction coordinates.[53] The potential for each of the relevant stationary points is fit to whatever data is available from experiment and theory. Thermodynamic data is incorporated to reproduce the reaction endo- or exothermicity. Finally, switching functions are incorporated to connect the asymptotic regions. The switching function parameters are adjusted (insofar as is possible) to yield the desired behavior away from the asymptotes. There are restrictions to fitting the switching function parameters. The switching functions must be well behaved in the sense that they do not create spurious local minima in the potential energy surface. Spurious local minima can occur when interaction terms involving a dissociating bond are not "switched off" fast enough. They can also arise when diagonal terms (which do not survive in the product potential) are "turned off" too soon. Therefore, care must be taken during the fitting

procedure. Ideally, a minimization routine should be used to ensure that undesired minima are not present on the potential-energy surface. The switching function parameters will also influence observables such the rate of intramolecular vibrational energy redistribution and the rate of reaction. The quality of the fit can be tested by performing preliminary calculations of reaction rates and making comparisons to experimental rates. Switching functions have been used to develop potentials for a wide variety of molecular systems.[54]

Connecting the potential-energy stationary points *via* switching functions is an *ad hoc* method of constructing a global potential-energy surface. There is often no information available regarding the interatomic forces at points displaced from the stationary points. Therefore, the switching function parameters must be fit intuitively. When *ab initio* information is available along the reaction path, it is possible to obtain a more meaningful fit of the potential-energy surface. The switching function parameters can be fit to the *ab initio* results. One such approach relies on *ab intio* results for geometries which lie on the intrinsic reaction coordinate (IRC).[55] The IRC is the steepest descent path in mass-weighted Cartesian coordinates that passes through the potential-energy surface saddle point from reactants to products.[56] The reaction coordinate s is defined as the signed distance along the IRC with $s=0$ at the saddle point. The *ab initio* information at each point of an IRC calculation includes the geometry, normal mode frequencies (with motion along the reaction coordinate, translations, and rotations projected out as described by Miller, Handy, and Adams[57]), the Hessian, the potential energy, and the potential-energy gradient.

Tucker and Truhlar[58] used information from *ab initio* calculations along the minimum energy path in their fit of a potential-energy surface for the $Cl^-(g)$ + $CH_3Cl(g)$ reaction. The surface was fit to the energy levels at three stationary points

and to scaled *ab initio* frequencies at these points and one additional point. Standard switching function methods were used to connect the stationary points. The additional (nonstationary) point that was included in the fit was not weighted as heavily as the stationary points. Requiring that the potential behave in accord with *ab initio* data at points between the stationary points removes some of the ambiguity associated with potentials parameterized with respect to the reaction coordinate(s). However, the bulk of the potential-energy surface is represented by a function which is not based on theoretical or experimental data.

One important consideration in constructing reaction-path potentials is symmetry invariance. The reaction-path methodology provides a description of a potential along a minimum energy path associated with a specific reaction coordinate. A global representation of the surface requires that all such equivalent paths be accessible and indistinguishable. Ischtwan and Collins[59] presented a method for using information along a reaction path to construct a potential-energy surface which is invariant to operations of the complete nuclear permutation inversion group.[60] The method is based on that reported by Schmelzer and Murrell[61] for defining an analytic S_4-symmetry-invariant potential function for tetra-atomic homonuclear molecules. To test the method, Ischtwan and Collins constructed a potential for NH_5^+ which allows hydrogen abstraction along two symmetry-equivalent reaction paths. A number of severe limitations of the potential function were noted. However, further development of and extension to the method are highly relevant considerations. If *ab initio* results along reaction paths (i.e., from IRC calculations) are used to construct global potential-energy surfaces for chemical dynamics calculations, it is imperative that the resultant potential function be symmetry invariant.

Restricted potental-energy functions which describe the potential-energy surface along or in the vicinity of the IRC are useful for applications such as

transition-state theory and semiclassical tunneling methods.[62] However, dynamics calculations can result in geometries which are far displaced from the minimum-energy path. It is necessary, therefore, to obtain a global representation of the potential-energy surface that is as accurate as possible for *all* molecular geometries. The methods cited earlier for defining potential-energy surfaces for tri- and tetra-atomics have been applied to chemical reactions for which electronic structure calculations at a significant number of points have been fit to obtain global potentials (see, for example, Ref. 38 and references therein). As electronic structure calculations become more accessible for polyatomics larger than three or four atoms, theoretical methods require extension so that *ab initio* results may be used effectively to construct accurate potential-energy surfaces for these systems.

Scope of Study

CF_2Br

Both experimental and theoretical studies have demonstrated that energy flow subsequent to mode-specific excitation occurs along specific pathways.[63] Nonstatistical energy distributions can persist for finite times following excitations, but any effects on reaction rates of covalently bonded molecules are generally not observable. That mode-selective effects in reactions are rarely observed in experiments may be due to several reasons, which have been discussed elsewhere.[64] This situation exists in spite of the fact that molecules display quasiperiodic behavior at and above their dissociation limits.[65]

Quasiperiodicity, as can be evidenced by a sharp peak in the power spectrum of an ensemble of classical trajectories, implies the presence of a well-defined molecular mode which is exhibiting regular dynamics. This type of behavior has been referred to as "mode-localized."[5]

It would seem that if localization of a molecular mode exists for times comparable to the reactive lifetime that mode-selective reaction rates should be possible. The results reported in Chapter IV for the CF_2Br radical demonstrate that regular dynamics persist in this molecule for times longer than that required for reaction. *Ab initio* methods were used to calculate the potential and classical trajectory methods were used to study the dynamics of the CF_2Br radical. Of particular interest is the relation of the dynamical behavior with respect to regular (quasiperiodic) *vs* chaotic motion to the reaction rates for mode-specific excitation.

The CF_2Br radical has been observed as a primary product of the 248 nm photolysis of CF_2Br_2.[66,67] Krajnovich, Zhang, Butler, and Lee[66] examined the photochemistry of CF_2Br_2 in crossed laser-molecular beams. They concluded that the only primary reaction channel is the elimination of a Br atom:

$$CF_2Br_2 + h\nu\,(248nm) \rightarrow CF_2Br + Br \ . \qquad (4)$$

They also detected CF_2 radicals which they attributed to efficient secondary photodissociation of the CF_2Br radical formed in reaction (4):

$$CF_2Br + h\nu\,(248nm) \rightarrow CF_2 + Br \ . \qquad (5)$$

Gosnell, Taylor, and Lyman[67] used ultrafast time-resolved absorption spectroscopy to study the photodissociation of CF_2Br_2. They also detected the CF_2Br radical as a primary product. However, they concluded that the CF_2 radical is formed in the ground or first-excited vibrational state of its ν_2 bending mode during the "unimolecular reaction of a vibrationally hot CF_2Br intermediate species." In addition, they concluded that the evolution of the CF_2Br absorption spectrum over 6 ps is indicative of slow intramolecular vibrational redistribution. These results are sufficiently intriguing to warrant a study of the dynamics of this system.

One of our main interests in this study is the nature of the CF_2Br dyanamics.

That is, is there any evidence for mode localization and if so, does it occur on a timescale of chemical interest. Power spectral analysis has found wide-spread use as a diagnostic (albeit subjective) means of elucidating the nature of the intramolecular dynamics. A discussion of power spectral methods is presented in Chapter II.

$\underline{N_2O_3}$

Mode selectivity is not generally observed at the energies required to break a chemical bond and the dissociation rates can usually be described by RRKM theory.[68] In contrast, the vibrational predissociation of van der Waals systems exhibits nonstatistical behavior. This is not surprising since van der Waals molecules are distinctly different from chemically bound systems. Nevertheless, they serve as informative examples of mode selective systems and help to illustrate some fundamental aspects of nonstatistical behavior. In an effort to understand mode selectivity in general, it is useful to study systems that are intermediate between van der Waals and chemically bound molecules. In this regard a series of studies have been reported of intramolecular conversions that have energy barriers of the order of 10-15 kcal/mol.[69,70,71,72] In this study, we investigate N_2O_3, a "van der Waals/chemically bound" molecule, .

Smith and Yarwood[73] have examined the kinetics of association and dissociation of N_2O_3 to probe the vibrational predissociation behavior in a system in which the bonding is intermediate in strength between chemical bonds and van der Waals bonds. In particular, they were interested in determining "how strong a dissociating bond must be for a system to conform to RRKM theory and what other factors influence the change in dynamics between the two limits."[73] They used time-resolved infrared absorption to obtain kinetic measurements for the reaction
They obtained a rate constant for the dissociation of the $(N_2O_3)^{\dagger}$ complex consistent

$$NO + NO_2 \rightleftharpoons (N_2O_3)^{\dagger} \ . \qquad (6)$$

with statistical rate theories. In contrast, rate constants obtained by Chewter, Smith, and Yarwood[74] employing high-resolution Fourier-transform infrared spectroscopy show that energy flow for the ν_1 mode (the nitroso stretch) of N_2O_3 is relatively slow. Their results indicate nonstatistical behavior. However, as pointed out by Smith and Yarwood,[73] the difference in the results obtained from the two studies may be due to enhanced energy flow from the ν_1 mode when the lower frequency modes are excited as in the case of the $(N_2O_3)^{\dagger}$ addition complex.

In the present study, classical trajectory methods were used to calculate vibrational predissociation rate constants for N_2O_3 for a variety of initial excitations of the nitroso- and nitro-group normal modes. The ν_1=3 excitation has been examined in order to compare to the experimental study of Chewter, Smith, and Yarwood.[74]

<u>SiH_5^-</u>

It is the goal of this work to use the results of *ab intio* IRC calculations to construct global potential-energy surfaces. Specifically, we are interested in the potential-energy surfaces for molecular isomerizations. Isomerizations generally involve the concerted motion of a number of atoms in the molecule in contrast to simple chemical reactions wherein the reaction progress is defined by displacement along a single chemical bond. Therefore, modeling isomerizations can be a more challenging procedure than modeling chemical reactions. One such isomerization process is Berry pseudorotation[75] in SiH_5^-. The Berry pseudorotation process in SiH_5^- has been studied using *ab initio* results and variational transition state theory with tunneling corrections.[76,77] The *ab initio* calculations reveal that the pseudorotation process is described by motion along one of the normal-mode directions. A number

of points were calculated along the IRC. In order to make application of the IRC results to the construction of a global potential-energy surface, the reaction coordinate *s* must be expressable in an analytic form which is suitable for mapping arbitrary geometries onto the IRC. Natanson, Garrett, Truong, Joseph, and Truhlar[78] have discussed some of the difficulties inherent in acheiving a *unique* projection of the system configuration space onto the IRC. For trajectory calculations, this mapping must be achieved analytically at each integration step.

Prudent application of the IRC results requires equitable consideration of the stationary and nonstationary points during the fitting procedure. This is difficult at best using standard switching function methods. Alternative methods are needed to facilitate the fitting procedure. In addition, care must be taken to provide for treatment of molecular geometries which do not lie on the reaction path.

A normal coordinate system can be defined for motion along the IRC which consists of *s*, the reaction coordinate mode, and the 3N-7 modes orthogonal to *s* designated by Q_k. In terms of the normal coordinates, the potential energy function $V(s,Q_1,Q_2,,\ldots,Q_{3N-7})$ can be approximated as,[57]

$$V(s,Q_1,Q_2,\ldots,Q_{3N-7}) = V_0(s) + \sum_{k=1}^{3N-7} \frac{1}{2}\omega_k(s)^2 Q_k^2 \ , \qquad (7)$$

which "has the form of a 'harmonic valley' about the reaction path."[57] $V_0(s)$ is the potential energy on the reaction path and the $\omega_k(s)$ are the (3N-7) frequencies for the modes orthogonal to the reaction path. In order to extend the reaction-path description of the potential-energy surface to a global representation, it is necessary to consider displacements in the directions orthogonal to s. Therefore, some knowledge of the potential-energy surface for arbitrary system configurations is required.

Since a complete definition of the potential-energy surface for a polyatomic molecule from *ab initio* calculations is prohibitive, it is necessary to carefully define

which areas of the surface are critical to a reasonable characterization of the surface and then to obtain the additional *ab initio* results at only those points. Symmetry of the system can be used to advantage for this process. For example, the system under consideration SiH_5^- has three equivalent reaction channels. *Ab initio* points intermediate between two of these channels should be used to define the surface at points intermediate between each of the three channels.

CHAPTER II

METHODS

Power Spectra

The autospectral density function provides a useful tool for ascertaining the nature of the intramolecular dynamics of polyatomic molecules.[24] Quasiperiodic components of the data will be evidenced in the autospectral density function by the appearance of sharp peaks at the mechanical frequencies of the underlying molecular motions.[24,79,80] In contrast, when the data are chaotic, the autospectral density function will relax and the spectrum will consist of intensity over a wide band of frequencies. Quantatatively, the autospectral density function can be shown, through application of Parseval's Theorem, to provide a measure of the "power" of the original data.[81,82]

The two-sided autospectral density function (also called the power spectral density function) of the function $x(t)$ is defined for both negative and positive frequency values by[83]

$$S_{xx}(f)=\int_{-\infty}^{\infty} R_{xx}(\tau)e^{-i2\pi f\tau}d\tau \qquad -\infty<f<\infty \ , \tag{8}$$

where $R_{xx}(\tau)$ is the ensemble averaged autocorrelation function

$$R_{xx}(\tau)=\langle x(t)x(t+\tau)\rangle \ , \tag{9}$$

τ is a time lag measured relative to time t ($t=0$ is often employed), and f is the mechanical frequency which is related to the angular frequency ω through

$$f = \frac{\omega}{2\pi} \ . \tag{10}$$

Under appropriate conditions, the ergodic hypothesis can be invoked and the ensemble average of Eq. (9) replaced by the appropriate time average over a single record.[80] However, the ergodic hypothesis is only strictly applicable for the case where *x(t)* is a stationary random process. A stationary process can be classified as either weakly or strongly stationary. The ergodic hypothesis is satisfied by the condition of weak stationarity; that is, the mean value of the process is a time invariant constant and the autocorrelation function depends only on τ [the autocorrelation function does not depend upon the value of t in Eq. (9)]. The condition of strong stationarity is satisfied when all possible moments and joint moments are invariant with time.

In practice, the data record often cannot be represented by a *continuous* function *x(t)* which extends over an *infinite* time history. It is therefore necessary to employ techniques by which *discrete* data records may be analyzed over *finite* times. The extension to finite times is accomplished by defining[84]

$$S_{xx}(f,T,k) = \frac{1}{T} X_k^*(f,T) X_k(f,T) \ , \tag{11}$$

where[85]

$$X_k(f,T) = \int_0^T x_k(t) e^{-i2\pi ft} dt \ , \tag{12}$$

is the *finite* Fourier transform of $x_k(t)$, $X_k^*(f,T)$ is the complex conjugate of $X_k(f,T)$, and the index k represents a *single* time history record. A second definition of the autospectral density function $S_{xx}(f)$ is given by[86]

$$S_{xx}(f) = \lim_{T\to\infty} \langle S_{xx}(f,T,k) \rangle \ , \tag{13}$$

where it can be shown that[87]

$$\lim_{T\to\infty} \langle S_{xx}(f,T,k) \rangle = \int_{-\infty}^{\infty} R_{xx}(\tau) e^{-i2\pi f\tau} d\tau \ , \tag{14}$$

in agreement with the definition of Eq. (8). The ensemble average is over the index k.

Discrete data records are treated by replacing the integral in Eq. (12) with the appropriate sum:

$$X_k(f_j,T) = \Delta t \sum_{n=0}^{N-1} x_{kn} \exp\left[\frac{-i2\pi jn}{N}\right] , \tag{15}$$

where Δt is the sampling interval, f_j is the jth frequency component of a set of N/2+1 discrete frequencies, and N is the total number of points in the sample. The total time T is related to N and Δt through

$$T = N\Delta t \ . \tag{16}$$

The two-sided autospectral density function can be estimated for finite, discrete data by averaging over an ensemble of Fourier transforms of the individual data records according to[88]

$$\hat{S}_{xx}(f_j) = \frac{1}{n_d N \Delta t} \sum_{k=1}^{n_d} |X_k(f_j,T)|^2 \ , \tag{17}$$

where n_d is the total number of sample records.

As previously noted, the two-sided autospectral density function is defined over the frequency range $-\infty < f < \infty$. A closely related function is the one-sided

autospectral density function[89]

$$\hat{G}_{xx}(f) = 2\hat{S}_{xx}(f) \qquad 0 \le f < \infty \ . \tag{18}$$

This spectral density function, defined only for positive values of the frequencies, is the function which is calculated in practice.

Spectral density function estimates can be obtained using a Fast Fourier Transform (FFT) algorithm.[90] (The FFT algorithm has received considerable notice due to the work of Cooley and Tukey[90] in 1965, however, the algorithm had been in use for sometime prior to that.) The FFT coefficients H_l can be normalized so that the total power (sum squared amplitude) in the frequency domain is equal to the total power of the original data in the time domain (through Parseval's Theorem):[91]

$$\sum_{n=0}^{N-1} |x_{kn}|^2 = \frac{1}{N}\sum_{l=0}^{N-1} |H_l|^2 \ , \tag{19}$$

where the x_{kn} are the discrete values of the data from record k. The intensity at an arbitrary frequency f_p represents the average power in the frequency range $(f_p - r/2) < f < (f_p + r/2)$ where $r = 1/T$ is the spectral resolution. Assuming the normalization convention of Eq. (19), the one-sided spectral density function is given in terms of the (N/2 + 1) FFT coefficients by

$$\begin{aligned} \hat{G}_{xx}(0) &= \frac{1}{N}|H_0|^2; \\ \hat{G}_{xx}(f_i) &= \frac{2}{N}|H_i|^2, \quad [i = 1,2,\ldots,(N/2-1)]; \\ \hat{G}_{xx}(f_{N/2}) &= \frac{1}{N}|H_{N/2}|^2. \end{aligned} \tag{20}$$

A discussion of alternative normalization procedures can be found in Ref. 82.

In the studies reported here, power spectral analysis is applied to the results of classical trajectory calculations for molecular systems. It is useful to transform quantities which have physical significance. The internal coordinates of a molecule (specifically, the bond lengths and bond, wag, and dihedral angles) satisfy this criterion. Therefore, in the present calculations the x_{kn} of Eq. (19) are the displacements of the internal coordinates from their time-averaged means. The x_{kn} are rendered dimensionless through division by the maximum value (again, relative to the time-average mean) achieved by a given internal coordinate during a particular trajectory. Spectra for individual internal coordinates were obtained directly through application of Eq. (20). Composite spectra were calculated by summing over the individual internal coordinate spectra. Both the individual internal coordinate and composite spectra were used in the analysis of the dynamics. The DRCFT subroutine which is a part of the IBM Engineering and Scientific Subroutine Library was employed to obtain the Fourier coefficients.

Noid, Koszykowski, and Marcus[24] reported methods for using the power spectrum of a *single* trajectory as a means of probing the regular *vs.* chaotic nature of intramolecular dynamics. The contention is that the single trajectory power spectrum provides an estimate for the autospectral density function. They reported results for the Hénon-Heiles[20] model for illustration. The power spectrum for the Hénon-Heiles system consist of two discrete peaks at the fundamental frequencies when the dynamics are quasiperiodic. A grassy, significantly broadened spectrum is observed when the dynamics are chaotic. However, the "chaotic" spectrum is still centered on certain frequencies.

Spectra of single trajectories have been used in other studies of regular and irregular dynamics with mixed results.[92,93,94] Some general conclusions have been drawn regarding the relationship of the appearance of the single trajectory power

spectrum to the underlying dynamics:[24] (1) Power spectra of systems undergoing regular dynamics consist of sharp peaks at the fundamental frequencies of the motion. (2) Power spectra corresponding to irregular dynamics tend to be grassy and broadened relative to those for regular dynamics with intensity over a wide range of frequencies. Dumont and Brumer[79] tested those conclusions by calculating power spectra for a number of model systems. Their results demonstrate that power spectra of single trajectories *cannot* in principle be used to distinguish between regular and irregular dynamics as they found spectra that appeared grassy and broadened that correspond to regular dynamics. They also showed that a trajectory which was classified as chaotic on the basis of its long time behavior (in terms of exploration of the energetically accessible phase space) exhibited short time regular dynamics due to trapping in the vacinity of a vague *torus*. A power spectrum of this single trajectory calculated over the "trapping" time could present the erroneous appearance of globally regular dynamics.

In addition to the ambiguities associated with using power spectra of single trajectories to identify regular and chaotic behavior, it is well established that there are problems associated with the power spectrum of a single time-history record.[79,80,82] In order to better understand those problems and the associated causes, it is appropriate to investigate the approximation upon which use of the single trajectory spectrum is based. In addition, a brief overview of the error analysis of power spectra will be presented to demonstrate the potential for error in trying to perform a detailed analysis of the single record power spectrum.

The single trajectory power spectrum $S_{xx}(f,T,k)$ has been assumed to approximate the autospectral density function $S_{xx}(f)$ in the infinite time limit according to

$$S_{xx}(f) = \lim_{T\to\infty} S_{xx}(f,T,k) \ . \tag{21}$$

This assumption is without sound theoretical basis.[79,80,82] As already discussed, the autospectral density function is obtained in the limit as T tends to infinity of the *ensemble averaged* function $S_{xx}(f,T)$. Furthermore, it has been demonstrated by Dumont and Brumer[79] that the single trajectory power spectrum only converges to the autospectral density function in the mean. That is, there is no "pointwise convergence, in frequency, of the single trajectory power spectrum to the autospectral density function in the $T\to\infty$ limit."[79] In addition, the estimate based on Eq. (21) does not become statistically more consistent with increasing T.[80] Increasing the time length of the data record only serves to increase the resolution of the spectrum. All of the additional data goes into the determination of additional spectral peaks. Therefore, there is no gain in accuracy of a given peak intensity from increasing the total time of the transformed data. In fact, for the limiting case where $x(t)$ is a Gaussian random process, the random error of the autospectral density function from a single data record can be shown to be equal to 1.[80] By using ensemble averaging, Eq. (17), the random error is substantially reduced. The random error ϵ_r is related to the total number of records in the ensemble n_d by[95]

$$\epsilon_r = \frac{1}{\sqrt{n_d}} \ . \tag{22}$$

There is a rapid decrease in the random error with increasing ensemble size.

The methods for analyzing error in the autospectral density function calculation, which are outlined in Bendat and Piersol,[80] are for application to stationary random processes. However, the methods can be extended to processes which are Gaussian over the time history considered. To test the validity of application of the error analysis methods to the internal coordinate time histories from

classical trajectory calculations, the internal coordinate time histories from two CF_2Br trajectories were fit to Gaussian curves. The histograms of the calculated internal coordinate values and the fitted Gaussian curves are shown in Figs. 1 and 2. The initial conditions for both trajectories corresponded to excitation of ν_6 to 35 kcal/mol. Figures 1 and 2 are for trajectories of total time length 45.0 ps and 16.6 ps, respectively. The sampling interval was 7.5 fs yielding a total of 6001 points and 2214 points, respectively. The data were placed in 100 bins of equal size over the range bounded by and inclusive of the minimum and maximum values achieved by a given internal coordinate during the course of the trajectory. The points for the Gaussian fit were calculated at the midpoints of each bin. Figures 1(a), 1(b), 2(a), and 2(b) are the C-F bond lengths. Although the bonds are treated as Morse oscillators in the trajectory calculations, the internal coordinate histories are reasonably well represented by the Gaussian fit. Figures 1(d), 1(e), and 1(f); and 2(d), 2(e), and 2(f) are the two Br-C-F bond angles and the F-C-F bond angle, respectively. As expected, the harmonic bond angles are well represented by the Gaussian fit. The most marked deviation from the Gaussian fit is for the C-Br bond length, Figs. 1(c) and 2(c). The deviation is most pronounced for the smaller sample size, Fig. 2(c). Although the internal coordinate histories are not equally representative of Gaussian processes, the fit is reasonable for the majority of the internal coordinate time histories. Therefore, it will be assumed that the error analysis methods for Gaussian processes are meaningful relative to the present trajectory calculations.

The failure of a power spectrum of a single data record to adequately represent the finite time autospectral density is illustrated by the results in Fig. 3. Figure 3(a) is a composite power spectrum (the composite spectrum was obtained by summing over the internal coordinate spectra) of a single trajectory for the CF_2Br radical at a

Figure 1. Gaussian fits of CF_2Br internal coordinate time histories. The initial conditions are for excitation of ν_6 to 35 kcal/mol. The sampling interval was 7.5 fs. The trajectory was followed for 45.0 ps. Panels (a) and (b) are for the C-F bonds, (c) is for the C-Br bond, (d) and (e) are for the Br-C-F angles, and (f) is for the F-C-F angle.

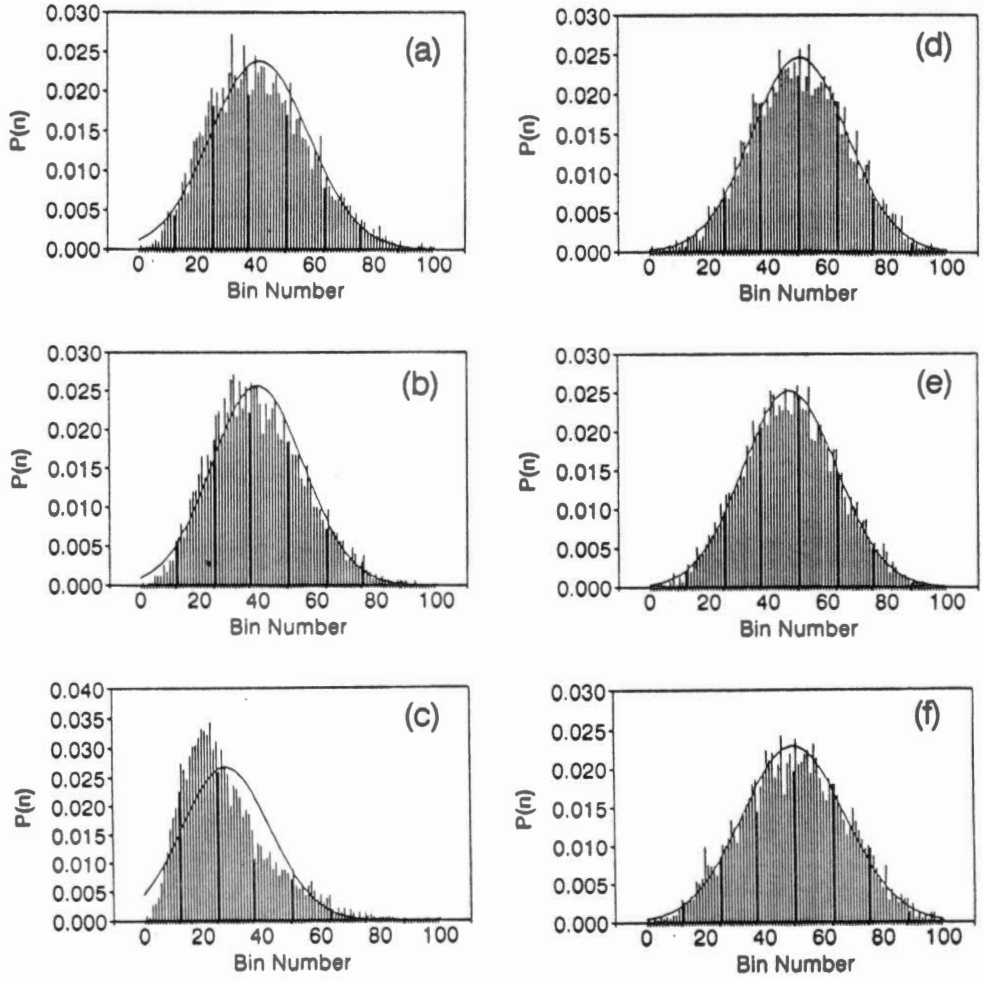
(a)
(b)
(c)
(d)
(e)
(f)
P(n)
Bin Number
0.000
0.005
0.010
0.015
0.020
0.025
0.030
0.035
0.040
0
20
40
60
80
100

Figure 2. Same as Fig. 1 except the trajectory was followed for 16.6 ps.

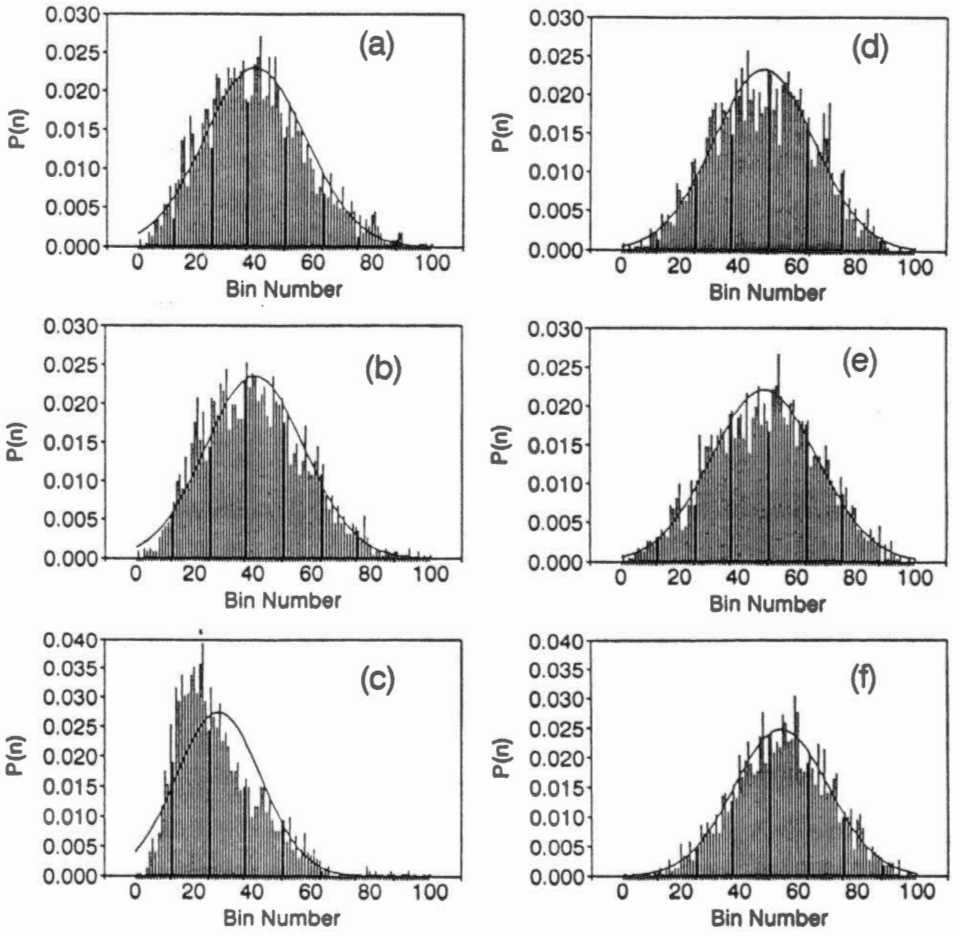
(a)
(b)
(c)
(d)
(e)
(f)
P(n)
Bin Number
0.000
0.005
0.010
0.015
0.020
0.025
0.030
0.035
0.040
0
20
40
60
80
100

Figure 3. Comparison of single and ensemble averaged CF_2Br composite power spectra. The total system energy is 41 kcal/mol. (a) single trajectory spectrum; (b) spectrum for a 20 trajectory ensemble.

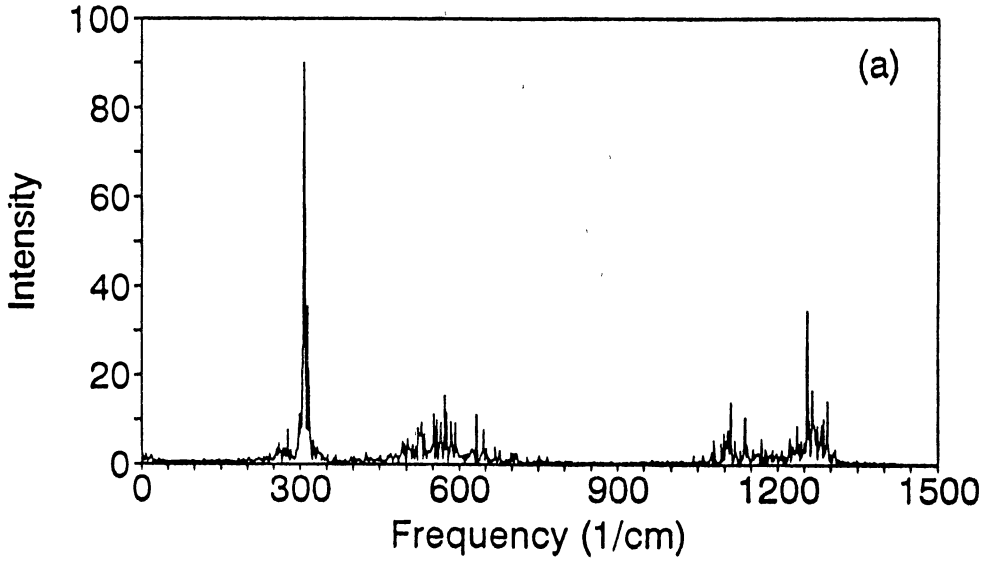
100
80
60
40
20
0
Intensity
(a)
0
300
600
900
1200
1500
Frequency (1/cm)

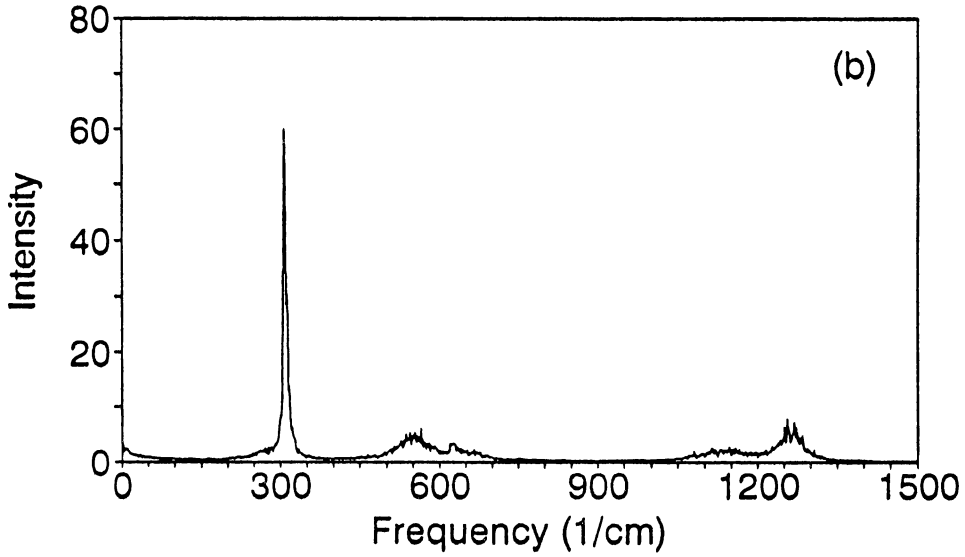
80
60
40
20
0
Intensity
(b)
0
300
600
900
1200
1500
Frequency (1/cm)

total system energy of 41 kcal/mol. Figure 3(b) is a composite power spectrum obtained by averaging the power spectra from an ensemble of 20 trajectories corresponding to the same initial conditions as for Fig. 3(a). The time length of the data samples was 20.16 ps resulting in a spectral resolution of 1.65 cm^{-1}. The grassy structure present in the single trajectory spectrum [Fig. 3(a)] which has been associated with chaotic system behavior smooths out when the spectra are averaged. This is due to the reduction in the random error as the number of records in the sample is increased [Eq. (22)]. The broad band low intensity structure is associated with relaxation (chaotic dynamics).[79] The sharp peak at approximately 307 cm^{-1} is associated with regular (quasiperiodic) dynamics.[79] The power spectrum of a larger ensemble of 50 trajectories displays the same qualitative structure as observed in Fig. 3(b). Specifically, the peak locations and intensities are comparable. The power spectrum for the larger ensemble is somewhat smoother as expected. The random errors associated with the 20- and 50- trajectory ensembles are .22 and .14, respectively. Given the similar qualitative appearance of the spectra for the two ensembles of 20 and 50 trajectories, larger ensemble sizes were not investigated. Ensembles of 50 trajectories were used to calculate the power spectra in the studies reported here.

Although the *estimated* autospectral density function can be easily calculated for finite times using appropriate ensemble averages, the *true* autospectral density function $S_{xx}(f)$ is strictly due to the infinite time limit [see Eq. (14)]. Since infinite time cannot be achieved in practice, finite time records must be employed. To what extent then can a finite-time approximation to the spectral density function $S_{xx}(f,T)$ be expected to represent $S_{xx}(f)$? Dumont and Brumer[79] extrapolated ($T \rightarrow \infty$) spectra from finite-time ensemble averaged power spectra. The extrapolated spectra are very similar in appearance to the finite-time ensemble averaged spectra. Those results are

encouraging in that they demonstrate that an appropriately averaged finite-time power spectrum can provide a reasonable estimate of the autospectral density function.

The autospectral density function of a periodic function can be represented by a single record provided that the time length of the sample covers one full vibrational period of the lowest frequency mode and the sampling frequency is at least twice that of the highest frequency component in the record. Therefore peaks due to regular motion are expected to be well defined in both the one trajectory and the ensemble averaged spectra. This is observed for the results in Fig. 3. The one sharp peak that is present in the single trajectory spectrum survives in the ensemble averaged spectrum. As the analysis of the results in our study of the CF_2Br radical relate to the determination of the presence/absence of regular intramolecular motion, it is of importance to establish that regular motion can be assigned on the basis of the power spectrum. The survival of the sharp peak to the ensemble average over the single trajectory power spectra demonstrates the presence of a quasiperiodic component in the underlying data. The molecular mode responsible for this periodic component can be approximately determined by examining the spectra of the individual internal coordinates.

By definition, the autospectral density function is proportional to the squared Fourier coefficients. As previously noted, the squares of the transformation coefficients provide, through Parseval's Theorem, a direct measure of the "power" or energy associated with a given frequency component of the data.[81] Alternative methods of data analysis based on power spectral techniques have been explored. Muckerman, Noid, and Child[96] have used the log of the Fourier transform of cross-correlations functions to define a criterion for chaos which is based on the number of spectral peaks with amplitudes exceeding a particular value (to eliminate consideration of peaks due to spectral noise). They made application of the method to the study of

a two-dimensional model Hamiltonian for H_2O. They determined that stochastic trajectories always have a total number of peaks exceeding 170 and a total number of peaks greater than 1.5 times the average number of peaks in the two "half" trajectories which constitute the total trajectory. Cho, Winter, Harris, Fleischmann, and Adams[97] applied this method to the study of chaotic vibrations in HCN using a three-dimensional model. However, they were unable to find a set of spectral correlations of dimension two or greater that reliably distinguished between chaotic and regular vibrations. Raff[98] has discussed the use of the magnitude of the Fourier coefficients (as opposed to the squared magnitude) to predict whether the reaction dynamics of a molecular system will be statistical or nonstatistical. The squared magnitudes amplify the major spectral intensities and diminish the low intensity peaks. Plots of the magnitude thus provide an amplified view of the low intensity structure.

A number of methods have been developed to calculate power spectra and are discussed in a recent review by Roy, Sumpter, Pfeffer, Gray, and Noid.[99] The methods reviewed include the FFT, MEM (maximum-entropy method), MUSIC, and ESPRIT methods. Emphasis is placed on models such as MUSIC and ESPRIT which depend "on the geometric aspects of a deterministic signal model in additive noise" with results presented to substantiate applicability of the methods as spectral estimators for molecular trajectory calculations. The benefit of the MUSIC and ESPRIT estimators is that they "require *much* less time-dependent information because these methods *do* exploit, in some manner, a presumed, underlying structure of that information." An example which was cited is the calculation of the power spectrum of a polymer molecule. The FFT method would require information regarding all of the atoms at hundreds of time steps whereas the MUSIC and ESPRIT methods only required 64 time steps. Hence, a substantial savings in computer time can be gained by using the newer techniques. However, investigations regarding the applicability of

the methods are limited and Roy *et al.*[99] recommended testing the results of the methods, as applied to a particular problem, by comparison to a spectrum calculated using a standard method such as the FFT.

An important consideration in the computation of discrete spectra is the sampling interval Δt. The sampling interval determines the value of the Nyquist cutoff frequency f_c.[100]

$$f_c = \frac{1}{2\Delta t} \quad . \tag{23}$$

The Nyquist frequency is the highest frequency that can be defined on the basis of the sampling interval. Frequencies in the data that are larger than f_c result in "aliasing." Aliasing occurs when spectral intensities at frequencies higher than f_c fold over into the autospectral density function at frequencies below f_c. Aliasing can be avoided by careful selection of Δt or by using filters to remove components of the data with frequencies which exceed f_c (See, for example, Ref. 80.).

Side-lobe leakage can contribute to error in the power spectrum estimation and therefore deserves mention. Side-lobe leakage results from the sampling of data for finite time T where the data function $x(t)$ is in effect multiplied by a rectangular window $u(t)$:[80]

$$u(t) = \begin{cases} 1 & 0 \le t \le T \\ 0 & otherwise \end{cases} \quad . \tag{24}$$

A description of side-lobe leakage and the data tapering (windowing) methods which can be employed to reduce the effect are given in Ref. 80. Spectra calculated with and without a data window are shown in Figs. 4(a) and 4(b), respectively. The plots in Fig. 4 are for an ensemble of 50 trajectories for CF_2Br for which ν_6 initially contained 35 kcal/mol of excitation energy. The Parzen data window[101] was employed for the calculation of the spectrum in Fig. 4(a). As can be seen by comparison of the

Figure 4. Comparison of CF_2Br spectra calculated with and without the use of a Parzen data window. The spectra are for ensembles of 50 trajectories. The initial conditions are for excitation of ν_6 to 35 kcal/mol. (a) spectrum calculated with the Parzen data window; (b) spectrum calculated without the Parzen data window.

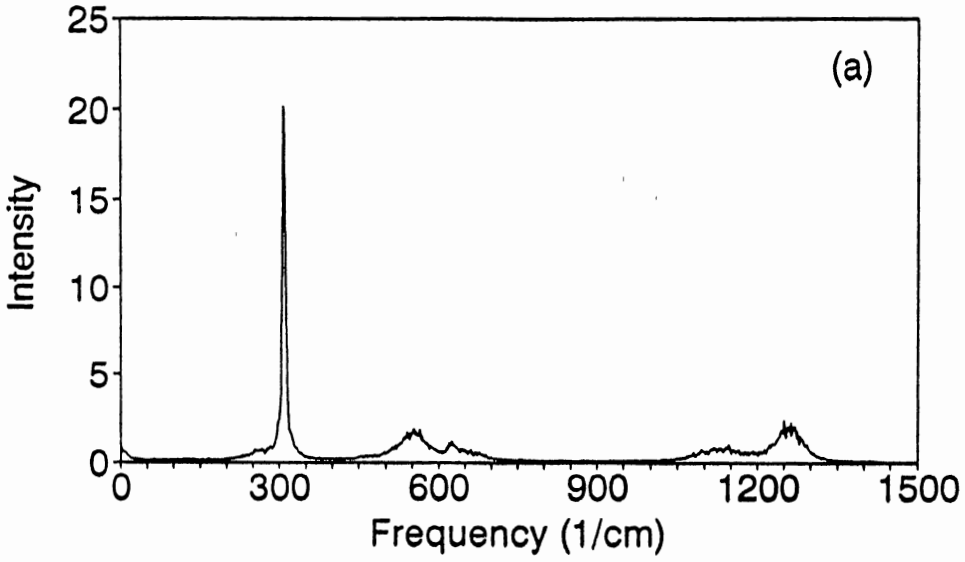
25
20
15
10
5
0
Intensity
(a)
0
300
600
900
1200
1500
Frequency (1/cm)

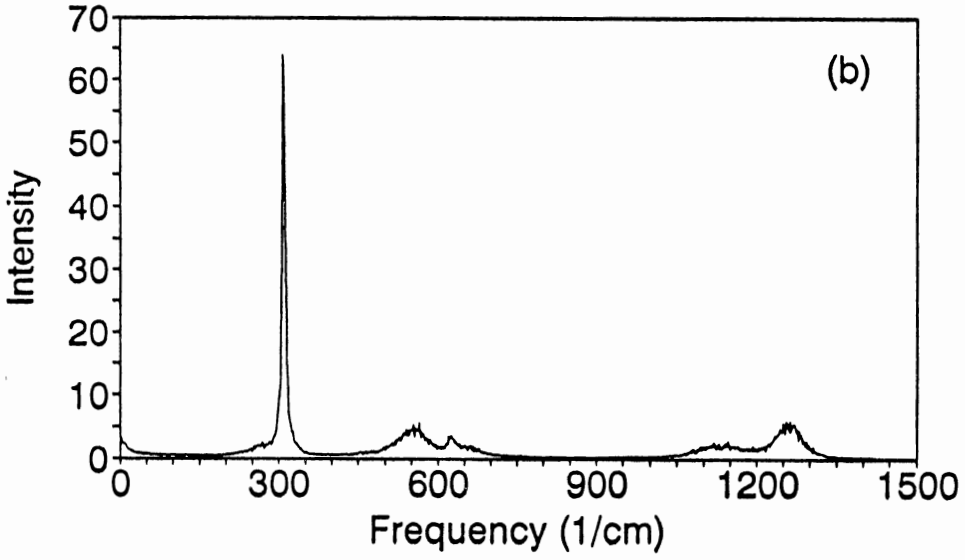
70
60
50
40
30
20
10
0
Intensity
(b)
0
300
600
900
1200
1500
Frequency (1/cm)

spectra in Fig. 4, the windowing technique did not alter the qualitative aspects of the spectrum. Namely, a quasiperiodic component is present in both spectra as evidenced by the sharp peak at approximately 307 cm^{-1}. The remaining structure is due to irregular motion with broad frequency bands which can be approximately assigned on the basis of the normal mode frequenies. The intensities are different in the two plots because the window "scales" the data at the beginning and end of the trajectory as can be seen by examination of the Parzen data window, Fig. 5. Methods exist for reducing the bias associated with windowing techniques.

Given that including the Parzen data window in the calculations does not alter the conclusions drawn from the spectra, windowing techniques were not included in the calculations presented in this thesis.

A matter of practical concern for the present trajectory calculations is averaging the spectra for data records of varying length. The current work is concerned with the reaction dynamics of the CF_2Br radical. The trajectories were terminated when the C-Br bond length exceeded 6 Å; however, the reactive lifetime was taken as the last inner turning point of the C-Br bond. Therefore, the trajectories in a given ensemble represent a wide range of lifetimes. In order to calculate appropriate ensemble averages, it is necessary for the spectra in a given ensemble to have the same spectral resolution. As previously noted, the resolution is determined by the time length of the data record. In order to obtain the same spectral resolution for each spectrum in a given ensemble, the internal coordinate time histories of trajectories for which the reactive lifetime was less than some predetermined value were padded with zeros.[82] Power spectra calculated using this method and power spectra calculated at an energy below the C-Br bond dissociation energy are similar in appearance. Therefore, it appears that the zero padding technique does not introduce any significant bias into the calculations.

Figure 5. Parzen data window.

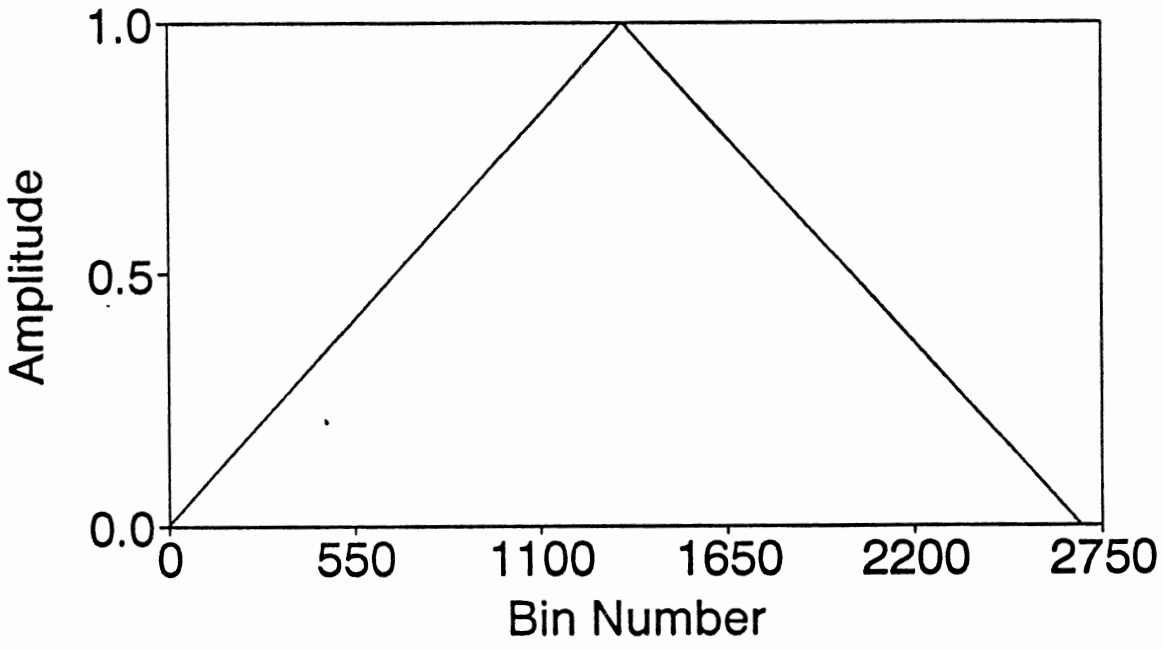
1.0
0.5
0.0
Amplitude
0
550
1100
1650
2200
2750
Bin Number

Trajectory Calculations

The GenDyn classical trajectory code was used in these studies.[102] The code is "general" in that it is applicable to the study of the intramolecular and reaction dynamics of any size polyatomic molecule (limited, of course, by computer memory and disk capacity) without requiring extensive reprogramming. A set of input data files are required to define structural and potential parameters and to set flags for runtime options. Standard options include a normal mode analysis (using the analytical second derivatives evaluated at the equilibrium structure of the molecule); specification of initial conditions using microcanonical Metropolis sampling, canonical sampling, or excitation of normal or local (bond) modes; calculation of time histories of normal and local mode energies; calculation of internal coordinate time histories; and determination of the reaction times.

The GenDyn code provides for specification of the potential energy V in terms of a number of standard potential functions including Morse or harmonic oscillators for the bonds, harmonic oscillators for the bond and wag angles, and a truncated cos series for the dihedral angles. The kinetic energy T is

$$T = \frac{1}{2}\sum_{i=1}^{3N}\frac{p_i^2}{m_i}\,, \tag{25}$$

where the p_i are the Cartesian momenta of the N atomic nuclei and the m_i are the atomic masses. The total system energy is given by the Hamiltonian H:[103]

$$H = T + V\,.$$

The equations of motion are defined used the Hamiltonian methodology:[103]

$$\dot{q}_j = \frac{\partial H}{\partial p_j}$$
$$-\dot{p}_j = \frac{\partial H}{\partial q_j} \; . \tag{27}$$

The q_j and p_j are the Cartesian coordinates and conjugate momenta, respectively. The derivatives are calculated analytically and the equations of motion integrated using a fourth-order Runge-Kutta-Gill routine.

The GenDyn code was modified to include attenuation of the potential parameters as functions of the bond lengths and dihedral angles. Switching functions (described in Chapter III) were used to accomplish the attenuation.

In the present studies, initial conditions for mode-specific excitations were selected by populating one of the normal modes with its ground-state energy plus an arbitrary excitation energy. Each of the other normal modes was assigned its calculated ground-state vibrational energy. Initial conditions were also considered for which the excitation energy was equipartitioned among the normal modes. Monte Carlo phase averaging was used (assuming harmonic normal-mode oscillators) to obtain the initial phases of the normal coordinates:[104]

$$Q = Q_e - (Q_e - \rho_-)\sin\left(\frac{\pi}{2} + \pi\xi'\right) \tag{28}$$

where Q_e is the equilibrium value of the normal coordinate (namely, zero), ρ_- is the classical inner turning point at energy E, and ξ' is a random number between zero and one. The normal mode velocity is simply:

$$\dot{Q} = \pm\sqrt{2T} \; . \tag{29}$$

The kinetic energy T for a given normal mode is the difference between the desired mode energy and the potential energy calculated using the phase averaged normal

coordinates. The sign of the velocity is determined using a random number. The normal coodinates and velocities were transformed to Cartesian coordinates and velocities using the linear transformation equations:[105]

$$q_i = \sum_{k=1}^{3N} l_{ij} Q_j \quad i=1,2,...,3N \quad , \tag{30}$$

where the the q_i are mass weighted Cartesian coordinates, the Q_j are normal coordinates, N is the total number of atoms in the molecule, and the l_{ij} are the normalized eigenvectors of the secular equation for the $\boldsymbol{F}$ matrix. The transformation equations for the velocities were obtained by taking the time derivative of both sides of Eqs. (30).

The energies calculated for the initial conditions obtained by populating the normal modes deviate from the desired energies. In addition, a spurious angular momentum is introduced. The angular momentum is removed by subtracting the linear velocity due to rotation from the initial velocity of each atom.[106] The coordinates and momenta are then scaled to obtain a fixed-energy ensemble (to within 10^{-5} kcal/mol).[106] The procedure sometimes requires several iterations. Rotational effects were not considered in these studies.

The trajectories were integrated until reaction occurred (fission of the appropriate bond was defined on the basis of the bond length reaching a critical extension) or until the integration time exceeded a value determined on the basis of preliminary calculations. The reactive lifetime of a trajectory was defined as the time up to the last inner turning point of the dissociating bond. Rate constants k were calculated by least-squares fitting the lifetimes to

$$\ln\left(\frac{N(t)}{N(0)}\right) = -kt \quad , \tag{31}$$

where N(t) is the number of undissociated trajectories at time t and N(0) is the total

number of trajectories in the ensemble. Initial conditions for which the excitation energy was assigned to the reaction coordinate mode resulted in a number of trajectories which did not undergo an inner turning point prior to dissociation. These zero-lifetime trajectories were retained both as a part of the total ensemble and counted in the number of unreacted trajectories at a given time. However, the points at $t=0$ were not included in the least-squares fits.

To investigate the mechanism for energy flow, the energies in the normal modes were calculated as a function of time. Although this type of analysis is qualitative (the sum of the normal mode energies can deviate significantly from the total system energy as calculated from the system Hamiltonian), it does provide some insight into the mechanism for energy flow from an initially excited mode. The methods are described elsewhere.[102]

$\underline{CF_2Br}$

Five excitation energies, measured relative to the zero-point energy of the harmonic normal modes (approximately 6 kcal/mol), were considered. The lowest excitation energy is 35 kcal/mol which is slightly higher than the C-Br bond well-depth of 33.3 kcal/mol used in this study. On the basis of time-of-flight distributions, Krajnovich, Zhang, Butler, and Lee[66] estimated the *maximum* product internal energy of the following reaction to be 39 kcal/mol:

$$CF_2Br_2 + h\nu\,(248\ nm) \rightarrow CF_2Br + Br\ . \qquad (32)$$

Since no information is available regarding the electronic state of the Br atom, it is conceivable that all of the product internal energy is in the form of CF_2Br vibrational energy. Thus, 39 kcal/mol corresponds to the excitation energy of the "hottest" CF_2Br intermediates in the photodissociation experiment of Krajnovich *et al.* The

three other excitation energies (45, 50, and 60 kcal/mol) were considered to determine what effect (if any) higher excitation energies might have on the relative behavior of the rate constants for mode-specific excitations.

Seven calculations were carried out at each of the five excitation energies. Six of these calculations involved mode-specific excitation of the individual normal modes. The seventh calculation at each of the five energies consisted of equipartitioning the excitation energy among the normal modes. (For a description of the methods used to select the initial conditions, see page 48).

Ensembles of 500 trajectories were calculated for each set of initial conditions. An integration stepsize of .15 fs was used. Conservation of energy was obtained to 5 significant figures. The trajectories were followed for 50 ps or until reaction (C-Br bond fission) occurred. The value of 50 ps was chosen as it exceeded the average reactive lifetime for trajectories at the lowest excitation energy considered. Reaction was defined to be complete when the C-Br bond length exceeded 6 Å.

The regular *vs* chaotic character of the intramolecular dynamics of the CF_2Br radical was investigated using power spectra. The techniques are discussed elsewhere (see page 24). Ensembles of 50 trajectories, which are subsets of the larger ensembles used to calculate the rate constants, were employed. The trajectory integration stepsize was .15 fs and sampling of the internal coordinate time histories was performed every fiftieth integration step; therefore the sampling interval was Δt=7.5 fs which yields a Nyquist cutoff frequency of 2222 cm^{-1}.

$\underline{N_2O_3}$

The initial conditions were selected using mode-specific excitations of the nitro- or nitroso-group normal modes (ν_1, ν_2, ν_3, and ν_4) and combinations thereof.

Initial conditions were also considered for which the excitation energy was equipartitioned among the normal modes. (See page 48 for a description of initial conditions selection methods.) Calculations were carried out for which the total system energy was the same for two or more sets of initial conditions or for which the energy in the excited mode was the same for two or more sets of initial conditions. All sets of initial conditions considered are given in Chapter IV on page 104. Ensembles of 200 trajectories were used to calculate the lifetimes unless otherwise noted.

An integration stepsize of 4.89×10^{-17} s was used. Conservation of energy to 10^{-4} kcal/mol was obtained. As previously noted, ensembles of 200 trajectories were calculated for each set of initial conditions, but ensembles of 400 trajectories were calculated for a few select sets of initial conditions to check convergence of the calculated rates. Reaction was considered complete when the N-N bond length exceeded 5 Å.

CHAPTER III

POTENTIAL-ENERGY SURFACES

CF_2Br

Ab initio calculations were performed by Jeff Hay[107] (at the Los Alamos National Laboratory) on CF_2Br at the Hartree-Fock level using the MESA electronic structure codes.[108] The details are given elsewhere.[109] The *ab initio* and experimental frequencies[110] for CF_2Br are given in Table I on page 54.

A brief analysis of the internal coordinate contributions to the *ab initio* normal modes follows. The lowest frequency mode υ_6 is almost exclusively Br-C-F bending. There is essentially no displacement of the other internal coordinates for υ_6 motion. Of the normal modes, υ_6 is the most localized in terms of internal coordinate motion in that the other modes correspond to some combination of internal coordinate displacements. The υ_2 and υ_4 modes correspond primarily to C-Br stretch motion. The υ_4 mode also involves motion directed along the axis connecting the Br atom and the center-of-mass of the CF_2 group. The υ_3 mode is predominantly F-C-F bending. The υ_1 and υ_5 modes correspond to the symmetric and asymmetric C-F stretches, respectively.

The three frequencies which have been determined experimentally (υ_1, υ_2, and υ_5) were reported (to within 1 cm^{-1}) in two independent studies.[110,111] In the study by Jacox,[110] it was noted that insufficient information was available to make symmetry assignments for the C-F stretching fundamentals. However, Prochaska and Andrews[111] have attributed the highest frequency fundamental to the symmetric C-F

TABLE I

CF_2Br FREQUENCIES

Mode	Frequency (cm^{-1}) Experimental[a]	Calculated[b]
CF_2Br		
ν_6		311
ν_4		331
ν_3		562
ν_2	684	676
ν_1	1138	1207
ν_5	1198	1326
CF_2		
ν_1	1222	1218
ν_2	663	647
ν_3	1124	1112

[a] CF_2Br frequencies from: Jacox, Ref. 110. CF_2 frequencies from: Kirchhoff *et al.*, Ref. 115.

[b] CF_2Br frequencies from *ab initio* calculations.[107] CF_2 frequencies from derived potential energy surface, Eq. (36).

stretch. Their assignment is inverted relative to the *ab initio* results whereby the asymmetric C-F stretch was found to be the highest frequency mode. Comparison of the values of the calculated and experimental frequencies (see Table I on page 54) reveals differences of 6 and 11 percent, respectively, for the C-F stretch frequencies (υ_1 and υ_5) while much closer agreement is observed for the υ_2 C-Br stretch frequency between the calculated (767 cm^{-1}) and experimental (684 cm^{-1}) value. Calculated frequencies for polyatomic molecules at the Hartree-Fock level are typically overestimated by 10-15 percent with the 6-31G basis used for the present calculations, or with the more accurate 6-31G* basis set.[112] Since there are only limited experimental data (to our knowledge, results have not been reported for the remaining three modes) and since the rate of C-Br bond fission is the quantity of interest in this study, we based the potential on the *ab initio* Hessian without modification.

A number of developments are given in the literature for obtaining the internal coordinate force constant matrix by transformation of the Cartesian Hessian *via* the **B** matrix. The methods described by Fogarasi and Pulay[113] were used in this study. (Note however that the method is due to Crawford and Fletcher.[114]) The complete CF_2Br internal force constant matrix (the internal coordinates are the three bonds and three bond angles defined in Fig. 6) was obtained by direct transformation of the Cartesian *ab initio* Hessian at the equilibrium geometry

$$f = A^t K A \ , \tag{33}$$

where (employing the notation of Fogarasi and Pulay[111]) $\boldsymbol{f}$ is the internal coordinate Hessian (for a set of complete and non-redundant internal coordinates), $\boldsymbol{K}$ is the Cartesian Hessian, and $\boldsymbol{A}$ is obtained from the $\boldsymbol{B}$ matrix through

$$A = uB^t(BuB^t)^{-1} \ . \tag{34}$$

The matrix **u** is the 3N X 3N diagonal matrix of the inverse nuclear masses. The

Figure 6. Definition of internal coordinates for CF_2Br.

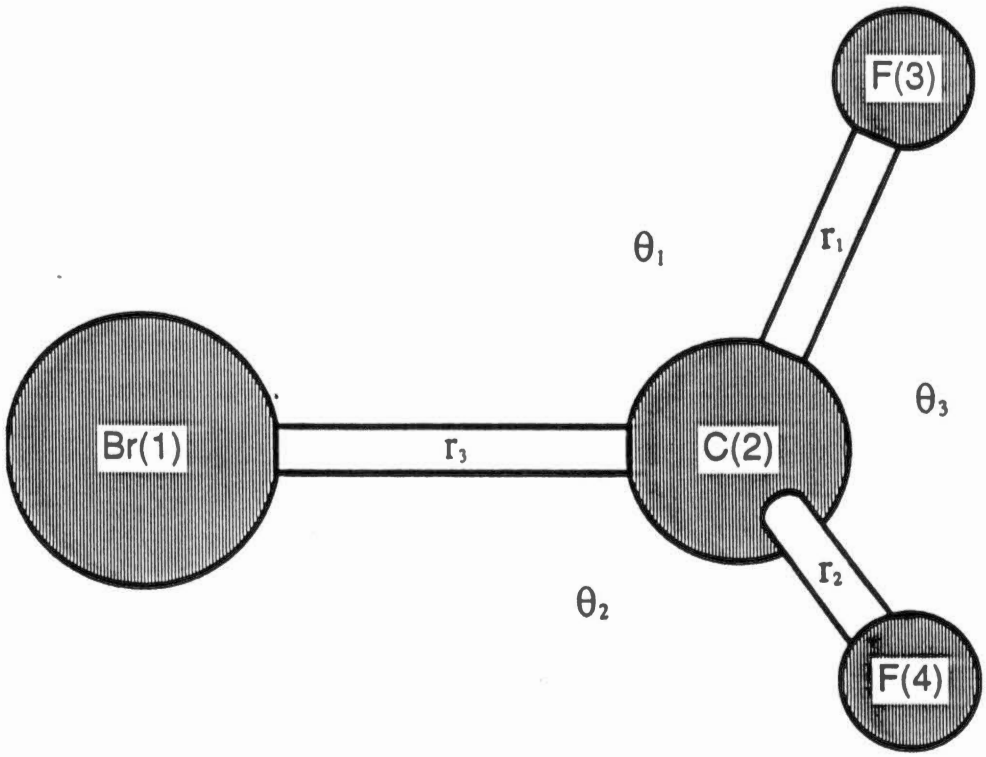
F(3)
θ1
r1
θ3
Br(1)
r3
C(2)
r2
θ2
F(4)

potential energy function is given in terms of f by

$$V = V_0 + \frac{1}{2} q^t f q \ , \tag{35}$$

where V_0 is the energy at the potential minimum and q is the column vector of the internal displacement coordinates. Thus, all quadratic potential interaction terms are explicitly accounted for in the potential energy function.

In the form of the potential used in the trajectory calculations, the diagonal harmonic oscillator terms for the bonds were replaced by Morse oscillators. Values of 33.3 and 127.4 kcal/mol were used for the C-Br and C-F well depths, respectively. These values were obtained from estimates for the ΔH^0_{diss} of the respective bonds. The full potential is

$$V = V_0 + \sum_{i=1}^{3} V(q_i) + \frac{1}{2}\sum_{i=4}^{6} f_{ii} q_i^2 + \frac{1}{2}\sum_{\substack{i,j=1 \\ i \neq j}}^{6} f_{ij} q_i q_j \ ; \tag{36}$$

where V_0 is the negative of the sum of the Morse well-depths; the q_i are the internal displacement coordinates with i=1, 2, and 3 corresponding to bonds 1, 2, and 3, respectively, and i=4, 5, and 6 corresponding to angles 1, 2, and 3, respectively; the $V(q_i)$ are Morse potentials; the f_{ii} are the bond angle harmonic force constants; and the f_{ij} are the interaction constants. The equilibrium structure for CF_2Br was taken to be the *ab initio* computed structure.[107] The potential energy and structural parameters are given in Table II on page 59.

TABLE II

CF_2Br POTENTIAL ENERGY AND STRUCTURAL PARAMETERS

Morse Parameters			
Bond	r_e (Å)	D_e (kcal/mol)	β ($Å^{-1}$)
CF_2Br			
r_1	1.346	127.4	1.993
r_2	1.346	127.4	1.993
r_3	1.953	33.3	2.411
CF_2			
r_1	1.346	127.4	1.87
r_2	1.346	127.4	1.87
Bond Angles			
Angle		θ_o (Degrees)	Force Constant (kcal/mol/rad^2)
CF_2Br			
θ_1		114.3	208.42
θ_2		114.3	208.42
θ_3		110.4	268.81
CF_2			
θ		104.8	332.70

TABLE II (Continued)

Off-Diagonal Potential Energy Terms[a]	
Interaction Term	Constant
CF_2Br	
r_1r_2	89.61
r_1r_3	59.14
r_2r_3	59.14
$\theta_1\theta_2$	78.25
$\theta_1\theta_3$	71.73
$\theta_2\theta_3$	71.73
$r_1\theta_1$	41.55
$r_1\theta_2$	-13.98
$r_1\theta_3$	53.41
$r_2\theta_1$	-13.98
$r_2\theta_2$	41.55
$r_2\theta_3$	53.41
$r_3\theta_1$	50.28
$r_3\theta_2$	50.28
$r_3\theta_3$	6.452
CF_2	
r_1r_2	224.7
$r_1\theta$	101.9
$r_2\theta$	101.9

[a]Units of energy are in kcal/mol, bond lengths are in Å, angles are in radians.

The CF_2 potential-energy function and equilibrium structure were taken from the microwave study of Kirchhoff, Lide, and Powell[115] except that the CF_2Br parameters for the C-F bond lengths and well depths were used. The CF_2 potential is given by

$$V = V_0 + \sum_{i=1}^{2} V(q_i) + \frac{1}{2} f_{33} q_3^2 + \frac{1}{2} \sum_{\substack{i,j=1 \\ i \neq j}}^{3} f_{ij} q_i q_j \ , \qquad (37)$$

where i=1 and 2 corresponds to r_1 and r_2, respectively, and i=3 corresponds to the bond angle. The remaining terms are as defined for Eq. (36). The calculated and experimental frequencies for CF_2 are given in Table I on page 54. (Note that the calculated frequencies for CF_2 are from the fit, not from the *ab initio* calculations.) Experimental frequencies for the CF_2 radical have been reported by a number of investigators.[115,116,117,118,119] Since the potential-energy surface is based on that reported by Kirchhoff, Lide, and Powell, the experimental frequencies given in Table I (see page 54) were taken from that study. The potential-energy and structural parameters for CF_2 are given in Table II (see page 59).

Switching functions were incorporated in the potential-energy function to smoothly connect the reactant and product regions of the potential-energy surface by attentuation of the force constants and equilibrium internal coordinate values as functions of the C-Br bond length (the reaction coordinate). The switching functions were chosen such that the potential energy first- and second-derivatives are continuous. The following form satisfies these criteria while remaining computationally inexpensive:

$$\gamma(r_{C-Br}) = \begin{cases} \gamma_p - (\gamma_p - \gamma_r)\exp[-\alpha(r_{C-Br} - r^0_{C-Br})^N] \ , & r_{C-Br} > r^0_{C-Br} \\ \gamma_r \ , & r_{C-Br} \leq r^0_{C-Br} \end{cases} ; \qquad (38)$$

where γ is a force constant or equilibrium internal coordinate (with subscripts p and r

denoting product and reactant, respectively), $r_{C\text{-}Br}$ is the C-Br bond length, and α and N are fitting parameters which determine the rate of attenuation and the bond-length range of the attenuation.

It was necessary to use two sets of values for the parameters α and N. The values of α=8.0 and N=4 were used to turn off the potential-energy coupling (off-diagonal) terms which appear in the CF_2Br potential but which do not appear in the CF_2 potential. These values of α and N were chosen to eliminate spurious local minima which occur if the interaction constants are not switched off before the C-Br bond achieves approximately 1 Å displacement from equilibrium.

The values of α=.25 and N=4 were used to attenuate the force constants and the remaining interaction constants (those which survive in the CF_2 potential). These values of α and N result in attenuation over about a 2 Å extension beyond the equilibrium value of the C-Br bond. Preliminary results obtained for a number of sets of values of α and N switching function parameters showed that local minima occur in the potential-energy surface unless the α and N parameters are chosen such that the attenuation of these constants terminates in the asymptotic region of the C-Br bond potential. The spurious local minima occurred when the Br-C-F angle force constants were turned off short of the C-Br bond potential asymptote allowing essentially free rotation of the CF_2 radical. The minima occurred in a region of the potential-energy surface far removed from the minimum energy path where we have no information about the forces. Most *ab initio* calculations are for the vicinity of the minimum energy path and therefore fail to provide critical information about the full-dimensional potential-energy surface which is needed for dynamics calculations since trajectories can deviate significantly from the minimum energy path. However, *ab initio* calculations for geometries along the minimum energy path provide information useful for treatments such as transition-state theory[120,121] and reaction-path

Hamiltonian theory.[57] (The determination and application of minimum energy paths are discussed in recent articles.[62,122]) However, unrestricted dynamics calculations require the forces for geometries far removed from the minimum-energy path.

The C-F bond well-depth is based on that for CF_2[123] and thus was not attenuated. Furthermore, there is only .042 Å difference between the *ab initio* equilibrium C-F bond length of CF_2Br and the experimental equilibrium C-F bond length of CF_2. Therefore, it seems reasonable to neglect attenuation of the equilibrium C-F bond length. The F-C-F equilibrium bond angle was attenuated between the reactant and products values using switching parameter values of $\alpha=.25$ and N=4.

Although at the energies employed in this study it is not possible for C-F bond fission to occur, it is necessary to turn off certain of the potential parameters as the C-F bonds extend. The potential parameters which are switched are those which do not occur in the potential of the products which would result from C-F bond fission. The final form for these potential-energy parameters, $\zeta(r_{C\text{-}Br},r_{C\text{-}F1},r_{C\text{-}F2})$, is given by:

$$\zeta(r_{C-Br},r_{C-F_1},r_{C-F_2}) = \gamma(r_{C-Br})\chi_1\chi_2 \ , \tag{39}$$

where

$$\chi_i = \begin{cases} \exp[-\alpha(r_{C-F_i}-r^o_{C-F_i})^N] \ , & r_{C-F_i} > r^o_{C-F_i} \\ 1 \ , & r_{C-F_i} \le r^o_{C-F_i} \end{cases} \ , \tag{40}$$

with $\gamma(r_{C\text{-}Br})$, α, and N as previously defined and $r_{C\text{-}F(i)}$ (i=1 or 2) being one of the C-F bond lengths. Diagonal terms which do not survive C-F bond fission were switched as functions of the C-F bond lengths using $\alpha=.25$ and N=4. Off-diagonal terms which do not survive C-F bond fission were switched using $\alpha=8.0$ and N=4. The equilibrium values of the internal coordinates were not switched as functions of

the C-F bonds.

N_2O_3

The enthalpy of dissociation for asymmetric N_2O_3 is $\Delta H^0(298\ K)=9.8$ kcal/mol.[74] A well-depth of 10.1196 kcal/mol was used in the calculations. The N-O well-depths are the same as those used by Rice and Thompson[124] in a study of the unimolecular decomposition of nitromethane. Bibart and Ewing[125] have estimated the ground-state torsional barrier for N_2O_3 to be of the order of 1 kcal/mol. We used two dihedral angles to describe the torsional motion each with a barrier of 0.6 kcal/mol, thus, the total torsional barrier is 1.2 kcal/mol. The structure for asymmetric N_2O_3 was taken from the microwave structure reported by Brittain, Cox, and Kuczkowski.[126]

The bond and angle definitions are shown in Fig. 7. The wag and dihedral angles are defined as follows: γ_1 is the angle between bond 3 and the plane of atoms 1, 2, and 5; γ_2 is the angle between bond 4 and the plane of atoms 1, 2, and 4; τ_1 is the angle between the plane of atoms 1, 2, and 3 and the place of atoms 1, 2, and 4; and τ_2 is the angle between the plane of atoms 1, 2, and 3 and the plane of atoms 1, 2, and 5. The equilibrium values of the internal coordinates are given in Table III on page 65.

TABLE III

N_2O_3 EQUILIBRIUM INTERNAL COORDINATES

Coordinate	Equilibrium Value[a,b]
r_1	1.864
r_2	1.142
r_3	1.202
r_4	1.217
θ_1	105.1
θ_2	112.7
θ_3	129.8
θ_4	117.5
γ_1	0.0
γ_2	0.0
τ_1	0.0
τ_2	180.0

[a]From Ref. 126.

[b]Bond lengths in units of angstroms. Angles in units of degrees.

Figure 7. Definition of internal coordinates for N_2O_3.

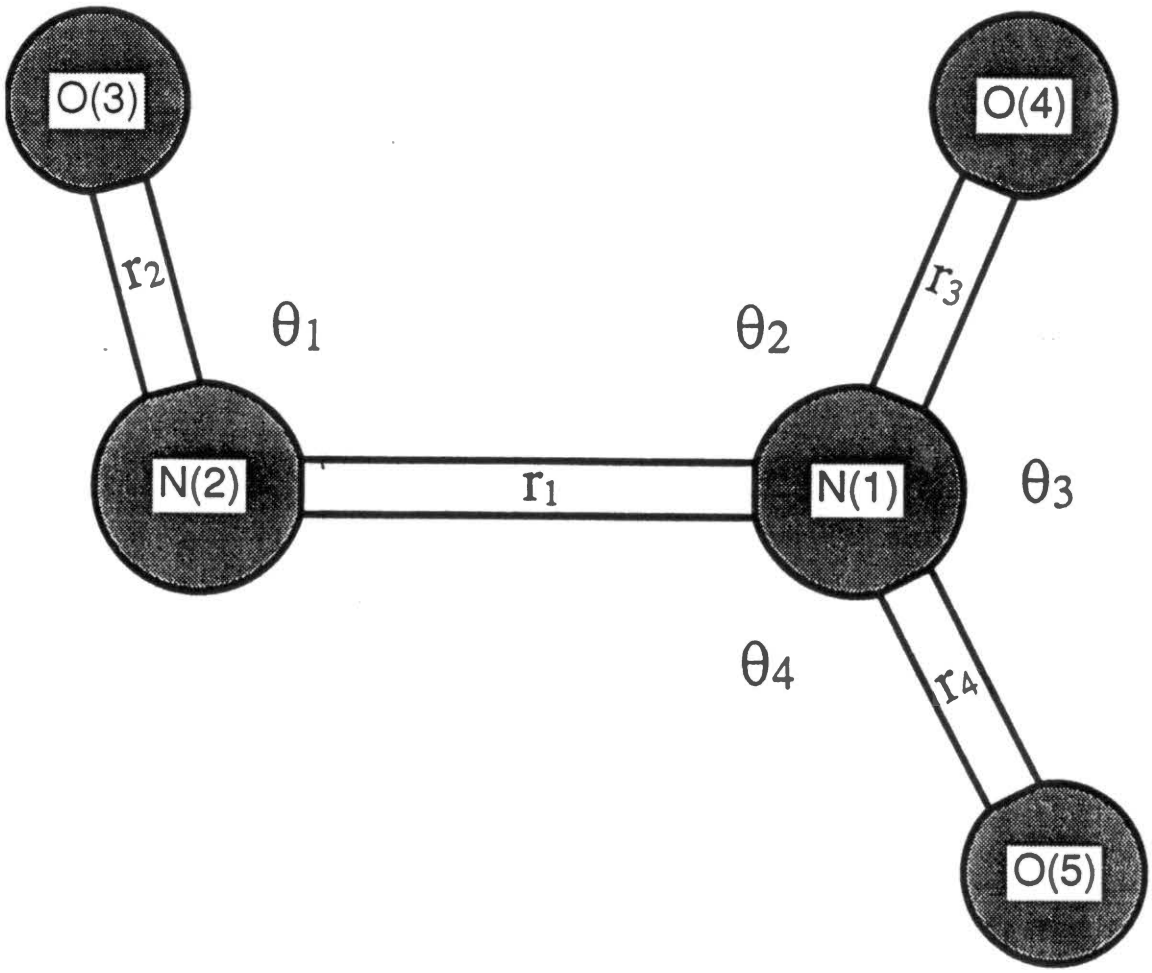
O(3)
O(4)
r2
r3
θ1
θ2
N(2)
r1
N(1)
θ3
θ4
r4
O(5)

The potential-energy surface used in this study was fit to the spectroscopic frequency assignments reported by Chewter, Smith, and Yarwood.[74] The form of the equilibrium potential is

$$V = \sum V(r_i) + \sum V(\theta_i) + \sum V(\gamma_i) + \sum V(\tau_i) + + k_{1,2}\theta_1\theta_2 + k_{1,4}\theta_1\theta_4 \ , \tag{41}$$

where

$$V(r_i) = D_{e_i}\{1-\exp[-\beta_i(r_i-r_{e_i})]\}^2 \ , \tag{42}$$

$$V(\theta_i) = \frac{1}{2}k_i(\theta_i-\theta_i^0)^2 \tag{43}$$

$$V(\gamma_i) = \frac{1}{2}k_i(\gamma_i-\gamma_i^0)^2 \ , \tag{44}$$

$$V(\tau_i) = \sum_{j=0}^{4} a_j\cos(j\tau_i) \ . \tag{45}$$

It is necessary to attenuate the β Morse parameters for bonds 3 and 4 and the force constants for bond angles 2 and 4 as functions of the dihedral angles. This is accomplished by using the following switching functions for β and $k_{\theta i}$:

$$\beta_i(\tau_j) = \beta_{i_P} + \frac{1}{2}(\beta_{i_R} - \beta_{i_P})(1 + A_j\cos\tau_j) \tag{46}$$

and

$$k_{\theta_i}(\tau_j) = k_{\theta_{i_P}} + \frac{1}{2}(k_{\theta_{i_R}} - k_{\theta_{i_P}})(1 + A_j\cos\tau_j) \ , \tag{47}$$

where $A_j=1$ for τ_1 and $A_j=-1$ for τ_2. Force constants for angles 1, 2 and 4, and for the wag and dihedral angles were attenuated as functions of the N-N bond length (r_1):

$$k(r_1) = k_P + (k_R - k_P)\exp[-\alpha(r_1 - r_{e_1})^N] , \quad (48)$$

where α=0.25 Å^{-6} and N=6. The equilibrium values of the internal coordinates (specifically r_3, r_4, θ_2, and θ_4) were not attenuated as functions of the dihedral angles.

The normal mode frequencies for the NO and NO_2 products are within 9 percent of the experimentally reported values.[127,128,129] On the basis of the good agreement between the calculated frequencies and the experimental values, the force constants for the radicals were not attenuated as a function of the N-N bond length. The calculated and experimental frequencies for N_2O_3 are given in Table IV. The calculated frequencies were fit to the experimental frequencies to within 10 cm^{-1} with the exception of ν_7. However, the frequency for this mode has not been observed in the gas phase. The experimental frequency for ν_7 was obtained from Raman studies of N_2O_3 in an NO matrix.[130] The normal mode assignments are those reported by Chewter, Smith, and Yarwood.[74] The potential parameters are given in Table V.

TABLE IV

N_2O_3 FREQUENCIES

Mode	Frequency (cm^{-1})	
	Experimental[a]	Calculated
ν_1	1832	1830
ν_2	1652	1658
ν_3	1305	1295
ν_4	773	781
ν_5	415	418
ν_6	241	236
ν_7	205	240
ν_8	622	622
ν_9	70	70

[a]See Ref. 74 and references therein.

TABLE V

N_2O_3 POTENTIAL PARAMETERS

Morse Parameters		
Bond	D_e (kcal/mol)	β ($Å^{-1}$)
r_1	10.1196[a]	2.7245
r_2	151.2596[b]	2.6398
r_3	72.1238[b]	2.9657
r_4	72.1238[b]	2.9850
Bond Angles		
Angle		k_θ(kcal/mol rad^2)
θ_1		93.0508
θ_2		62.3297
θ_3		247.8154
θ_4		59.1528
Wag Angles		
Angle		k_γ(kcal/mol rad^2)
γ_1		38.7729
γ_2		38.7729
Dihedral Angles		
cos series coefficient		a_i(kcal/mol)
a_0		0.3120
a_2		-0.3000
a_4		-0.0120
Coupling Terms		
Angles		k (kcal/mol rad^2)
$\theta_1\theta_2$		80.7136
$\theta_1\theta_4$		37.1219

[a] ΔH^0(298 K) from Ref. 74, with zero-point energy correction.
[b] From Ref. 124 and references therein.

SiH_5^-

In a pentacoordinated compound of trigonal-bipyramidal structure, Berry pseudorotation[75] is a concerted motion of the atomic nuclei by which the axial ligands exchange with two of the equatorial ligands. As an example, consider the Berry pseudorotation process in SiH_5^-. Three of the H atoms occupy the equatorial positions and two of the H atoms occupy the axial positions of the trigonal bipyramid. One of the equatorial H atoms will remain fixed during Berry pseudorotation; this is the anchor atom. The angle formed by the two axial H atoms and the Si atom (which is 180° in the trigonal-bipyramidal structure) begins to close at the same time that the angle formed by the other two equatorial H atoms and the Si atom (which is 120° in the trigonal-bipyramical structure) begins to open. The transition state structure for Berry pseudorotation is a square pyramid with the anchor atom at the apex and the other four H atoms in the basal positions. At the transition state, two reaction paths are available. One path leads to the originating trigonal-bipyramidal structure. The second path leads to a trigonal-bipyramidal structure which is equivalent to the original structure except that the axial H atoms are exchanged with two of the equatorial H atoms. As dynamicists, we are interested in studying the effects of this type of large amplitude motion on intramolecular vibrational energy redistribution.

Ab initio and semiempirical calculations at various levels of theory were employed by Gordon, Windus, Burggraf, and Davis[76] to study the minimum energy path for the Berry pseudorotation process in SiH_5^-. The results of Gordon *et al.* show that, at the level of theory considered, the D_{3h} trigonal bipyramid is a minimum on the potential-energy surface and that the C_{4v} tetragonal pyramid is a transition-state structure for Berry pseudorotation. The minimum-energy path connecting the D_{3h} and C_{4v} structures is of C_{2v} symmetry. The *ab initio* barrier height was calculated to be between 2.5 and 3.0 kcal/mol.

Gordon *et al.*[76] examined the normal mode eigenvectors of SiH_5^- and determined that ν_9, one of the two degenerate lowest frequency normal modes, corresponds to motion along a Berry pseudorotation pathway. In addition, the dynamic reaction coordinate (DRC)[131] method was applied at the AM1 level of theory. The trajectory was initiated in the direction of ν_9. The trajectory proceeded from the initial equilibrium structure, through the transition state, to an equivalent isomeric structure for which the two H atoms which were initially axial were equatorial and two of the original equatorial H atoms were axial. The DRC trajectory results show that motion in the direction of ν_9 is appropriate to a Berry pseudorotation pathway.

The geometry, internal coordinate Hessian, potential energy, and projected normal mode frequencies at nine points were taken from the intrinsic reaction coordinate (IRC) *ab initio* results of Gordon *et al.*[76] at the RMP2/6-31G(d) level of theory. Gordon *et al.* determined that reasonable agreement was obtained between the *ab initio* results calculated at this level of theory and the results for which electron correlation or diffuse functions in the basis set were included. The barrier height at this level of theory is 2.5 kcal/mol. The potential-energy surface was derived directly from the internal coordinate Hessian and has the following form:

$$V = V_0(s) + \frac{1}{2}\sum_i f_{ii} q_i^2 + \sum_{\substack{i,j \\ i \neq j}} f_{ij} q_i q_j \qquad (49)$$

where $V_0(s)$ is the potential energy as a function of the reaction coordinate s, the q_i are the internal displacement coordinates (in this case, bonds and bond angles), and the f_{ii} and f_{ij} are the internal coordinate force and interaction constants, respectively. The force/interaction constants and "equilibrium" geometries are functions of s.

It was necessary to define a set of redundant internal coordinates to obtain a

potential-energy surface that is symmetric with respect to the equivalent H atoms. Sewell[132] has demonstrated that potentials which do not possess symmetry with respect to equivalent nuclei result in aphysical behavior when used in classical trajectory calculations. Specifically, dynamics calculations were carried out for a potential-energy surface for SiF_4 that was defined as a function of a set of nonredundant internal coordinates which excluded one of the bond angles. The values of the bond angles were monitored during the trajectory calculations. The bond angle which was not included in the definition of the potential function achieved values which are physically unrealizable. In particular, the bond angle was found to "close" almost completely. This is clearly not a realistic result.

The internal coordinates used in this study are the five Si-H bond lengths and the ten H-Si-H bond angles. The Cartesian coordinate Hessian was transformed to the internal coordinate Hessian by Gordon *et al.*[76] at all points along the IRC except for the point at equilibrium. The equilibrium value of one of the bond angles is 180° which results in singularities in the Hessian transformation equations. Therefore the transformation to the internal coordinate Hessian could not be performed analytically at equilibrium. To circumvent this problem, the internal coordinate force/interaction constants were determined at equilibrium for another set of redundant internal coordinates. The internal coordinates used are the five bond lengths and eight of the ten bond angles. The two bond angles which were excluded are the H_{ax}-Si-H_{ax} angle (H_{ax} represents an axial H atom in the trigonal-bipyramidal structure) and the H_{eq}-Si-H_{eq} angle (H_{eq} represents an equatorial H atom in the trigonal-bipyramidal structure) which excludes the anchor H atom (the anchor H atom is the apex atom of the square pyramid transtition-state structure).

Each of the force/interaction constants from the Hessian defined in terms of 13 internal coordinates was multiplied by the quotient of the number of symmetry

equivalent terms in the 13 and 15 internal coordinate representations of the Hessian. This quotient is just a scaling factor which disperses the values of the force constants for n symmetry equivalent terms over m ($m>n$) symmetry equivalent terms. There are no symmetry equivalent terms for the potential-energy terms involving the H_{ax}-Si-H_{ax} angle. Since this angle was neglected in the set of 13 internal coordinates, there are no *ab initio* results for the force/interaction constants for this bond angle. Inspection of plots of some of the *ab initio* angle-angle interaction constants for the H_{ax}-Si-H_{ax} angle reveal that these constants diverge as equilibrium is approached from the direction of any two of the transition states. This is illustrated in Fig. 8 which is a plot of the interaction constant for the H_{ax}-Si-H_{ax} angle and one of the H_{ax}-Si-H_{eq} angles (where H_{eq} is not the anchor atom). The points at transition states 1 and 2 are the left- and right-most points of Fig. 8, respectively. The equilibrium structure occurs at a value of the reaction coordinate of about 2.09. Fitting these *ab initio* points for the interaction constant to a continuous function requires that the function pass through zero. Since no *ab initio* information is available for potential terms involving the H_{ax}-Si-H_{ax} angle, an obvious choice is to set each of the potential terms involving the H_{ax}-Si-H_{ax} angle to zero at equilibrium. This choice eliminates singularities in the potential-energy function which occur at equilibrium when the H_{ax}-Si-H_{ax} angle is identically 180°. A normal mode analysis was performed at the equilibrium geometry using the force/interaction constants so obtained and the frequencies were found to be in agreement with the *ab initio* frequencies. The fit at equilibrium was therefore judged to be accurate.

The *ab initio* calculations were only carried out for one of the three equivalent reaction paths which is accessible from any given equilibrium configuration corresponding to a particular set of three H atoms in the equatorial positions. A global dynamical simulation of the Berry pseudorotation process requires that all three

Figure 8. Plot of a SiH_5^- *ab initio* interaction constant *vs* the reaction coordinate.

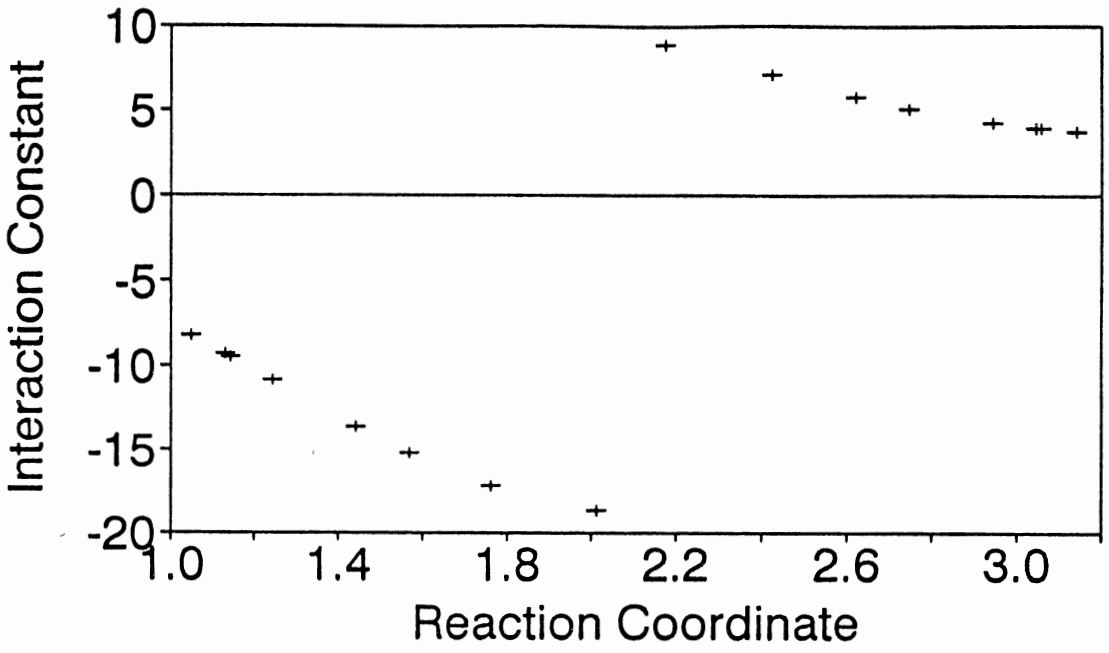
Interaction Constant
10
5
0
-5
-10
-15
-20
1.0
1.4
1.8
2.2
2.6
3.0
Reaction Coordinate

of the equivalent paths be accessible. The force/interaction constants and geometries (henceforth referred to as potential parameters) for the other two paths were obtained from the one reaction path for which *ab initio* results were available by consideration of the symmetry of the system.

Dynamical calculations result in geometries which deviate from the minimum energy path. These geometries must be mapped onto the minimum energy path at each integration step in order to define the potential parameters as a function of the reaction coordinate s.[78] The Berry pseudorotation process has been examined in cyclic phosphoranes by considering how closely the structural distortions of these molecules follow the "Berry exchange coordinate."[133] The Berry exchange coordinate used in that study was defined by plotting the absolute value of the sum of angular distortions from a square pyramid geometry *vs.* the absolute value of the sum of angular distortions from a trigonal-bipyramid geometry. (The distortions from the square-pyramid geometry were adjusted to the same scale as those from the trigonal-bipyramid geometry.) However, this definition of the reaction coordinate does not provide an analytical function that can be used in dynamics calculations. Such a function was defined by expressing the reaction coordinate in terms of a set of dihedral angles. These angles are formed between the planes of the two axial H atoms and each of the equatorial H atoms. The dihedral angles were calculated at the *ab initio* points on the IRC. The relationship between the IRC coordinate s and the values of the dihedral angles is linear within acceptable accuracy. The dihedral angles were used as the reaction coordinates in the fit.

Cubic spline methods[104] were used to fit the potential-energy surface to the nine *ab initio* points. (Note that cubic spline methods are covered in a number of excellent references, many of which are given in Ref. 104.) Traditional switching functions are inappropriate for this system because some of the *ab initio* force

constants are not monotonic functions of the reaction coordinate(s). A cubic spline fit of each of the potential parameters was made between transition state one and transition state two and between transition state one and transition state three.

Preliminary trajectories were calculated for a surface which connected two of the transition states. The energy conservation for these trajectories was not satisfactory. It was determined that sharp extrema which occur at equilibrium in the cubic spline fit of a number of the potential parameters were the source of the problem, and numerical integration of the equations of motion when the trajectories passed through the equilibrium geometry was inaccurate. Excluding point eight from the fits resulted in a smoother and more gradual "turn over" in the cubic spline functions at equilibrium. Trajectories calculated on the potential-energy surface fit to only the other eight points had satisfactory energy conservation. It should be noted that the sharp extrema are artifacts of the assumptions used to fit the potential-energy function at the equilibrium structure. An alternative definition of the internal coordinates might eliminate these difficulties.

It was determined that the number of points available in the region of the potential between points six and seven (see Fig. 9) is inadequate to obtain a good fit. (Figure 9 is the same as Fig. 8 except that the "fitted" point at equilibrium is included and the point numbers are marked for reference.) The plots of cubic splines for potential parameters with an extremum at the equilibrium geometry or multiple extrema showed extraneous "waves." (Note that the extrema correspond to local or global maxima and minima.) Seventh-degree polynomials were used to interpolate additional points between points six and seven. The polynomials were fit to the eight *ab initio* points connecting a given transition state to the equilibrium structure (again, point eight was excluded from the fit). Plots were made of the polynomial fits and compared with plots of the *ab initio* points. The polynomials are well behaved for all

Figure 9. Same as Fig. 8 except that the "fitted" point at equilibrium is included and the transition states and point numbers are marked.

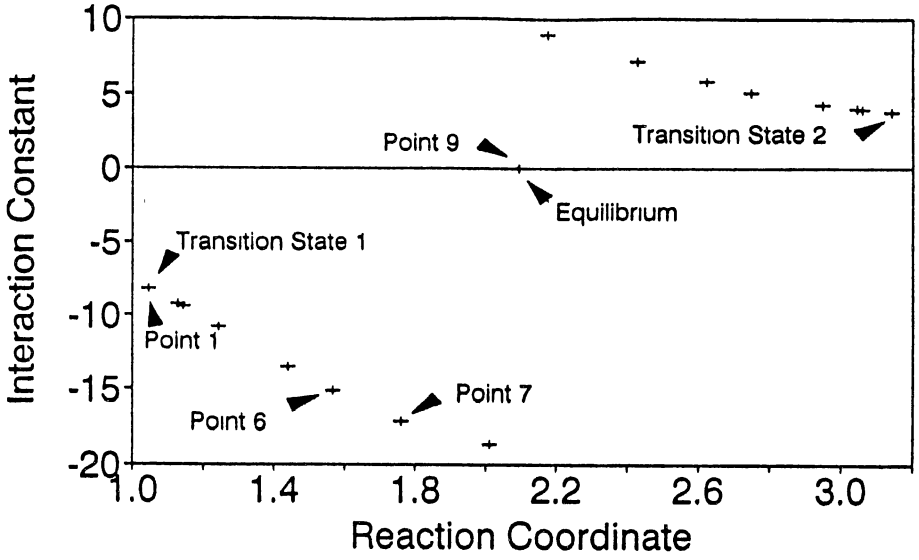
Interaction Constant
10
5
0
-5
-10
-15
-20
1.0
1.4
1.8
2.2
2.6
3.0
Reaction Coordinate
Point 9
Transition State 2
Equilibrium
Transition State 1
Point 1
Point 6
Point 7

of the fits. It was determined that the inclusion of five additional interpolated points is adequate to eliminate the extraneous behavior of the spline functions. If additional *ab initio* results become available, the interpolated points should be tested against *ab initio* points between points six and seven to ascertain the accuracy of the interpolation method. Again, symmetry can be used to define two of the reaction paths once one of the reaction paths has been fit. The potential energy along the IRC was parameterized with respect to the dihedral angles using cubic splines on the same grid as used for the potential parameters. The present form of the potential does not connect all three reaction channels in an equitable manner.

CHAPTER IV

RESULTS AND DISCUSSION

CF_2Br

Rate constants were calculated for selective excitation of each of the CF_2Br normal modes and for equipartitioning of the excitation energy among the normal modes. The calculated rate constants for ensembles of 500 trajectories are given in Table VI on page 84. Two values are given for the rate constants for ν_4 excitations because the decay curves exhibit two distinct regions. Representative decay curves are shown in Fig. 10 for excitation to 35 kcal/mol. The first values of the rate constants in Table VI for ν_4 excitation were obtained by least-squares fitting the points in the initial linear region (corresponding to fast decay) of the decay curves to Eq. (31). The second value is the analogous quantity for the remaining points (corresponding to slow decay). Decay curves for 500 trajectory ensembles for which the initial excitation energy was partitioned into one of the other normal modes and for equipartition of the excitation energy displayed only a single region of decay.

Excluding the ν_4 rate constants corresponding to the region of fast decay, comparison of the rate constants in Table VI at a given energy reveals no evidence of mode selectivity. The largest spread between any two rate constants at a particular energy is less than a factor of two. All rate constants for mode-specific excitations (again, excluding ν_4 rate constants for the region of fast decay) are comparable to the equipartition rates. However, the ν_4 rate constants corresponding to fast decay are as much as an order of magnitude greater than their isoenergetic counterparts. As

TABLE VI

CF_2Br RATE CONSTANTS (ps^{-1})

Energy (kcal/mol)	ν_6	ν_4[a]	ν_3	ν_2	ν_1	ν_5	Equipartition
41	0.02	0.17 0.02	0.02	0.02	0.02	0.02	0.02
45	0.05	0.38 0.05	0.06	0.06	0.05	0.06	0.06
51	0.15	1.4 .17	0.15	0.15	0.13	0.15	0.16
56	0.25	3.6 .26	0.27	0.30	0.24	0.23	0.23
66	0.54	13 .70	0.51	0.60	0.51	0.56	0.50

[a]Two rate constants are reported at each energy for excitation of ν_4. The first value is for the initial steep region of the decay curve. The second value is for the remaining portion of the decay curve.

Figure 10. Representative CF_2Br decay curves for an excitation energy of 35 kcal/mol. (a) ν_4 initially contains the excitation energy. Two distinct regions of decay are present. (b) ν_6 initially contains the excitation energy. Only one region of decay is observed. (c) ν_1 initially contains the excitation energy. Only one region of decay is observed.

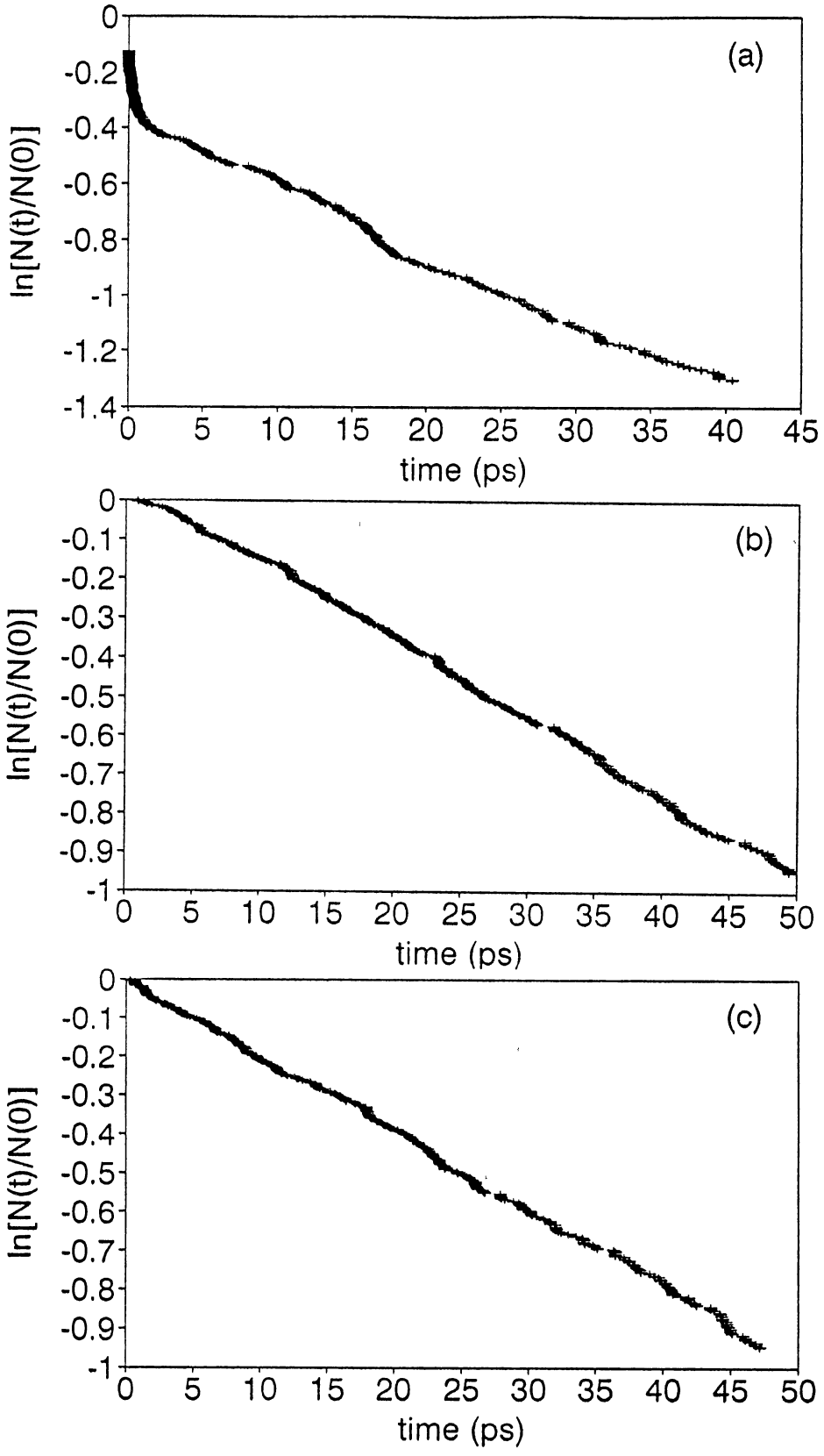
(a)
ln[N(t)/N(0)]
0
-0.2
-0.4
-0.6
-0.8
-1
-1.2
-1.4
0 5 10 15 20 25 30 35 40 45
time (ps)
(b)
ln[N(t)/N(0)]
0
-0.1
-0.2
-0.3
-0.4
-0.5
-0.6
-0.7
-0.8
-0.9
-1
0 5 10 15 20 25 30 35 40 45 50
time (ps)
(c)
ln[N(t)/N(0)]
0
-0.1
-0.2
-0.3
-0.4
-0.5
-0.6
-0.7
-0.8
-0.9
-1
0 5 10 15 20 25 30 35 40 45 50
time (ps)

noted in Chapter III, ν_4 motion involves displacement along the Br-CF_2 center-of-mass coordinate. It is, therefore, not surprising that the rates for excitation of the reaction coordinate mode show this behavior.

Plots of the rate constants k versus the total energy E are shown in Fig. 11. All of the rate constants are plotted in Fig. 11(a) with the exception of those for ν_4 excitation for the region of fast decay. The latter are shown in Fig. 11(b); the rate constants for equipartition of the excitation energy are also shown for reference. Again, there is very little spread in the rate constants in Fig. 11(a), and the rate constants increase monotonically with increasing total system energy as expected.

Although the rate constants show no evidence of mode specificity (excluding excitation of ν_4), power spectra show that the dynamics are not globally chaotic (at least during the finite time interval sampled, namely 20.16 ps). Figure 12(a) shows a composite power spectrum (sum of the individual internal coordinate spectra) which corresponds to the first 20.16 ps for an ensemble of 50 trajectories for ν_6 (Br-C-F bending) initially excited to 35 kcal/mol. The structured areas can be assigned in terms of the CF_2Br normal modes. The maximum of the sharpest and most intense band occurs in the vicinity of 307 cm^{-1} which is slightly lower than the ν_6 normal mode frequency of 311 cm^{-1}. The reaction coordinate mode ν_4 (normal mode frequency of 331 cm^{-1}) appears as the broad structure located at the base of the ν_6 peak. The ν_4 band is also red-shifted as expected. The structured region in the range from about 500 to 700 cm^{-1} appears to have two maxima which can be attributed to ν_3 and ν_2 (normal mode frequencies of 562 and 676 cm^{-1}, respectively). The ν_2 maximum is red-shifted considerably from the normal mode frequency. This is not unexpected since this mode involves C-Br stretch motion. The broad high frequency bands can be attributed to the C-F stretch modes (normal mode frequencies of 1207 and 1326 cm^{-1}). As discussed in Chapter II, the internal coordinate time histories for

Figure 11. CF_2Br rate constants *vs* total system energy. (a) rate constants excluding those for excitation of ν_4: □, ν_1; ∗ , ν_2; +, ν_3; ×, ν_5; ■, ν_6; and ▲, equipartion of energy. (b) ν_4 rate constants for the region of fast decay with the equipartion rate constants shown for reference: +, ν_4 and ▲, equipartion of energy.

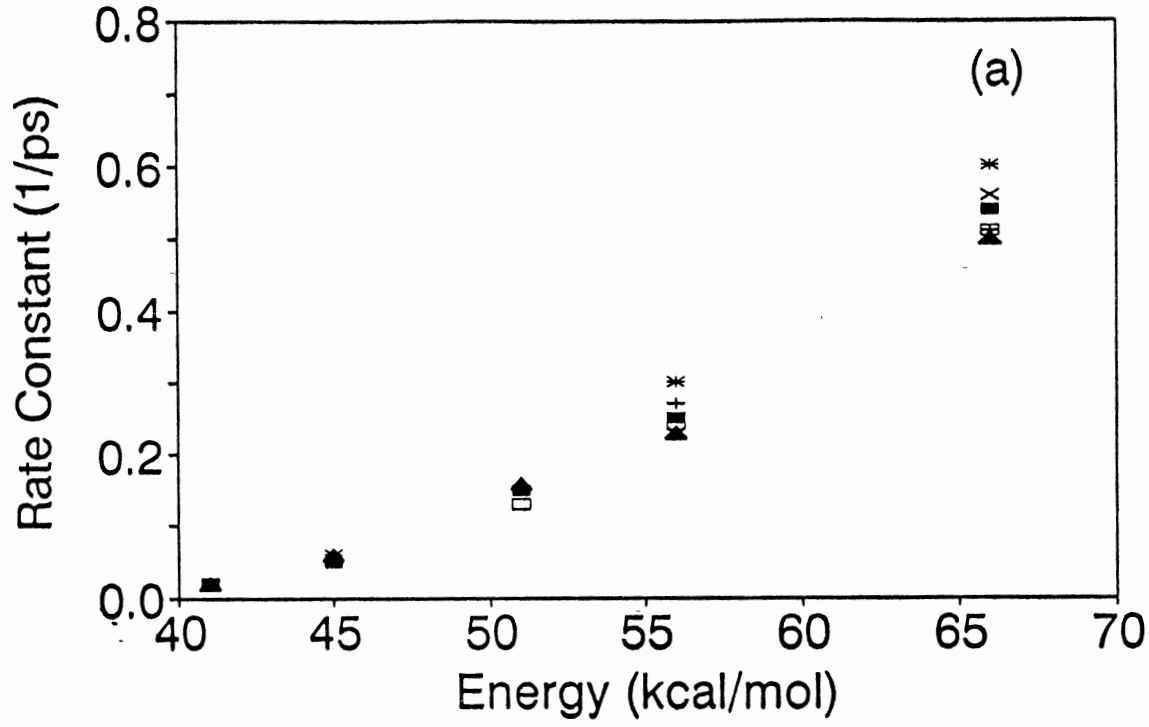
(a)
Rate Constant (1/ps)
0.0
0.2
0.4
0.6
0.8
40
45
50
55
60
65
70
Energy (kcal/mol)

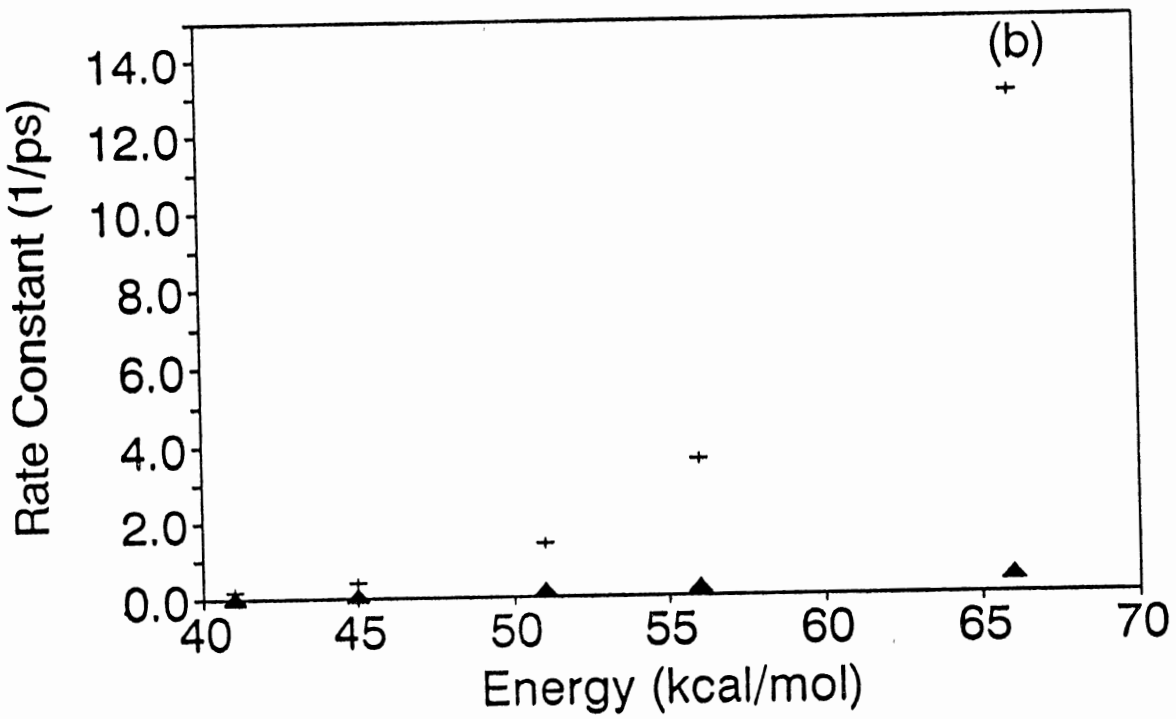
(b)
Rate Constant (1/ps)
0.0
2.0
4.0
6.0
8.0
10.0
12.0
14.0
40
45
50
55
60
65
70
Energy (kcal/mol)

Figure 12. CF_2Br power spectra for excitation of ν_6 to 35 kcal/mol. Power spectra are for the first 20.16 ps of an ensemble of 50 trajectories.
(a) composite spectrum; (b) spectrum of one of the Br-C-F angles;
(c) same as for (b) except with an expanded ordinate scale.

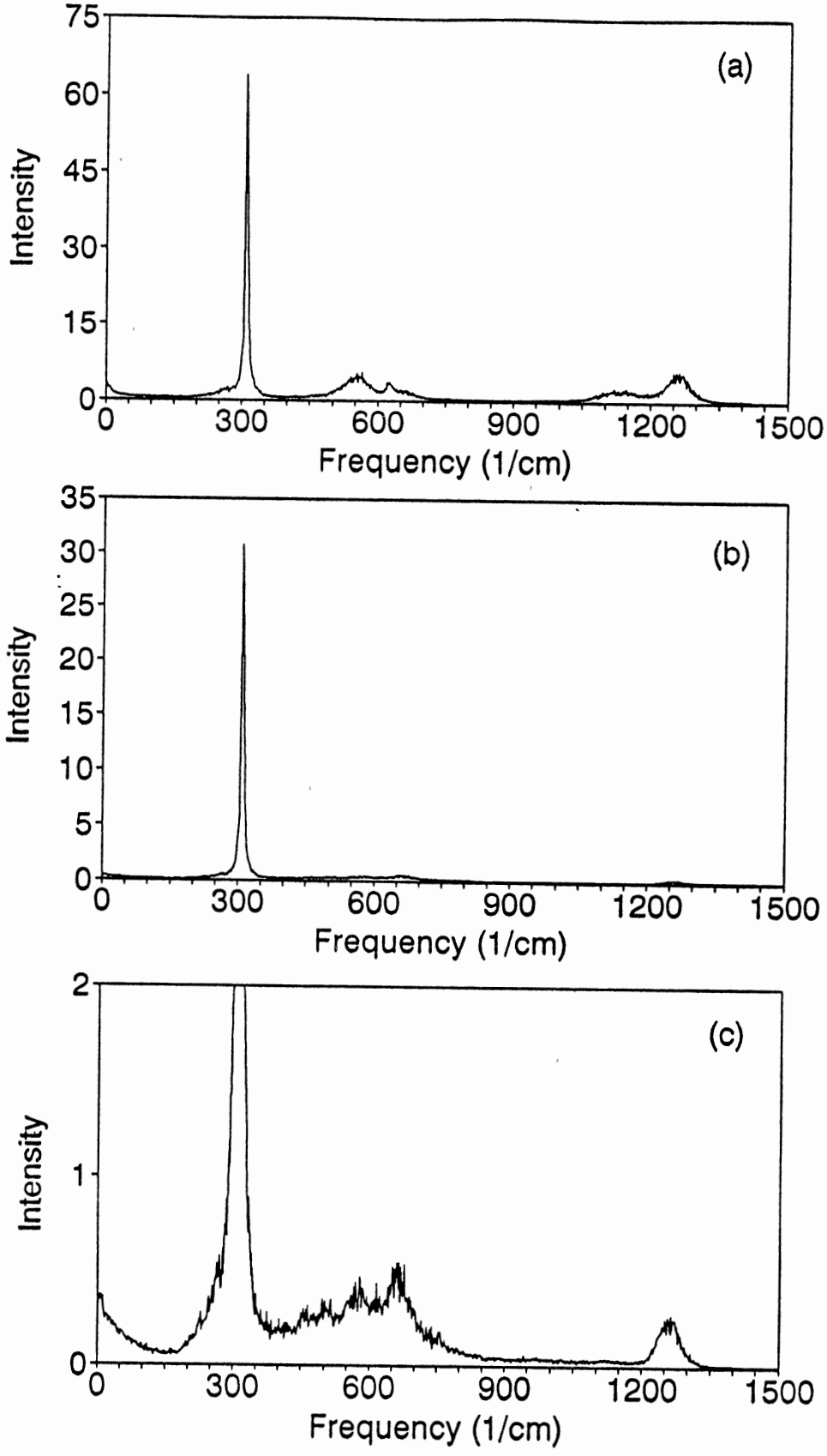
(a)
Intensity
75
60
45
30
15
0
0
300
600
900
1200
1500
Frequency (1/cm)
(b)
Intensity
35
30
25
20
15
10
5
0
0
300
600
900
1200
1500
Frequency (1/cm)
(c)
Intensity
2
1
0
0
300
600
900
1200
1500
Frequency (1/cm)

reactive trajectories were padded with zeros beyond the time of the last inner turning point of the C-Br bond. Therefore, effects due to translation and due to the product vibrational motion do not contribute to the spectra.

To determine the origin of the sharp peak at 307 cm^{-1}, the power spectra for the individual internal coordinates were examined. A power spectrum for one the Br-C-F angles is shown in Fig 12(b); it is one of the components of the spectrum in Fig. 12(a). The spectrum clearly demonstrates that the peak at 307 cm^{-1} is due to Br-C-F bending. There are no sharp peaks of comparable intensity present in the other internal coordinate spectra. In terms of an internal coordinate description of the normal modes, ν_6 is the "purest" normal mode corresponding almost solely to Br-C-F bending with the remainder of the normal modes described by motion which is due to some combination of internal coordinate displacements. Figure 12(c) is the same spectrum as Fig. 12(b) with the ordinate scale expanded. Even though the Br-C-F bend (θ_1) spectrum has a sharp peak at about the ν_6 normal mode frequency, this expanded scale reveals that the bend is mixing with other molecular modes. Structured areas are present in the vicinity of all of the other normal mode frequencies although at intensities almost two orders of magnitude less than observed for the ν_6 peak.

The power spectra provide an *average* frequency domain picture of the dynamics over the finite time of the data sample. Therefore, power spectra were calculated for 5 ps time windows of a 45 ps time history which is longer than the average reaction lifetime ($1/k$=42 ps) for the same initial conditions as Fig. 12. These spectra are shown in Fig. 13. Figure 13(a) is for the first 5 ps, Fig. 13 (b) is for the second 5 ps, etc. The important feature of these spectra is that the spectral structure is preserved over the reactive lifetime as evidenced by the last window, Fig. 13(i) (40-45 ps). No shift in the maximum of the 307 cm^{-1} peak is observed.

Figure 13. CF_2Br power spectra for excitation of ν_6 to 35 kcal/mol. An ensemble of 50 trajectories was employed. The individual spectra represent 5 ps time windows of a 45 ps trajectory which is inclusive of the average reaction lifetime for the stated initial conditions. (a) 0-5 ps; (b) 5-10 ps; (c) 10-15 ps; (d) 15-20 ps; (e) 20-25 ps; (f) 25-30 ps; (g) 30-35 ps; (h) 35-40 ps; (i) 40-45 ps.

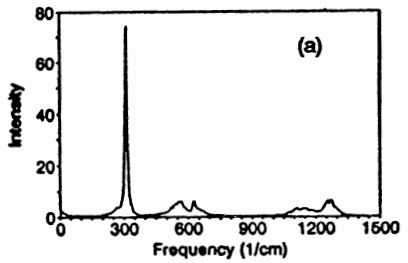
(a)
Intensity
Frequency (1/cm)
0
20
40
60
80
0
300
600
900
1200
1500

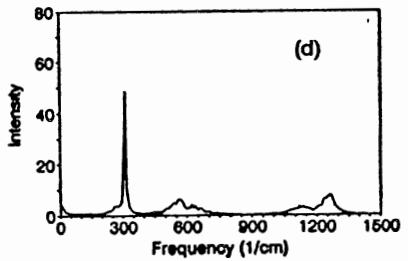
(d)
Intensity
Frequency (1/cm)
0
20
40
60
80
0
300
600
900
1200
1500

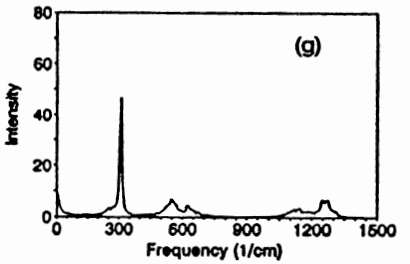
(g)
Intensity
Frequency (1/cm)
0
20
40
60
80
0
300
600
900
1200
1500

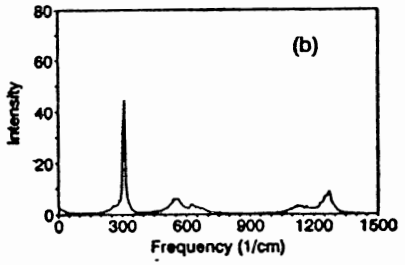
(b)
Intensity
Frequency (1/cm)
0
20
40
60
80
0
300
600
900
1200
1500

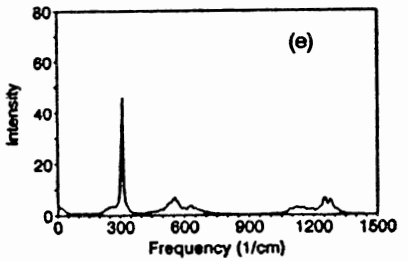
(e)
Intensity
Frequency (1/cm)
0
20
40
60
80
0
300
600
900
1200
1500

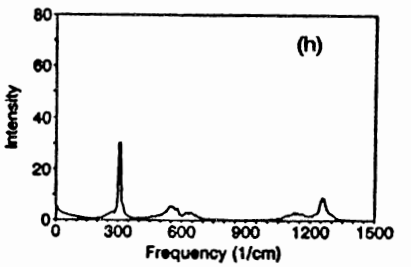
(h)
Intensity
Frequency (1/cm)
0
20
40
60
80
0
300
600
900
1200
1500

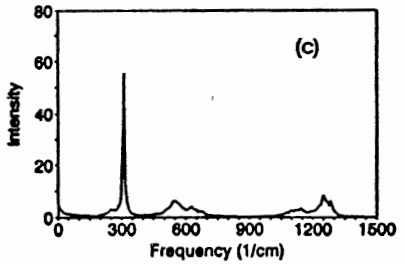
(c)
Intensity
Frequency (1/cm)
0
20
40
60
80
0
300
600
900
1200
1500

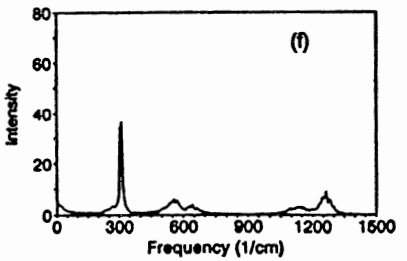
(f)
Intensity
Frequency (1/cm)
0
20
40
60
80
0
300
600
900
1200
1500

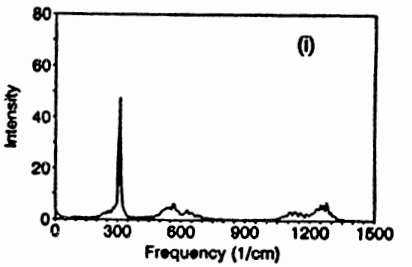
(i)
Intensity
Frequency (1/cm)
0
20
40
60
80
0
300
600
900
1200
1500

The spectra in Figs. 12 and 13 are for initial excitation of ν_6 which is almost exclusively Br-C-F bending. However, *all* of the normal modes involve some Br-C-F bending. Thus, the Br-C-F bends are excited irrespective of which normal mode is initially excited. The ν_1 mode involves the least amount of Br-C-F bending relative to other internal coordinate motions. Therefore, it is interesting that the peak at 307 cm^{-1} is still present when ν_1 is the excited mode. The power spectrum in Fig. 14(a) is for initial excitation of ν_1 to 35 kcal/mol for an ensemble of 50 trajectories. The sharp Br-C-F bending peak is still present. The power spectrum for the Br-C-F bend (θ_1) is shown in Fig. 14(b) for the same initial conditions as for Fig. 14(a). There is a very small increase in the intensity of the structured regions corresponding to mixing of the Br-C-F bend with other modes. This is displayed more graphically in Fig. 14(c) where the ordinate scale has been expanded to provide a better perspective of the structured regions. Some of the intensity at integer multiples of the frequency of the sharp ν_6 peak may be due to overtones, however, the broad appearance of the bands at higher frequencies suggests that structure is not due solely to overtone intensity.

To determine if the spectral structure in the vicinity of 307 cm^{-1} persists with increasing energy, power spectra were calculated for 60 kcal/mol excitation in modes ν_6 and ν_1 (see Figs. 15 and 16, respectively). Figures 15(a) and 16(a) are composite power spectra for ensembles of 50 trajectories. Figures 15(b) and 16(b) are the power spectra of one of the Br-C-F angles. The peak at approximately 307 cm^{-1} is still present and can be attributed to Br-C-F bending by examining Figs. 15(b) and 16(b). The Br-C-F bending motion still exhibits regular dynamics relative to the other internal coordinate motions even at very high energy. The composite spectra also retain structure which can be attributed to molecular motions associated with the other normal modes. For example, the two bands located between about 1050 and

Figure 14. CF_2Br power spectra for excitation of ν_1 to 35 kcal/mol. Power spectra are for an ensemble of 50 trajectories. The trajectories were calculated for 20.16 ps. (a) composite spectrum; (b) spectrum for one of the Br-C-F angles; (c) same as (b) except with an expanded ordinate scale.

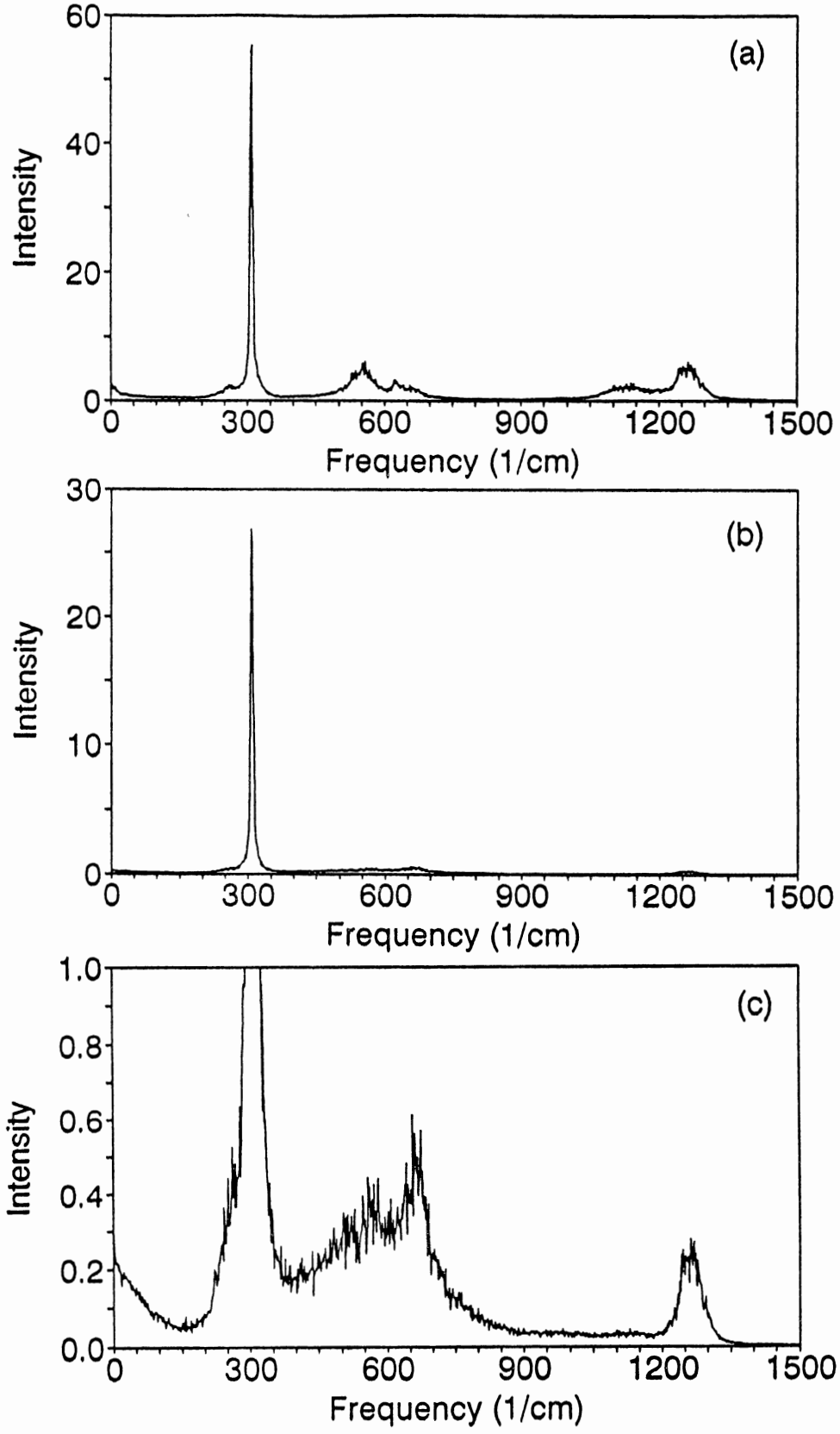
(a)
Intensity
60
40
20
0
0
300
600
900
1200
1500
Frequency (1/cm)
(b)
Intensity
30
20
10
0
0
300
600
900
1200
1500
Frequency (1/cm)
(c)
Intensity
1.0
0.8
0.6
0.4
0.2
0.0
0
300
600
900
1200
1500
Frequency (1/cm)

Figure 15. Power spectra for excitation of ν_6 to 60 kcal/mol. Power spectra are for a 50 trajectory ensemble. The trajectories were calculated for 20.16 ps. (a) composite spectrum; (b) spectrum for one of the Br-C-F angles.

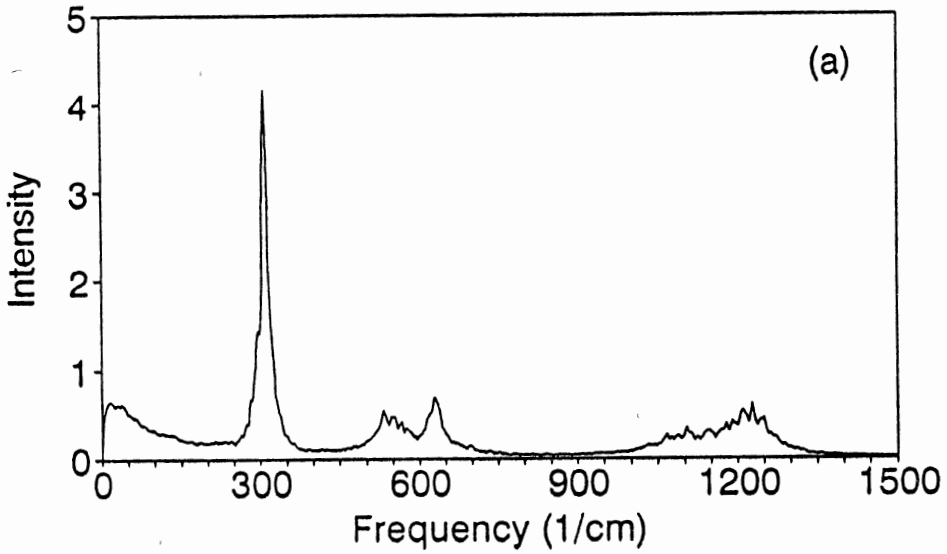
(a)
Intensity
Frequency (1/cm)
0
1
2
3
4
5
0
300
600
900
1200
1500

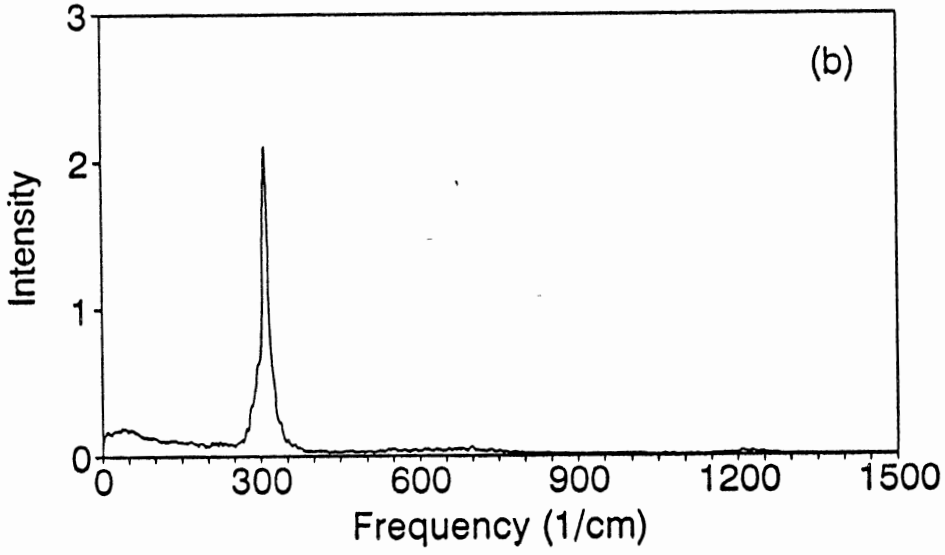
(b)
Intensity
Frequency (1/cm)
0
1
2
3
0
300
600
900
1200
1500

Figure 16. Same as Fig. 15 except for excitation of ν_1.

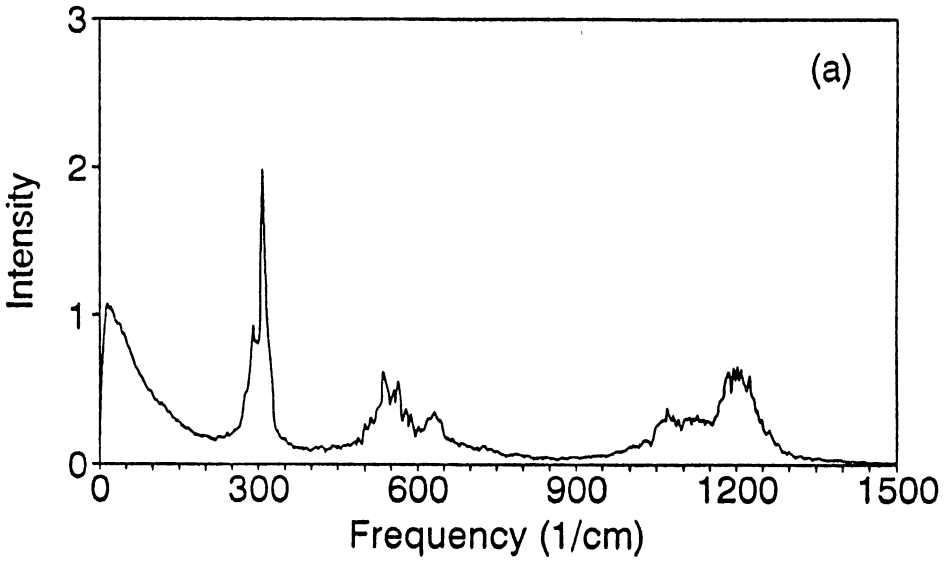
(a)
Intensity
3
2
1
0
0
300
600
900
1200
1500
Frequency (1/cm)

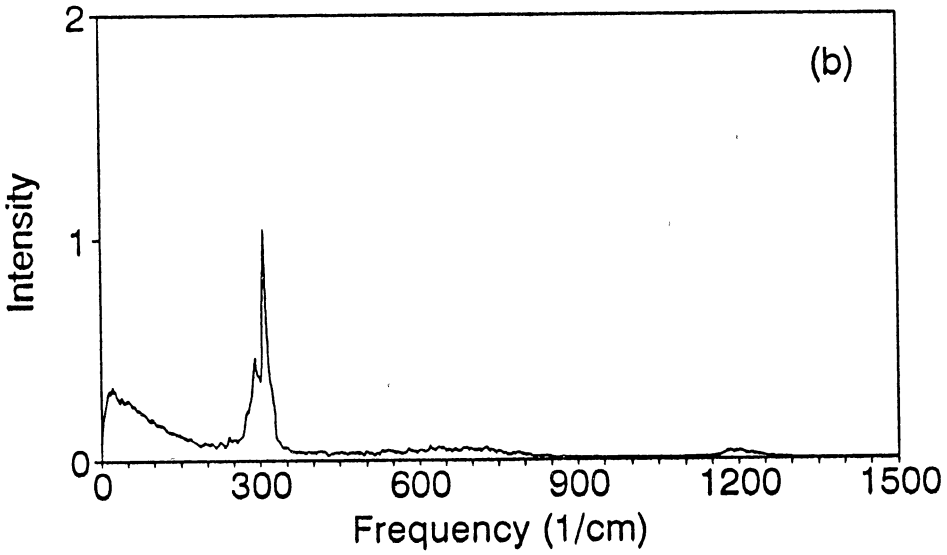
(b)
Intensity
2
1
0
0
300
600
900
1200
1500
Frequency (1/cm)

1350 cm^{-1} are due to C-F stretching (normal mode frequencies of 1207 and 1326 cm^{-1}). The localized nature of the peak at 307 cm^{-1} suggests that a difference should be evident in the rate constants for excitation of the ν_6 mode relative to the other modes. The initial conditions selection methods employed in this study do not result in excitation of a "pure" mode. Rather some combination of modes is initially excited, albeit the bulk of the excitation resides in the mode of interest (as evidenced by observation of mode-specific rates for studies wherein the same excitation scheme was employed[134]). A decrease in the rate for ν_6 excitation would require "pure" excitation of the C-Br-F bend. The eigenvectors for this mode contain some displacement in the other internal coordinates. The displacement in the F-C-F bend is almost two orders of magnitude less than that for the Br-C-F bends for a given excitation energy. The bond displacements are almost negligible. Nevertheless, *some* excitation energy will initially reside, because of the approximate energy assignment, in all of the internal coordinates when ν_6 initially contains the excitation energy. The mode energies for the initial conditions are also somewhat smeared by the scaling procedure[106] used to obtain isoenergetic ensembles of trajectories. These factors might be sufficient to account for the observation of statistical rate constants for ν_6 excitation. Even though the peak is well-defined in the power spectra (indicative of regular dynamics), the mode is still weakly coupled to other modes as illustrated by the expanded-scale power spectra in Figs. 12(c) and 14(c). This coupling may be sufficient to account for the nonselectivity of ν_6 excitation.

The sharp spectral structure attributed to the Br-C-F bends has been observed for bending vibrations in other molecules.[25] However, this effect is not always observed in the power spectra of bending vibrations. The internal coordinate power spectra of the F-C-F angle in CF_2Br does not have sharp spectral features. The spectra are very broadened.

To investigate the difference in appearance of the spectra for the two types of angles, the potential interaction constants for the angles were examined. Potential coupling has been found to be an important factor in the mode-specific behavior of molecules.[135] All of the potential interaction constants for the Br-C-F bends are "switched off" as the C-Br bond extends. Therefore the coupling between the harmonic bend angle and other molecular degrees of freedom is at a maximum at the equilibrium structure. However, the potential interaction constants for the F-C-F angle for terms in the potential which survive C-Br bond fission increase in magnitude with extension of the C-Br bond. The difference in the magnitudes of the potential-energy coupling terms for the bond angles at geometries displaced from equilibrium may explain the observed differences in the spectral structures.

N_2O_3

Quasiclassical trajectories were used to study vibrational predissociation in N_2O_3. Rate constants were calculated by fitting the trajectory lifetimes to Eq. (31). Calculations were carried out for various excitations of the nitro- and nitroso-group normal modes (ν_1, ν_2, ν_3, and ν_4) and combinations of these modes. All sets of initial conditions considered are shown in Table VII on page 121 along with the calculated lifetimes. (All lifetimes are calculated for ensembles of 200 trajectories unless otherwise noted.)

Calculations were carried out for which the total system energy was the same for two or more sets of initial conditions or for which the energy in the excited mode was the same for two or more sets of initial conditions. Specifically, in the first four sets of initial conditions shown in Table VII, the energy in the excited mode is 18.3 kcal/mol with the unexcited modes containing zero-point energy. The lifetimes for ν_1 and ν_2 are approximately four times longer than observed for ν_4. Initial conditions for

TABLE VII

CALCULATED LIFETIMES FOR N_2O_3

Excitation[a]	Total Energy[b]	Lifetime[c]
$3.00\nu_1$ (18.30)	25.90	9.7
$3.36\nu_2$ (18.29)	26.13	9.9
$4.45\nu_3$ (18.31)	26.68	2.1
$7.70\nu_4$ (18.29)	27.39	0.9[d]
$3.28\nu_1$ (19.77)	27.36	8.0[e]
$4.64\nu_3$ (19.01)	27.36	2.2[f]
$0.36\nu_1$ (4.52), $0.40\nu_2$ (4.28), $0.52\nu_3$ (3.76), $0.86\ \nu_4$ (3.03), $1.60\nu_5$ (2.51), $2.84\nu_6$ (2.25), $2.77\nu_7$ (2.25), $1.08\nu_8$ (2.80), $0.59\nu_9$ (2.01)	27.39	3.9[e]
$0.08\nu_1$ (3.03), $0.14\nu_2$ (3.03), $0.32\nu_3$ (3.03), $0.86\nu_4$ (3.03), $2.04\nu_5$ (3.04), $4.01\nu_6$ (3.04), $3.92\nu_7$ (3.04), $1.21\nu_8$ (3.04), $14.76\nu_9$ (3.04)	27.32	3.0
$3.28\nu_1$ (19.77), ⅓ zero-point energy in other modes	22.35	16.6[g]
$7.70\nu_4$ (18.29), ⅓ zero-point energy in other modes	21.39	1.7
$3.00\nu_3$ (16.58)	24.43	14.4
$4.00\nu_3$ (16.65)	25.01	3.2[d]
$7.00\nu_4$ (16.73)	25.83	2.0[d]
$5.91\nu_4$ (14.30)	23.40	2.4
$2.00\nu_2$ (11.84), ν_3 (5.55)	23.39	12.2
$2.00\nu_3$ (9.25), ν_2 (7.11)	22.35	9.1
$2.00\nu_2$ (11.84), ν_4 (3.35)	21.92	17.3

[a]Excitations given in terms of quanta per mode with the excited mode energy shown in parentheses. Fractional quantum numbers were used to obtain isoenergetic mode and total system energies. [b]Units of energy are kcal/mol. [c]Units of time are ps. [d]199 trajectory ensemble. [e]400 trajectory ensemble. [f]395 trajectory ensemble. [g]100 trajectory ensemble.

a total system energy of 27.4 kcal/mol include ν_1=3.28, ν_3=4.64, ν_4=7.70, and equipartition of the excitation energy among all of the normal modes. The lifetime of ν_1 is approximately 8 times longer than for ν_4 and 3.6 times longer than for ν_3. The set of initial conditions for which the energy was equipartitioned among all of the normal modes gives a lifetime of 3.9 ps, which is about one-half that observed when all of the excitation energy is placed into ν_1 (τ=8.0 ps).

The results indicate that the ν_4 bending mode is the most efficient mode for initiating cleavage of the N-N bond both for initial conditions for which the energy in the excited mode is initially at the same value and for which the total system energy is initially at the same value. The symmetric stretch appears to be the second most effective mode, again for both types of initial excitations. The behavior of excited ν_1 and ν_2 appears to be similar with both of these modes having calculated lifetimes about 4.5 times longer than for excited ν_3 and about 10 times longer than for excited ν_4 when the energy in the excited mode is 18.3 kcal/mol. Inspection of the N_2O_3 normal modes reveals that the nitro group bend (ν_4) and symmetric stretch (ν_3) normal modes involve motions with significant components directed along the N-N bond. In contrast, the nitroso group stretch (ν_1) and the nitro group asymmetric stretch (ν_2) do not have significant components of motion projected along the N-N bond. Therefore, one would intuitively expect that excitation energy deposited in ν_3 or ν_4 would enhance the rate of vibrational predissociation relative to placing the energy in ν_1 or ν_2 (in the absence of other factors such as nonlinear resonances). It thus appears that the significant projection of ν_3 and ν_4 onto the N-N bond may account for the enhancement in the vibrational predissociation rate for excitation of these modes relative to ν_1 or ν_2.

As discussed in Chapter I, Waite and Miller[27] illustrated the role of motion directed along the reaction coordinate in mode-specific behavior in some studies of

the Henon-Heiles system. They calculated quantum-mechanical rate constants for tunneling using one- and three-barrier potentials. There are modes for the one-barrier potential for which no component of the motion is directed along the reaction coordinate and the results are mode-specific. There are no modes for the three-barrier potential which do not project onto at least one of the reaction coordinates. Statistical behavior was observed even at energies at which the motion is quasiperiodic and, thus, where mode-specific behavior might be expected.

Casassa, Stephenson, and King[28] also considered the importance of "geometrical factors" in the $(NO)_2$ dissociation. They refer to the V→T model developed by Ewing,[29] which includes as a parameter the effective component of the initial vibrational motion along the weak bond. Ewing's model reproduces the observed mode specificity for the $(HF)_2$ system for which one of the modes (ν_2) has a *significant* projection along the van der Waals bond. However, the results of Casassa *et al.* indicate that these factors solely cannot account for the mode specificity observed for $(NO)_2$. However, both the ν_1 and ν_4 modes in $(NO)_2$ have only *slight* projections along the N-N bond. For N_2O_3 there are slight projections for the nitroso group stretch (ν_1) and the nitro group asymmetric stretch (ν_2) (slow energy transfer) and significant projections for the nitro group symmetric stretch (ν_3) and bend (ν_4) modes (fast energy transfer).

Chewter, Smith, and Yarwood[74] reported vibrational predissociation lifetimes for the $n\nu_1$ (n=1 to 4) bands of N_2O_3. The linewidths observed for transitions in the $3\nu_1$ band were used to estimate a lifetime $>$ 150 ps for $3\nu_1$, which they report as a lower limit to the lifetime for vibrational predissociation to NO + NO_2. In addition, Chewter *et al.* used the simplified statistical adiabatic channel model (SACM)[136] to calculate first-order rate constants. They obtained a value of 65×10^{11} s^{-1} for the energy of the $3\nu_1$ transition (assuming J=0). This corresponds

to a lifetime of .15 ps. On the basis of the disparity between the experimental and RRKM lifetimes, Chewter *et al.* concluded that "at least in this respect, N_2O_3 exhibits markedly 'non-RRKM behavior.'"

The lifetime calculated with trajectories for ν_1=3 (9.7 ps) falls between the experimental and RRKM lifetimes reported by Chewter *et al.*[74] The difference between the trajectory and experimental lifetimes may be due in part to zero-point energy effects.

Zero-point energy leakage in classical trajectory studies has been discussed in several articles.[134(g),137,138] The well-depth of the dissociating bond in N_2O_3 is only 10.1196 kcal/mol. Therefore, the inclusion of the full zero-point energy (10.2 kcal/mol) may lead to vibrational predissociation rates that are too high due to aphysical flow of zero-point energy. The use of fractional zero-point energy has been explored by Guan, Uzer, MacDonald, and Thompson.[134(g)] They noted little change in the relative rates as a function of the initial excitation sites when the zero-point energy was reduced by two-thirds in a study of dissociation of H_2O_2. To examine zero-point energy effects in N_2O_3, ensembles of 100 trajectories were calculated for the ν_1=3 and the ν_4=7.70 excitations with the initial energy in each of the remaining normal modes initially at one-third of the zero-point energy for that mode. The lifetimes for these ensembles are 16.6 and 1.7 ps, respectively. The lifetimes for these same excitations using the full zero point energy are 9.7 and 0.9 ps, respectively. There is about an order of magnitude difference in the calculated lifetimes for excitaiton of ν_1 relative to ν_4 independent of the value used for the zero-point energy. These results suggest that zero-point energy leakage does not affect the qualitative behavior of the calculated vibrational predissociation lifetimes, only their magnitudes.

Figure 17 is a plot of the vibrational predissociation rate constants k versus

Figure 17. Rate constants *vs* total system energy for N_2O_3 for various initial conditions: (⊡) ν_1 excitations; (♦) ν_2 excitations; (×) ν_3 excitations; (◇) ν_4 excitations; (▵) ν_1 excitation with 1/3 zero-point energy; (▲) ν_4 excitation with 1/3 zero-point energy; (□) excitations of combinations of modes; (+) equipartition of energy for which the same *excitation* energy (in excess of the zero-point energy) is placed in each mode; and (o) equipartition of energy for which the same *total* energy is placed in each mode.

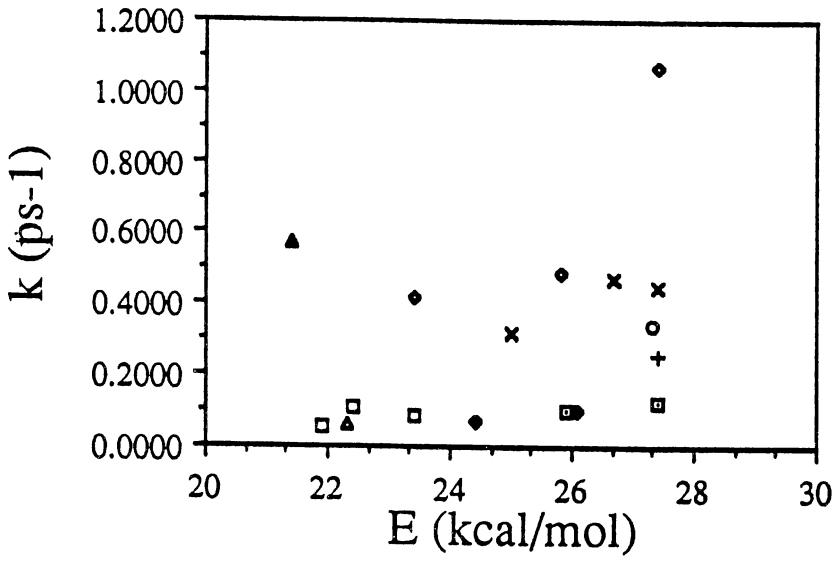
1.2000
1.0000
0.8000
0.6000
0.4000
0.2000
0.0000
k (ps-1)
20
22
24
26
28
30
E (kcal/mol)

the total system energy E for all the initial conditions considered. If the system behaves statistically (i.e., if the rate of intramolecular energy randomization is much faster than the rate of the N-N bond fission), the rate constants should display a monotonically increasing dependence on the total system energy independent of the manner in which the energy is initially partitioned into the molecule. Examination of Fig. 17 reveals a scatter of the rate constants with no functional dependence on the total system energy. In other words, the rate is dictated by the manner in which the energy is initially partitioned among the normal modes and that despite the imprecise method employed for initial state selection, fluctuations in the rates are observed.

As discussed in Chapter I (see pg. 20), rate constants for dissociation of the $(N_2O_3)^\dagger$ association complex are statistical[73] in contrast to the nonstatistical rates obtained for N_2O_3.[74] Smith and Yarwood[73] have attributed the statistical behavior of the $(N_2O_3)^\dagger$ association complex to enhanced energy flow from the ν_1 mode when the lower frequency modes of the complex are excited (as is the case for the $(N_2O_3)^\dagger$ complex). Smith[139] pointed out that there may be additional reasons that the results of the association reaction agree so well with statistical calculations. The first reason that he stated relates to intrinsically non-RRKM behavior. That is, there might be different time-scales for energy flow from the ν_1 mode into different modes in the association complex. However, he notes that energy flow into the low frequency modes (which are excited during formation of the complex) may be very rapid. The complex might then survive long enough for subsequent flow from the low frequency modes into the "stiffer modes" so that those states participate in determining the density of states. Therefore, statistical theories would hold. To investigate the mechanism for energy flow, five trajectory ensembles were used to perform a limited analysis of the energy in the normal vibrational modes. Figures 18 through 21 are plots of the normal mode energies *vs* time in units of akma (.978 ps/20 akma). The

plots in Fig. 18 are for initial conditions for which ν_6=14 (9.77 kcal/mol) with all other modes containing one-tenth zero-point energy for a total system energy of 10.758 kcal/mol. Figure 18 shows rapid energy flow from ν_6. The predominant mechanism for relaxation of ν_6 is *via* ν_5 which is a low frequency (415 cm^{-1}) bending mode of the $(N_2O_3)^{\dagger}$ complex. Limited energy flow into ν_1 (the nitroso group stretch) is also observed. Energy is beginning to transfer into ν_4 (nitro group bend) just prior to termination of the trajectories.

Figure 19 corresponds to initial conditions for which ν_5=7.70 (9.80 kcal/mol) with the other modes containing one-tenth zero-point energy for a total system energy of 10.766 kcal/mol. Energy flow from ν_5 is primarily into ν_6 (the reaction coordinate mode). Once again, some initial energy flow into ν_1 is observed with ν_4 picking up energy near the end of the trajectories. Figure 20 represents initial conditions for which ν_6=5.44 (4.00 kcal/mol), ν_1=.55 (5.49 kcal/mol), and the other modes contain one-tenth zero-point energy for a total system energy of 10.22 kcal/mol. Energy flow from ν_6 is initially rapid, flowing predominantly into ν_5. No decay of energy from ν_1 is observed. Figure 21 is for ν_6=5.66 (4.15 kcal/mol) and ν_1=.67 (6.12 kcal/mol), with the other modes containing one-third zero-point energy. The interesting difference between the plots in Fig. 21 and the plots in the Figs. 18, 19, and 20 is that the increase in zero-point energy apparently strengthens the coupling to ν_4 as evidenced by an earlier onset of energy flow into that mode. No significant loss of energy is detected for ν_1 for the 0.25 ps timescale. The calculations for ν_4 were extended to 0.5 ps, however, ν_1 remained relatively uncoupled to the other modes.

Figure 18. Plots of normal mode energies *vs* time for N_2O_3. Initial conditions are for excitation of ν_6 to 9.77 kcal/mol. The other modes contain one-tenth of their zero-point energies. The total system energy is 10.758 kcal/mol. (a) ν_6 , ν_7 , and ν_9 ; (b) ν_4 , ν_5 , and ν_8 ; (c) ν_1 , ν_2 , and ν_3.

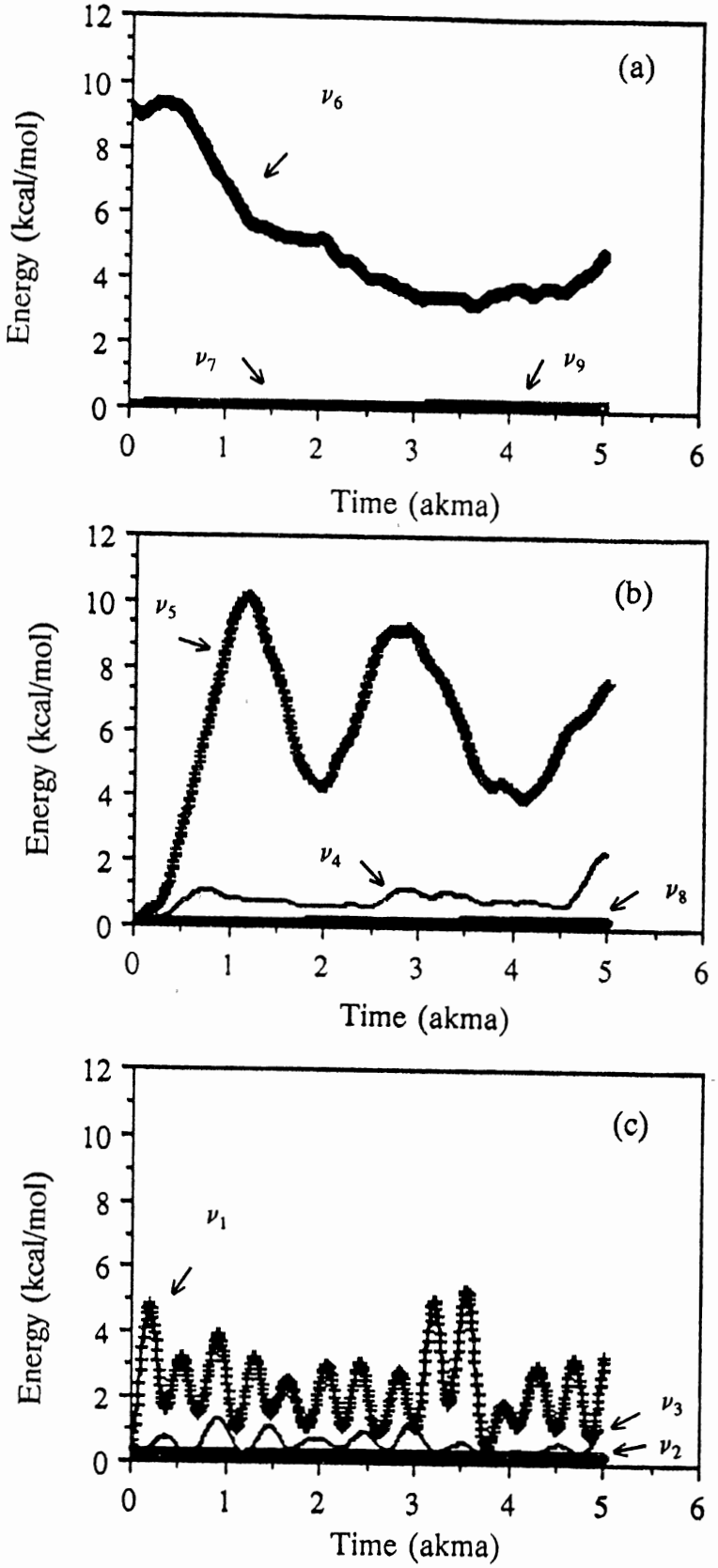
(a)
ν_6
ν_7
ν_9
Energy (kcal/mol)
Time (akma)
(b)
ν_5
ν_4
ν_8
Energy (kcal/mol)
Time (akma)
(c)
ν_1
ν_3
ν_2
Energy (kcal/mol)
Time (akma)

Figure 19. Same as Fig. 18 except for excitation of ν_5 to 9.80 kcal/mol. The total system energy is 10.766 kcal/mol.

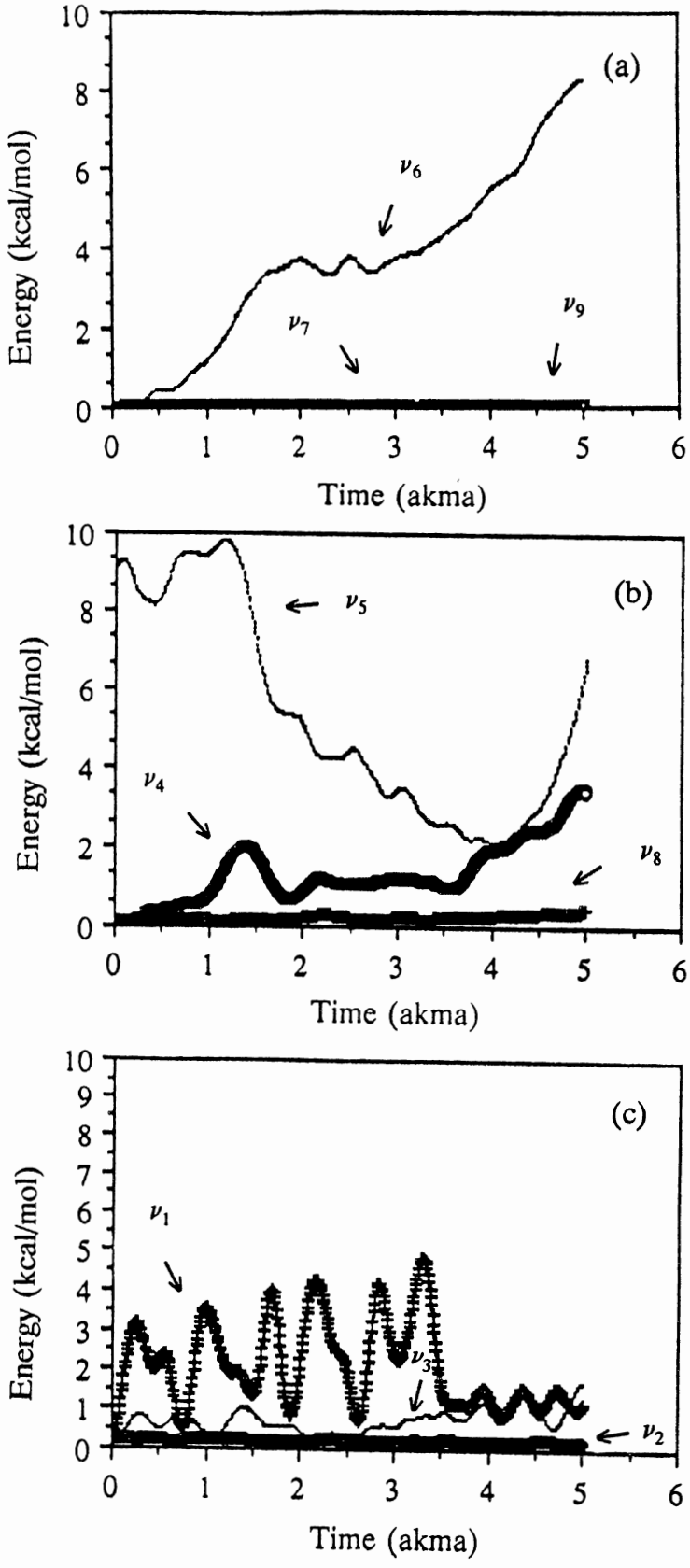
(a)
Energy (kcal/mol)
Time (akma)
ν_6
ν_7
ν_9
(b)
ν_5
ν_4
ν_8
(c)
ν_1
ν_3
ν_2

Figure 20. Same as Fig. 18 except for excitation of ν_6 to 4.00 kcal/mol and ν_1 to 5.49 kcal/mol. The total system energy is 10.22 kcal/mol.

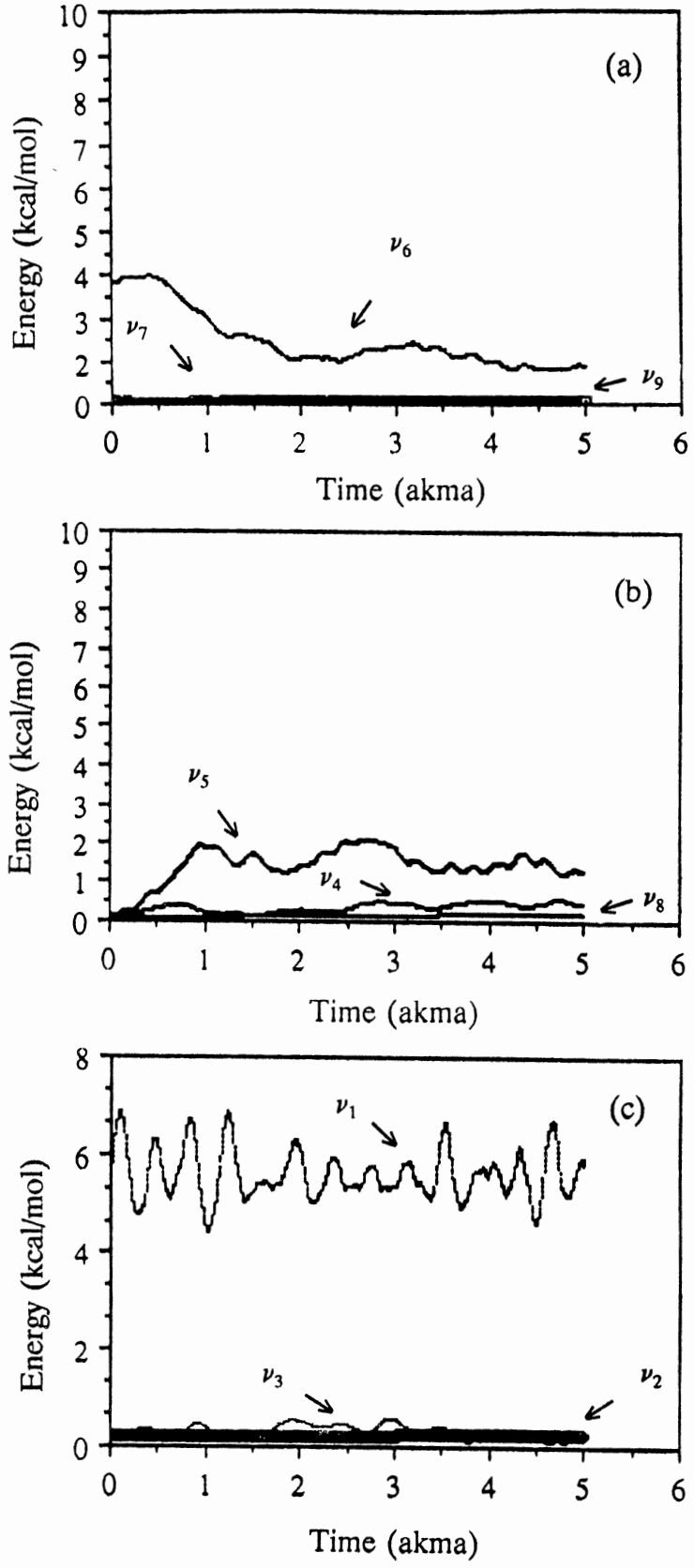
(a)
Energy (kcal/mol)
Time (akma)
ν_6
ν_7
ν_9
(b)
Energy (kcal/mol)
Time (akma)
ν_5
ν_4
ν_8
(c)
Energy (kcal/mol)
Time (akma)
ν_1
ν_3
ν_2

Figure 21. Same as Fig. 18 except for excitation of ν_6 to 4.15 kcal/mol and ν_1 to 6.12 kcal/mol with the other normal modes containing one-third of their zero-point energies.

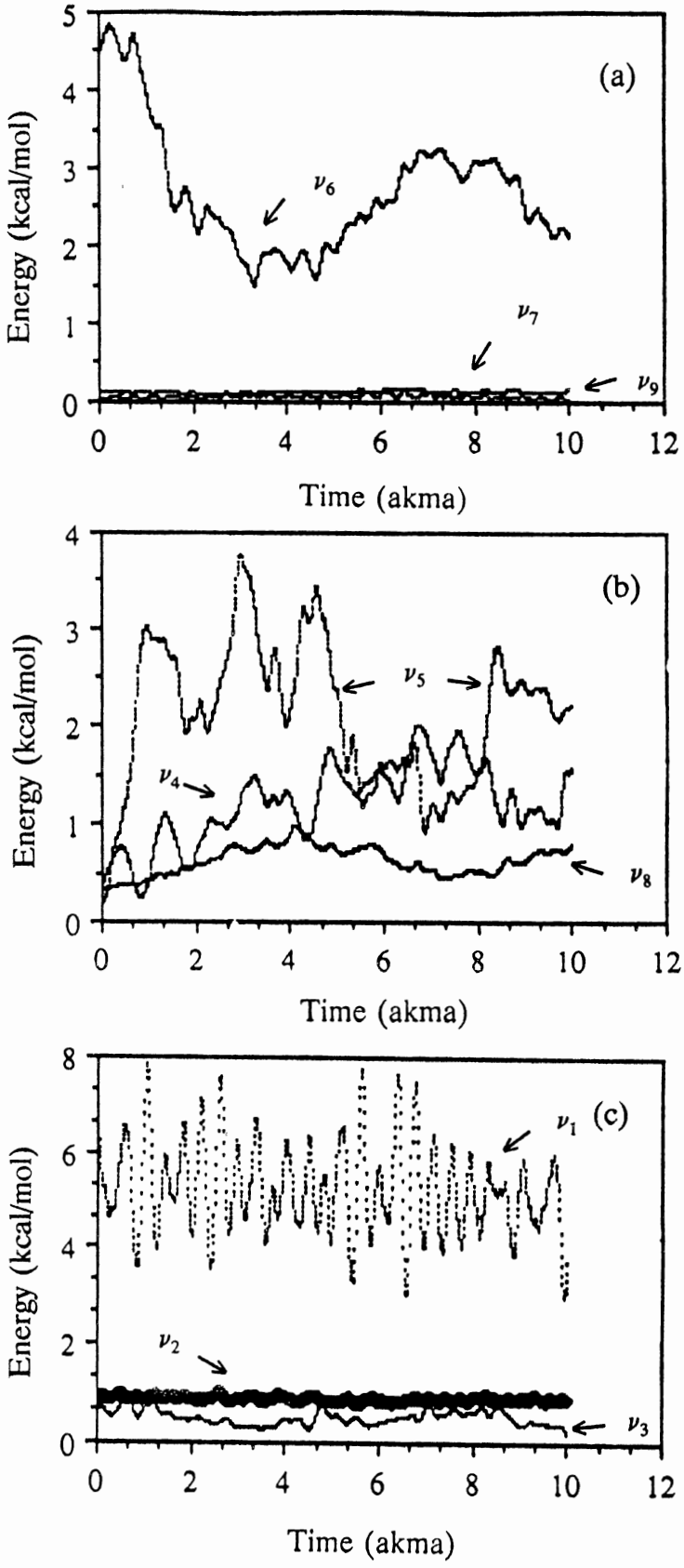
(a)
Energy (kcal/mol)
Time (akma)
ν_6
ν_7
ν_9
(b)
Energy (kcal/mol)
Time (akma)
ν_5
ν_4
ν_8
(c)
Energy (kcal/mol)
Time (akma)
ν_1
ν_2
ν_3

SiH_5^-

To determine the quality of the fitted surface for SiH_5^-, a normal mode analysis was performed at each of the *ab initio* points. The calculated normal mode frequencies at the eight points included in the cubic spline fits are within 1 cm^{-1} of the *ab initio* values. The normal mode frequencies at the point that was excluded from the fits are given in Table VIII with the *ab initio* frequencies given for comparison. The frequencies calculated from the fit are in good agreement with the *ab initio* frequencies with the exception of ν_8. However, differences of this magnitude are not uncommon even for potential-energy surfaces of polyatomic molecules at the equilibrium geometry. Since the equations of motion cannot be integrated successfully without excluding point eight, the quality of the fit was judged to be acceptable. It would be desirable to calculate the normal mode frequencies at additional *ab initio* points to determine the quality of the fit for different regions along the IRC.

Preliminary trajectory calculations revealed a significant flaw in the fitted potential-energy surface. Since the potential only connects three transition states which are accessible from one equilibrium configuration of the molecule, trajectory calculations are limited to energies below the pseudorotation barrier height, namely 2.5 kcal/mol. Therefore, it was necessary to use intial conditions with individual normal mode energies well below their zero-point energies. The initial conditions for the trajectories corresponded to placing 1.229 kcal/mol of energy in the reaction coordinate mode ν_9 and a total of .004 kcal/mol in the other normal modes. As previously noted, certain of the potential parameters from the *ab initio* results are divergent at equilibrium. At a value of the reaction coordinate of approximately 140°, the cubic spline fits abruptly begin to "switch" the potential parameters to the equilibrium structure values (the reaction coordinate is 120° at equilibrium).

TABLE VIII

HARMONIC NORMAL-MODE FREQUENCIES (CM^{-1})

	Fitted Potential	Ab Initio
ν_1	2017	2018
ν_2	1460	1460
ν_3	1609	1609
ν_4	1079	1079
ν_5	1989	1989
ν_6	1976	1976
ν_7	1083	1092
ν_8	1157	1109
ν_{10}	578	587
ν_{11}	1270	1270
ν_{12}	1243	1243

Figure 22 is a plot of the cubic spline fit to the *ab initio* points in Fig. 8. The steep "switching" region is between the equilibrium structure and a value of the reaction coordinates of 140° on either side of equilibrium. Figure 23(a) is a plot of the minimum energy path between TS 1 and TS 3. The minimum of the potential-energy surface occurs at $\xi_1=\xi_3=120°$. The reaction coordinates are $\xi_1=90°$ and $\xi_3=180°$ at TS 3 and $\xi_1=180°$ and $\xi_3=90°$ at TS 1. Figure 23(b) is a plot of ξ_3 *vs.* ξ_1 from a trajectory calculation. This figure illustrates significant divergence from the reaction path at approximately 140° as the trajectory approachs equilibrium. That this occurs near the value of the reaction coordinate where "switching" between the divergent functions begins cannot be mere coincidence. Since, the current form of the potential-energy surface results in the potential energy for geometries which are displaced from the minimum energy path being isoenergetic with geometries on the minimum energy path, the floppy molecule that results when a number of the potential parameters are "switched" to zero at equilibrium apparently allows trajectories to transverse the region between two reaction channels. Examination of the values of all three of the dihedral angles revealed that some of the trajectories appeared to follow two reaction paths simultaneously in this region of the potential-energy surface. This, of course, corresponds to a geometry intermediate between two channels. The limited form of the potential reported here does not account for this situation.

The problems encountered can be attributed to maintaining the symmetry of the molecule and therefore to the use of redundant internal coordinates. Ischtwan and Collins[59] noted similar concerns regarding an approximate potential for $NH_3^+ + D_2$ obtained from reaction path results. A more judicious choice of internal coordinates might be sufficient to eliminate the problems encountered here. It should also be noted that the results presented here demonstrate that an accurate fit to the harmonic

vibrational frequencies does not guarantee a reasonable form for the potential-energy surface.

Figure 22. Cubic spline fit of the *ab initio* interaction constants shown in Fig. 8.

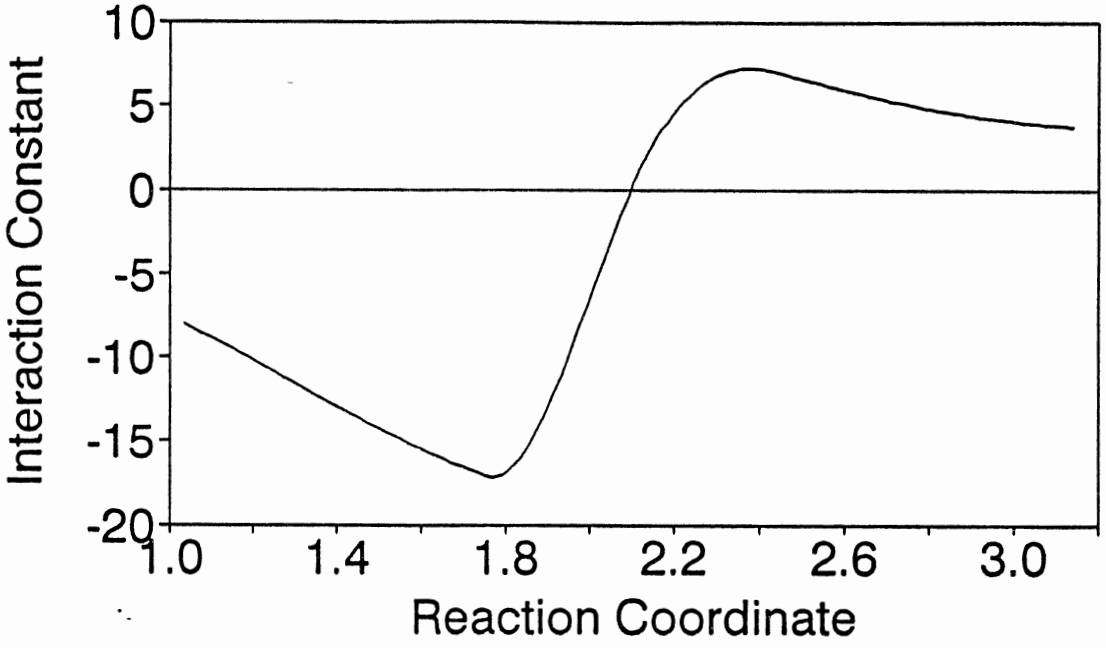
10
5
0
-5
-10
-15
-20
Interaction Constant
1.0
1.4
1.8
2.2
2.6
3.0
Reaction Coordinate

Figure 23. Plots of the SiH_5^- reaction coordinates ξ_3 *vs.* ξ_1. (a) minimum energy path (b) results from a trajectory calculation.

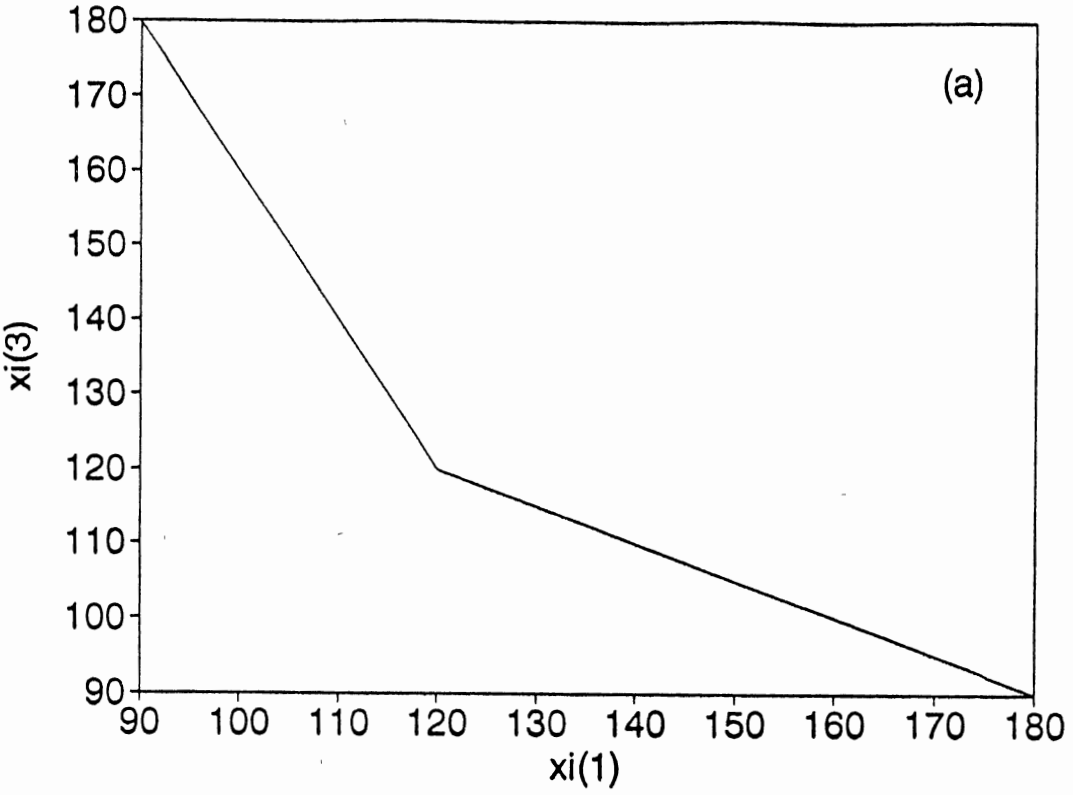
(a)
180
170
160
150
140
130
120
110
100
90
xi(3)
90 100 110 120 130 140 150 160 170 180
xi(1)

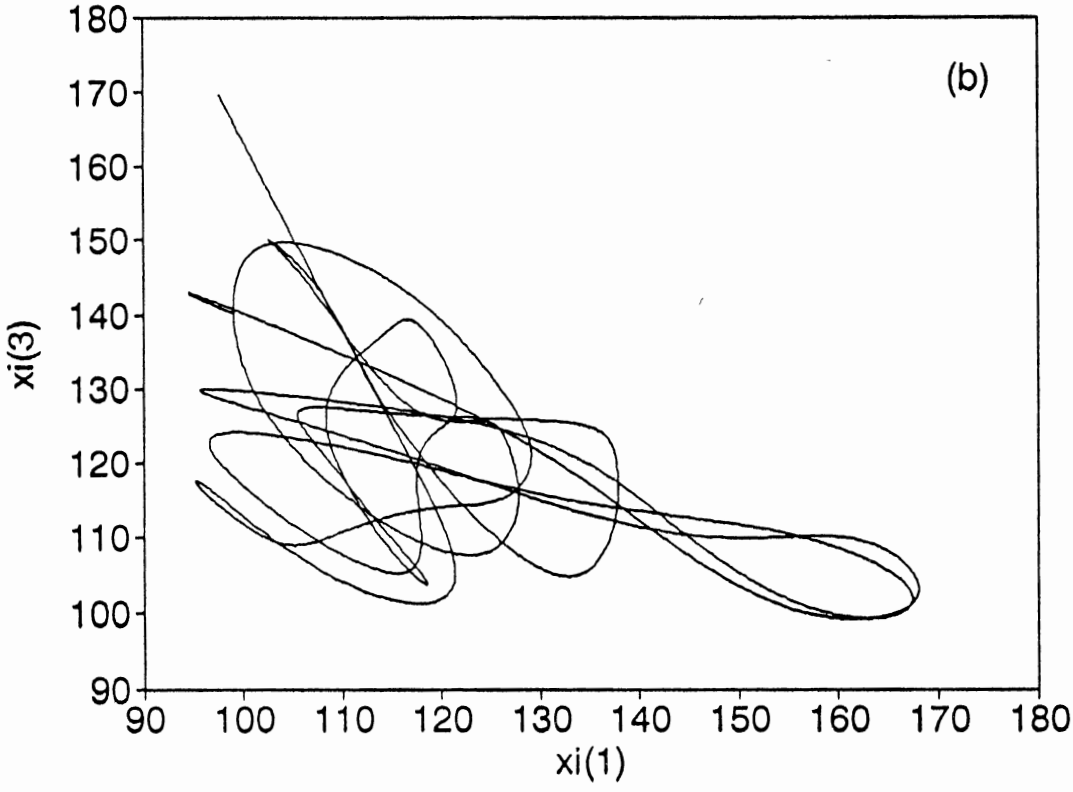
(b)
180
170
160
150
140
130
120
110
100
90
xi(3)
90 100 110 120 130 140 150 160 170 180
xi(1)

CHAPTER V

CONCLUSIONS

CF_2Br

The computed power spectra of the CF_2Br system demonstrate localization in the frequency domain. A sharp peak is present at about the ν_6 (Br-C-F bend) frequency in all of the power spectra that were examined for various initial conditions. Furthermore, in a series of power spectra for 5 ps time windows of a 45 ps time history, the peak remains well-defined over the entire time history. The power spectra show the presence of regular dynamics at excitation energies well above the C-Br bond dissociation energy. However, the calculated rate constants show that sufficient interaction must be occurring between ν_6 and other modes to prevent a decrease in the rate of reaction when ν_6 initially contains all of the excitation energy. The rate constants demonstrate mode selectivity only with respect to direct excitation of the reaction coordinate mode; there is no selectivity in the rates for excitations of the other normal modes. Furthermore, except for ν_4, the rate constants are comparable to those for equipartition of the excitation energy among the normal modes.

These results demonstrate that for the CF_2Br Hamiltonian used in this study, regular dynamics is not a sufficient condition for mode-specific reaction rates. Additional studies employing state-specific initial conditions would be useful for examining the effect of regular dynamics on the rate of chemical reaction. Another prospective direction for future studies is the identification and characterization of the

molecular modes which are responsible for the sharp peaks in the power spectra. The internal coordinate description used in the studies reported here provide a limited, but physically intuitive, description of the molecular dynamics.

N_2O_3

We have used classical trajectories to study mode-selective vibrational predissociation in N_2O_3. The results are in accord with the conclusion of Chewter, Smith and Yarwood[74] that N_2O_3 vibrational predissociation exhibits non-RRKM behavior. We find strong mode-selective behavior as evidenced by the variation in the rate as a function of the initial partitioning of energy among the normal modes. This variation in the rates can be explained by the extent to which the excited modes project onto the reaction coordinate. The nitro group bending (ν_4) and symmetric stretching (ν_3) modes involve motion with significant components directed along the N-N bond (approximately the reaction coordinate), while the nitroso group stretch (ν_1) and the nitro group asymmetric stretch (ν_2) do not. The trajectory results show that ν_4 mode excitation is the most efficient in promoting dissociation and ν_3 is the second most effective mode. The lifetimes for ν_1 and ν_2 excitations are significantly longer than those for ν_3 and ν_4 excitations.

The calculations for the energy in the normal modes as a function of time suggest that the dominant pathway for energy flow out of the N-N stretch (ν_6) is *via* the ν_5 bending mode. From ν_5 energy flows into the ν_4 (nitro group bend) mode. For the timescales and initial conditions examined, ν_1 remains relatively uncoupled from the other modes. A more comprehensive investigation of the mechanistic pathways for energy flow could be accomplished by employing larger ensembles and a larger variety of initial conditions. To truly test the proposal made by Smith regarding the statisticality of the rates for the association complex, initial conditions should be

considered which include initial excitation of the low frequency complex modes.

It would be instructive in future studies to examine theoretically the role of projection in chemically bound molecules such as HFCO for which mode-localized behavior has been demonstrated experimentally.[12]

SiH_5^-

The results of the studies reported here for fitting the SiH_5^- potential-energy surface demonstrate that accurate determination of a global potential-energy surface requires information for regions displaced from the minimum-energy path. Specifically for SiH_5^-, additional *ab initio* information is required for regions between the reaction channels. We must therefore conclude that the information provided by an *ab initio* IRC calculation is not sufficient to allow for a global description of the potential-energy surface suitable for a full dynamical investigation of molecular isomerizations such as the Berry pseudorotation process in SiH_5^-. *Ab initio* results for intermediate regions of the potential might be incorporated into the potential-energy surface by using a technique similar to that applied by Wall and Porter[39] to rotate a Morse curve between two reaction paths.

An additional consideration is definition of a set of coordinates which is appropriate to the problem under investigation. A Hamiltonian based on curvilinear normal modes and local modes has recently been reported for benzene.[140] Cubic and quartic terms were included in the expressions for the potential and kinetic energies. Higher order derivatives from *ab initio* calculations are being reported more frequently. Continued development of methods to use these derivatives to construct accurate potential-energy surfaces is certainly warranted.

Another course for further studies is to test the validity of interpolation methods in discrete regions of the potential-energy surface to obtain additional points

for a global fit. Successful application of interpolation results could lead to significant savings in the computer time required to obtain an adequate number of points for the fit.

Cubic spline methods were employed to fit the *ab initio* results for SiH_5^-. It would be useful to explore the use of other methods which have been successfully applied to tri- and tetra-atomic systems to determine the applicability to treating systems of higher dimensionality.

General Conclusions

Sewell, Schranz, Thompson, and Raff[135] investigated factors which are related to the statistical and nonstatistical behavior of reaction rates for 1,2-difluoroethane, disilane, and the 2-chloroethyl radical. They concluded that three factors can collectively account for nonstatistical behavior: Internal energies which are close to the dissociation energy, no large changes in the bond energies as a function of motion along the reaction coordinate, and the existance of a formation coordinate that is strongly coupled to the reaction coordinate but only weakly coupled to the other internal coordinates. They tested their conclusions by considering the results of a number of other studies and determined that the trends they had observed appear to be generally applicable.

The CF_2Br radical has been studied at an internal energy of 35 kcal/mol which is just above the dissociation threshold used in the calculations of 33.3 kcal/mol. Motion along the C-Br bond dissociation coordinate produces no change in the value of the C-F bond well depths. In addition, quasiperiodic motion with respect to the Br-C-F bend mode is present in the radical. One would therefore anticipate that the rate of C-Br bond fission would be retarded (relative to the equipartition rates) when the excitation energy is initially placed in the Br-C-F bend mode. That this is not

observed leads to consideration of the potential coupling between internal coordinates of the radical. The coupling between the Br-C-F angles and the other internal coordinates is attenuated to zero as the C-Br bond extends. Given the anharmonic form of the C-Br bond potential, these coupling terms are less than their equilibrium values over a significant fraction of the individual trajectory lifetimes. In contrast, the coupling terms between the F-C-F angle and the other internal coordinates increases as the C-Br bond extends. Since the diagonal potential-energy functions for the angles are harmonic, this explains why the Br-C-F angles demonstrate quasiperiodic dynamics while the F-C-F angle does not. However, additional factors must be considered to explain the lack of nonstatisticality in the reaction rates for excitation of the Br-C-F mode.

This may be due to the methods used for initial conditions selection. Much more careful consideration of the initial conditions might lead to selectivity in the reaction rates since the selectivity is, apparently, subtle. However, the weakly bound N_2O_3 demonstrates that factors such as the degree of projection of the excited mode onto the reaction coordinate mode can have a profound effect on the reaction rates for mode-specific excitations (even using the imprecise initial conditions selection methods employed in these studies). When there are significant differences between the degrees of projection of the individual modes onto the reaction coordinate mode (such as is the case for N_2O_3), selectivity is observed. However, factors such as projection are expected to be more pronounced in weakly bound molecules because other effects (such as nonlinear resonances) that can enhance intramolecular vibrational energy redistribution are often absent. Since it has been demonstrated experimentally (e.g., HFCO[12]) that mode localized behavior in chemically bound molecules requires precise excitation of the localized mode, it is expected that "clean" initial conditions are an important factor.

If the effects of factors such as regular dynamics are subtle, an accurate potential-energy surface must be used to ensure that any selectivity that these factors might impart to the dynamics are accurate. The construction of such surfaces requires judicious use of available experimental data and *ab initio* results. While progress has been made in this area,[30] there remains a need to develop methods for the determination of accurate global potential-energy surfaces to describe the reaction dynamics of polyatomic molecules. The construction of such potential-energy surfaces requires the use of global functions and global coordinates.[141] In addition, the use of interpolation methods to extend *ab initio* results could reduce the computational cost of the *ab initio* calculations required to characterize a global potential-energy surface. For example, in regions of the potential-energy surface which are "well behaved" (e.g., along the minimum-energy path), interpolation appears to provide a reasonable approach to the determination of additional points.

REFERENCES

1. C. N. Hinshelwood and C. J. M. Fletcher, Nature **131**, 24 (1933).

2. I. Oref and B. S. Rabinovitch, Acc. Chem. Res. **12**, 166 (1979).

3. K. N. Swamy, W. L. Hase, B. C. Garrett, C. W. McCurdy, and J. F. McNutt, J. Phys. Chem. **90**, 3517 (1986).

4. G. Hose and H. S. Taylor, J. Chem. Phys. **76**, 5356 (1982).

5. G. Hose and H. S. Taylor, Chem. Phys. **84**, 375 (1984).

6. W. L. Hase, R. J. Duchovic, K. N. Swamy, and Ralph J. Wolf, J. Chem. Phys. **80**, 714 (1984).

7. R. J. Wolf and W. L. Hase, J. Chem. Phys. **73**, 3779 (1980).

8. W. L. Hase and R. J. Wolf, in *Potential Energy Surfaces and Dynamics Calculations*, edited by D. G. Truhlar (Plenum Press, New York, 1981), p. 37.

9. C. W. Patterson, J. Chem. Phys. **83**, 4618 (1985).

10. M. Shapiro, R. D. Taylor, and P. Brumer, Chem. Phys. Lett. **106**, 325 (1984).

11. M. J. Coggiola, P. C. Cosby, and J. R. Peterson, J. Chem. Phys. **72**, 6507 (1980).

12. Y. S. Choi and C. B. Moore, J. Chem. Phys. **94**, 5414 (1991).

13. K. K. Lehmann, B. H. Pate, and G. Scoles, in *Mode Selective Chemistry*, (Kluwer, Netherlands, 1991), pp. 17-23.

14. B. H. Pate, K. K. Lehmann, and G. Scoles, J. Chem. Phys. **95**, 3891 (1991).

15. R. M. Hedges, Jr., and W. P. Reinhardt, Chem. Phys. Lett. **91**, 241 (1982).

16. D. W. Noid and M. L. Koszykowski, Chem. Phys. Lett. **73**, 114 (1980).

17. D. L. Bunker and W. L. Hase, J. Chem. Phys. **59**, 4621 (1973).

18. E. B. Wilson, Jr., J. C. Decius, and P. C. Cross, *Molecular Vibrations* (Dover, New York, 1980).

19. R. B. Shirts and W. P. Reinhardt, J. Chem. Phys. **77**, 5204 (1982).

20. M. Hénon and C. Heiles, Astron. J. **69**, 73 (1964).

21. B. Barbanis, Astron. J. **71**, 415 (1966).

22. A. J. Lichtenberg and M. A. Lieberman, *Regular and Stochastic Motion* (Springer-Verlag, New York, 1983).

23. See, for example: D. W. Noid and B. G. Sumpter, Chem. Phys. Lett. **121**, 187 (1985).

24. D. W. Noid, M. L. Koszykowski, and R. A. Marcus, J. Chem. Phys. **67**, 404 (1977).

25. T. D. Sewell, D. L. Thompson, and R. D. Levine, submitted for publication, J. Phys. Chem.

26. R. S. Dumont and P. Brumer, J. Chem. Phys. **88**, 1481 (1988).

27. B. A. Waite and W. H. Miller, J. Chem. Phys. **74**, 3910 (1981).

28. M. P. Casassa, J. C. Stephenson, and D. S. King, J. Chem. Phys. **89**, 1966 (1988).

29. G. Ewing, Chem. Phys. **29**, 253 (1978).

30. S. Dasgupta and W. A. Goddard III, J. Chem. Phys. **90**, 7207 (1989).

31. S. Sato, J. Chem. Phys. **23**, 592 (1955).

32. See, for example: J. P. Bergsma, B. J. Gertner, K. R. Wilson, and J. T. Hynes, J. Chem. Phys. **86**, 1356 (1987).

33. J. I. Steinfeld, J. S. Francisco, and W. L. Hase, *Chemical Kinetics and Dynamics* (Prentice Hall, New Jersey, 1989).

34. P. J. Kuntz, E. M. Nemeth, J. C. Polanyi, S. D. Rosner, and C. E. Young, J. Chem. Phys. **44**, 1168 (1966).

35. N. C. Blais and D. G. Truhlar, J. Chem. Phys. **61**, 4186 (1974).

36. D. G. Truhlar, B. C. Garrett, N. C. Blais, J. Chem. Phys. **80**, 232 (1984).

37. F. B. Brown, R. Steckler, D. W. Schwenke, D. G. Truhlar, and B. C. Garrett, J. Chem. Phys. **82**, 188 (1985).

38. J. N. Murrell, S. Carter, S. C. Farantos, P. Huxley, and A. J. C. Varandas, *Molecular Potential Energy Functions* (Wiley, New York, 1984).

39. F. T. Wall and R. N. Porter, J. Chem. Phys. **39**, 3112 (1963).

40. D. R. McLaughlin and D. L. Thompson, J. Chem. Phys. **59**, 4393 (1973).

41. N. Sathyamurthy and L. M. Raff, J. Chem. Phys. **63**, 464 (1975).

42. N. Sathyamurthy and L. M. Raff, J. Chem. Phys. **66**, 2191 (1977).

43. N. Sathyamurthy and L. M. Raff, J. Chem. Phys. **72**, 3163 (1980).

44. C. L. Stroud and L. M. Raff, J. Chem. Phys **72**, 5479 (1980).

45. N. Sathyamurthy, R. Rangarajan, and L. M. Raff, J. Chem. Phys. **64**, 4606 (1976).

46. N. Sathyamurthy, J. W. Duff, C. Stroud, and L. M. Raff, J. Chem. Phys. **67**, 3583 (1977).

47. C. Stroud and L. M. Raff, J. Chem. Phys. **46**, 313 (1980).

48. J. N. L. Connor, W. Jakubetz, and J. Manz, Mol. Phys. **29**, 347 (1975).

49. J. M. Bowman and A. Kuppermann, Chem. Phys. Lett. **34**, 523 (1975).

50. S. K. Gray, J. S. Wright, and X. Chapuisat, Chem. Phys. Lett. **48**, 155 (1977).

51. J. S. Wright and S. K. Gray, J. Chem. Phys. **69**, 67 (1978).

52. See, for example: C. S. Sloane and W. L. Hase, Faraday Discuss. Chem. Soc. **62**, 210 (1977).

53. T. D. Sewell and D. L. Thompson, J. Phys. Chem. **95**, 6228 (1991).

54. See, for example: (a) A. J. Marks and D. L. Thompson, J. Chem. Phys. **95**, 8056 (1991); (b) P. M. Agrawal, D. L. Thompson, and L. M. Raff, J. Chem. Phys. **88**, 5948 (1988); (c) B. M. Rice, L. M. Raff, and D. L. Thompson, J. Chem. Phys. **85**, 4392 (1986). (d) B. G. Sumpter and D.L. Thompson, J. Chem. Phys. **86**, 3301 (1987).

55. K. Fukui, J. Phys. Chem. **74**, 4161 (1970).

56. D. G. Truhlar, A. D. Isaacson, and B. C. Garrett, in *Theory of Chemical Reaction Dynamics*, edited by M. Baer (Chemical Rubber, Boca Raton, FL, 1985), p. 65.

57. W. H. Miller, N. C. Handy, and J. E. Adams, J. Chem. Phys. **72**, 99 (1980).

58. S. C. Tucker and D. G. Truhlar, J. Am. Chem. Soc. **112**, 3338 (1990).

59. J. Ischtwan and M. A. Collins, J. Chem. Phys. **94**, 7084 (1991).

60. P. R. Bunker, *Molecular Symmetry and Spectroscopy* (Academic Press, New York, 1979), p. 24.

61. A. Schmelzer and J. N. Murrell, Int. J. Quantum Chem. **28**, 287 (1985).

62. D. G. Truhlar and M. S. Gordon, Science **249**, 491 (1990).

63. T. Uzer, Phys. Rep. **199**, 73 (1991).

64. D. L. Thompson, "Mode Specificity in Intramolecular Conversions," in the **Proceedings of the Twenty-Fourth Jerusalem Symposium on Quantum Chemistry and Biochemistry**, *Mode Selective Chemistry*, edited by J. Jortner, B. Pullman, and R. D. Levine (Kluwer Academic Publishers, The Netherlands, 1991), pp. 261-272.

65. T. D. Sewell, D. L. Thompson, and R. D. Levine, "Mode Selectivity in the Classical Power Spectra of Highly Vibrationally Excited Molecules," J. Phys. Chem., submitted.

66. D. Krajnovich, Z. Zhang, L. Butler, and Y. T. Lee, J. Phys. Chem. **88**, 4561 (1984).

67. T. R. Gosnell, A. J. Taylor, and J. L. Lyman, J. Chem. Phys. **94**, 5949 (1991).

68. P. J. Robinson and K. A. Holbrook, *Unimolecular Reactions* (Wiley-Interscience, New York, 1972).

69. Y. Guan, G. C. Lynch, and D. L. Thompson, J. Chem. Phys. **87**, 6957 (1987).

70. Y. Guan and D. L. Thompson, Chem. Phys. **139**, 147 (1989).

71. H. Gai and D. L. Thompson, Chem. Phys. Lett. **168**, 119 (1990).

72. A. Preiskorn and D. L. Thompson, J. Chem. Phys. **91**, 2299 (1989).

73. I. W. M. Smith and G. Yarwood, Faraday Disc. Chem. Soc. **84**, 205 (1987).

74. L. A. Chewter, I. W. M. Smith, and G. Yarwood, Mol. Phys. **63**, 843 (1988).

75. R. S. Berry, J. Chem. Phys. **32**, 933 (1960).

76. M. S. Gordon, T. L. Windus, L. W. Burggraf, and L. P. Davis, J. Am. Chem. Soc. **112**, 7167 (1990).

77. T. L. Windus and M. S. Gordon, private communication.

78. G. A. Natanson, B. C. Garrett, T. N. Truong, T. Joseph, and D. G. Truhlar, J. Chem. Phys. **94**, 7875 (1991).

79. R. S. Dumont and P. Brumer, J. Chem. Phys. **88**, 1481 (1988).

80. J. S. Bendat and A. G. Piersol, *Random Data Analysis and Measurement Procedures*, 2nd ed. (Wiley, New York, 1986).

81. M. L. Boas, *Mathematical Methods in the Physical Sciences*, 2nd ed. (Wiley, New York, 1983).

82. W. H. Press, B. P. Flannery, S. A. Teukolsky, and W. T. Vetterling, *Numerical Recipes* (Cambridge University Press, New York, 1989).

83. Reference 80, Eq. (5.27).

84. Reference 80, Eq. (5.56).

85. Reference 80, Eq. (5.57).

86. Reference 80, Eq. (5.59).

87. Reference 80, pp. 130-132.

88. Reference 80, Eq. (11.101).

89. Reference 80, through substitution of Eq. (11.101) into Eq. (11.102).

90. See, for example: J. W. Cooley and J. W. Tukey, Math. of Comp. **19**, 297 (1965).

91. Reference 82, Eq. (12.1.10).

92. G. E. Powell and I. C. Percival, J. Phys. A **12**, 2053 (1979).

93. S. C. Farantos and J. N. Murrell, Chem. Phys. **55**, 205 (1981).

94. D. Carter and P. Brumer, J. Chem. Phys. **77**, 4208 (1982).

95. Reference 80, Eq. (8.154).

96. J. T. Muckerman, D. W. Noid, and M. S. Child, J. Chem. Phys. **78**, 3981 (1983).

97. Y. J. Cho, P. R. Winter, H. H. Harris, E. D. Fleischmann, and J. E. Adams, J. Phys. Chem. **94**, 1847 (1990).

98. L. M. Raff, private communication.

99. R. Roy, B. G. Sumpter, G. A. Pfeffer, S. K. Gray, and D. W. Noid, Phys. Rep. **205**, 109 (1991).

100. Reference 80, Eq. (10.12).

101. See, for example, Reference 82, pp. 425-427.

102. For a description of the original version of the GenDyn code, see: K. L. Bintz, M. S. Thesis, Oklahoma State University, (1986).

103. H. Goldstein, *Classical Mechanics* (Addison-Wesley, Reading, Massachusetts, (1980).

104. L. M. Raff and D. L. Thompson, in *Theory of Chemical Reaction Dynamics*, edited by M. Baer (Chemical Rubber, Boca Raton, 1985), Vol. III.

105. E. B. Wilson, Jr., J. C. Decius, and P. C. Cross, *Molecular Vibrations* (Dover, New York, 1980).

106. W. L. Hase, D. G. Buckowski, and K. N. Swamy, J. Phys. Chem. **87**, 2754 (1983).

107. P. J. Hay, private communication.

108. Molecular Electronic Structure Applications (MESA), P. W. Saxe, R. L. Martin, B. H. Lengsfield III and M. Page.

109. K. L. Bintz, D. L. Thompson, T. R. Gosnell, and P. J. Hay, submitted for publication.

110. M. E. Jacox, Chem. Phys. Lett. **53**, 192 (1978).

111. F. T. Prochaska and L. Andrews, J. Am. Chem. Soc. **100**, 2102 (1978).

112. W. J. Hehre, L. Radom, P. v. R. Schleyer, and J. Pople, *Ab Initio Molecular Orbital Theory* (Wiley, New York, 1986).

113. G. Fogarasi and P. Pulay, in *Vibrational Spectra and Structure*, edited by J. R. Durig (Elsevier, Amsterdam, 1985).

114. B. L. Crawford, Jr. and W. H. Fletcher, J. Chem. Phys. **19**, 141 (1951).

115. W. H. Kirchhoff, D. R. Lide, Jr., and F. X. Powell, J. Mol. Spec. **47**, 491 (1973).

116. J. B. Burkholder, C. J. Howard, and P. A. Hamilton, J. Mol. Spec. **127**, 362 (1988).

117. C. W. Mathews, Can. J. Phys. **45**, 2355 (1967).

118. D. E. Milligan, D. E. Mann, M. E. Jacox, and R. A. Mitsch, J. Chem. Phys. **41**, 1199 (1964).

119. D. E. Milligan and M. E. Jacox, J. Chem. Phys. **48**, 2265 (1968).

120. H. Eyring, J. Chem. Phys. **3**, 107 (1935).

121. M. G. Evans and M. Polyani, Trans. Faraday Soc. **31**, 875 (1935).

122. H. B. Schlegel, in *Ab Initio Methods in Quantum Chemistry*, edited by K. P. Lawley (Wiley, New York, 1987) Vol. I.

123. M. W. Chase, Jr., C. A. Davies, J. R. Downey, Jr., D. J. Frurip, R. A. McDonald, and A. N. Syverud, JANAF Thermochemical Tables, 3rd ed. [J. Phys. Chem. Ref. Data **14**, Suppl. No. 1 (1985)].

124. B. M. Rice and D. L. Thompson, J. Chem. Phys. **93**, 7986 (1990).

125. C. H. Bibart and G. E. Ewing, J. Chem. Phys. **61**, 1293 (1974).

126. A. H. Brittain, A. P. Cox, and R. L. Kuczkowski, Trans. Faraday Soc. **65**, 1963 (1969).

127. G. Herzberg, *Spectra of Diatomic Molecules* (Van Nostrand Reinhold, New York, 1950).

128. G. R. Bird, J. C. Baird, A. W. Jache, J. A. Hodgeson, R. F. Curl, Jr., A. C. Kunkle, J. W. Bransford, J. Rastrup-Andersen, and J. Rosenthal, J. Chem. Phys. **40**, 3378 (1964).

129. R. L. Sams and W. J. Lafferty, J. Mol. Spec. **56**, 399 (1975).

130. E. M. Nour, L. H. Chen, and J. Laane, J. Phys. Chem. **87**, 1113 (1983).

131. J. J. P. Stewart, L. P. Davis, and L. W. Burggraf, J. Comp. Chem. **8**, 1117 (1987).

132. Thomas D. Sewell, private communication.

133. R. R. Holmes and J. A. Deiters, J. Am. Chem. Soc. **99**, 3318 (1977).

134. (a) Y. Guan, G. C. Lynch, and D. L. Thompson, J. Chem. Phys. **87**, 6957 (1987); (b) T. Uzer, B. D. McDonald, Y. Guan, and D. L. Thompson, Chem. Phys. Lett. **152**, 405 (1988); (c) H. Gai, D. L. Thompson, and G. A. Fisk, J. Chem. Phys. **90**, 7055 (1989); (d) Y. Guan and D. L. Thompson, Chem. Phys. **139**, 147 (1989); (e) H. Gai and D. L. Thompson, Chem. Phys. Lett. **168**, 119 (1990); (f) K. L. Bintz and D. L. Thompson, Chem. Phys. Lett. **187**, 166 (1991); (g) Y. Guan, T. Uzer, B. D. MacDonald, and D. L. Thompson, in *Advances in Molecular Vibrations and Collision Dynamics*, Vol. 1B, edited by J. M. Bowman and M. Ratner, (JAI Press, Greenwich, Connecticut, 1991), p. 81.

135. See, for example: T. D. Sewell, H. W. Schranz, D. L. Thompson, and L. M. Raff, J. Chem. Phys. **95**, 8089 (1991).

136. J. Troe, J. Chem. Phys. **79**, 6017 (1983).

137. J. M. Bowman, B. Gazdy, and Q. Sun, J. Chem. Phys. **91**, 2859 (1989).

138. W. H. Miller, W. L. Hase, and C. L. Darling, J. Chem. Phys. **91**, 2863 (1989).

139. I. W. M. Smith, private communication.

140. Y. Zhang, S. J. Klippenstein, and R. A. Marcus, J. Chem. Phys. **94**, 7319 (1991).

141. K. Fukui, Accts. Chem. Res. **14**, 363 (1981).

VITA

Karen W. Bintz

Candidate for the Degree of

Doctor of Philosophy

Thesis: THEORETICAL INVESTIGATIONS OF FACTORS WHICH AFFECT THE MODE-SPECIFIC BEHAVIOR OF UNIMOLECULAR REACTION DYNAMICS

Major Field: Chemistry

Biographical:

Personal Data: Born in Pryor, Oklahoma, March 31, 1960, the daughter of Jack T. and Thelma L. Walker. Married to Daniel G. Bintz, O. D., on December 22, 1985.

Education: Graduated from Pryor High School, Pryor, Oklahoma, in May, 1978; received Bachelor of Science Degree in Chemistry from Northeastern State University, Tahlequah, Oklahoma, in May, 1984; received Master of Science Degree in Chemistry from Oklahoma State University, Stillwater, Oklahoma, December, 1986; completed requirements for the Doctor of Philosophy Degree at Oklahoma State University in July, 1992.

Professional Experience: Teaching Assistant, Department of Chemistry, Oklahoma State University, August, 1984, to May, 1985; Research Assistant, Department of Chemistry, Oklahoma State University, June, 1984, to July, 1984, June, 1985, to September, 1986, and January, 1990, to July, 1992.